2022

Accuracy of photogrammetry, intraoral scanning, and conventional impression techniques for full-arch implant-supported prostheses: an in-vitro study

BOSTON UNIVERSITY

HENRY M. GOLDMAN SCHOOL OF DENTAL MEDICINE

THESIS

ACCURACY OF PHOTOGRAMMETRY, INTRAORAL SCANNING, AND CONVENTIONAL IMPRESSION TECHNIQUES FOR FULL-ARCH IMPLANT-SUPPORTED PROSTHESES: AN IN-VITRO STUDY.

By

LEA GEORGE HAJJAR

D.D.S., Université Saint-Joseph de Beyrouth, 2018

C.A.G.S., Boston University, 2021

Submitted in partial fulfillment of the

requirements for the degree of

Master of Science in Dentistry

in the Department of Restorative Sciences and Biomaterials

2022

READERS' APPROVAL

First Reader: _____

Russell A. Giordano II, D.M.D., C.A.G.S., D.M.Sc.

Associate Professor and Director, Division of Biomaterials

Assistant Dean for Biomaterials & Biomaterials Research

Second Reader: _____

Yuwei Fan, M.Sc., Ph.D.

Research Associate Professor

Third Reader: _____

Konstantinos Michalakis, D.D.S., C.A.G.S., M.Sc, M.Sc, Ph.D.

Professor and Chair

Fourth Reader:_____

Peixi Liao, B.D.S., D.Sc.D., C.A.G.S.

Clinical Associate Professor of Prosthodontics

Fifth Reader:_____

Ali Abdallah, B.D.S., D.Sc.D., C.A.G.S.

Clinical Assistant Professor of Prosthodontics

CHAIR'S APPROVAL

Chair:_____

Konstantinos Michalakis, D.D.S., C.A.G.S., M.Sc, M.Sc, Ph.D.

Professor and Chair

DEDICATION

I would like to dedicate this work to my family without whom, none of this would have ever been possible:

To my father ***George*** and my mother ***Sawsan***, there are no words to express how eternally grateful I am to your unconditional love and support. You have sacrificed so much for us and have set the highest example of how perseverance, hard work, and determination are the backbones of success. I dedicate this work to you in the hopes that it will bring me one step closer to being able to give back all that you have done for us.

My sister ***Lyn*** and my brother ***Rayan***, thank you for your endless support and optimism under any circumstances, and despite the distance.

ACKNOWLEDGEMENTS

I want to express my profound gratitude to the faculty, staff, and residents at Boston University Goldman School of Dental Medicine for the incredible four years I spent completing the combined CAGS/MSD program in Prosthodontics.

Dr. Russel Giordano, thank you for being an exceptional research advisor and mentor. The knowledge and experience I have developed as your student have been transformational. Thank you for your guidance, support, and encouragement, which allowed me to always carry out this work serenely, and in good atmosphere.

Dr. Yuwei Fan, thank you for your outstanding - round-the-clock - mentorship. Your endless guidance, patience and support have without a doubt made me a better researcher, and for that, I am forever grateful. The execution and success of this project would not have been possible without your unmatched attention to detail and the invaluable contribution of your time and resources.

Dr. Konstantinos Michalakis, I had the great pleasure of knowing you and working with you in my final year at BU. The short, yet extremely valuable time together had a great impact on my education. Thank you for always raising more questions and challenging me to think critically. Your willingness to lend an ear and your meticulous thought process have been most fruitful.

Dr. Peixi Liao, you are a true pioneer of the digital era in BUGSDM. I was lucky to have matriculated the same year that you joined the faculty staff at the Prosthodontics department. Thank you for all the countless clinical and laboratory lessons you have taught me in the most considerate way, and for inspiring me to further submerge into the world of digital dentistry.

Dr. Ali Abdallah, thank you for being an exemplary senior co-resident and always having my back during my three years of residency. I am grateful for everything you have taught me then, and for everything I continue to learn from you now, as my faculty. You are an invaluable resource on the clinic floor, and the Department of Prosthodontics is lucky to have you.

Dr. Andre Hashem, you have once told me that "simplicity is the ultimate sophistication", and it has stuck with me through everything you have taught me. Your eye for art and perfection is incomparable. Thank you for always sharing your wealth of knowledge with me, and for going above and beyond to ensure that I had access to the equipment necessary for the realization of this project.

Dr. Hiroshi Hirayama, you have been a guide, a mentor, and a role model to me throughout every step in the past 4 years. To say I appreciate your time would be an understatement. Thank you for all the lessons, advice, and support. I will forever treasure the perspective and insights you have shared with me and the skills you have taught me. I am a better Prosthodontist today because of you.

Dr. Minglei Zhao, you are a key member of the Biomaterials laboratory. Thank you for always being present, with a smile on your face, and offering to lend a helping hand. It has really been great working with you.

Dr. Alexander Bendayan, you have always known exactly what to say or do to set your residents on the right path. Thank you for your enormous support and encouragement.

I would like to express my deep gratitude as well to ***Ms. Milly Koo*** for her invaluable administrative support and coordination.

My sincere thanks extend to the members of the jury for their interest in my thesis, by agreeing to examine my work and enrich it with their comments and suggestions.

ACCURACY OF PHOTOGRAMMETRY, INTRAORAL SCANNING, AND CONVENTIONAL IMPRESSION TECHNIQUES FOR FULL-ARCH IMPLANT-SUPPORTED PROSTHESES: AN IN-VITRO STUDY.

LEA GEORGE HAJJAR

Boston University, Henry M. Goldman School of Dental Medicine, 2022

Major Professor: Russell Giordano II, D.M.D., D.M.Sc., Director and Associate Professor, Department of Restorative Sciences and Biomaterials

ABSTRACT

Objectives: The purpose of this in vitro study is to measure and compare the accuracy of the conventional impression, the intraoral scanner, and the photogrammetry techniques for full-arch implant-supported dental prostheses at the abutment level.

Methods: An edentulous maxillary master model containing 6 implant abutment replicas (RP analog for screw-retained abutment straight from NobelReplace® Multi-unit Abutment Plus Replica) was fabricated. A reference STL of the master model was obtained using a desktop scanner (inEos X5, Dentsply Sirona) with high trueness and precision and served as the control STL. Three impression techniques were performed: the intraoral scanning (IOS) group (TRIOS 3 Battery Cart, 3Shape A/S), the photogrammetry (PTG) group (ICam 4D Generation 3, Imetric), and the conventional (CNV) group. Ten impressions from each group were tested. Scan bodies in each STL file acquired from the different impression techniques were converted to implant abutment replicas using a digital library. Three tests were completed to compare the different

registration techniques. A 3D deviation test between the experimental group and the reference was done on an inspection software (IScan4D Dental Version 9.1.104; Imetric) using a “best fit” algorithm to obtain the root mean square values, and on another inspection software (IScan3D Dental Version 9.1.104; Imetric) using spatial similarity transformation. The second test was meant to assess the angular deviations of the implant abutment replicas using a reverse engineering software (Geomagic Control X 2020.1; 3D Systems). The final test for cross-arch distances was done on an inspection software (IScan3D Dental Version 9.1.104; Imetric) which allows to determine the 3-dimensional coordinates for each implant by using the origin point and compare the cross-arch distance deviations as well as deviations at the x-, y-, and z- coordination. Trueness and precision were the two parameters used to define the accuracy of a system. The term "trueness" was used to see how close the measurements from the experimental files of each group were to those of the reference file. The term "precision" was defined as to see how close the measurements of each experimental files were to each other within the same group. The 3D discrepancies were then calculated and the trueness and precision of the three impression techniques were assessed and compared statistically ($\alpha = 0.05$).

Results: The root mean square of 3D deviation values through the ICP “best-fit” method showed statistically significant differences between the PTG and CNV group ($p < .0001$), and the PTG and IOS group ($p < .0001$). The CNV and IOS group did not show statistically significant differences ($p = 0.8626$) through the “best-fit” method, but significant differences were observed via the “spatial similarity” method ($p = 0.0041$). Both methods however showed the best results in terms of trueness for the PTG group, followed by the CNV group and least the IOS group. In terms of precision, PTG showed the best results, followed by the IOS group and least the CNV group. The angular deviation test using the “best-fit” alignment method showed that the PTG and CNV

had no statistically significant difference ($p = 0.7955$) and were equivalent. However, both showed a statistically significant difference to the IOS group ($p < .0001$), which had the highest angular deviation. Finally, in terms of cross-arch distances, the photogrammetry group showed optimal results followed by the IOS group and then the CNV group. In general, the shorter the inter-arch distance, the lower the deviation was. A larger deviation was observed on longer inter-arch distances. Considering the deviations on the 3 axes of each implant, the CNV technique had the highest deviation in the X-axis (longitudinal) and the IOS technique showed the highest deviation on the Y-axis (lateral) and Z-axis (vertical). The PTG technique experienced significantly less deviation on the X-axis, Y-axis, and the Z-axis.

Conclusion: Within the scope of this study, the photogrammetry technique reported the best accuracy in terms of trueness and precision of implant positions for complete-arch implant rehabilitation. Conventional impressions showed better accuracy results than intraoral scanning in the 3D deviations test and global angular deviation test, however the latter exhibited better results in terms of accuracy in terms of cross-arch distances test.

TABLE OF CONTENTS

LIST OF TABLES

LIST OF FIGURES

LIST OF EQUATIONS

LIST OF ABBREVIATIONS

ANOVA	Analysis of Variance
CAD/CAM	Computer-Aided Design / Computer-Aided Manufacturing
CBCT	Cone Beam Computed Tomography
CMM	Coordinate measuring machine
CNV	Conventional impression
DICOM	Digital Imaging and Communications in Medicine
GMGX	Geomagic
ICP	Iterative Closest Point algorithm
IMP	Implant
IOS	Intraoral scan
ISO	International Standards Organization
MOE	Margin of Error
MU	Multi-unit abutment
PMMA	Polymethyl Methacrylate
PTG	Photogrammetry group
PVS	Polyvinyl siloxane
RMS	Root means square
RP	Regular platform
SB	Scan body
SD	Standard Deviation
SIG	Significance
STL	Standard Tessellation Language
Y-TZP	Yttria-stabilized tetragonal zirconia polycrystal
3D	Three dimension

Chapter 1: INTRODUCTION

Due to the significant enhancement in quality of life compared to treatment with conventional dentures, implant-supported full-arch prostheses have become the treatment of choice for edentulous patients. Transferring the information of the implant position to obtain an accurately fitting framework has traditionally been one of the major challenges of this treatment methodology.

The Glossary of Prosthodontics defines the impression in dentistry as “a negative likeness or copy in reverse of the surface of an object; an imprint of the teeth and adjacent structures”.(1)

In a clinical setting, the purpose of an impression entails the transfer of the dimensions of soft and hard tissues from the patient’s mouth to a three-dimensional model.(2) If the fabricated restoration is to fit accurately, the cast or virtual model created from this impression should be as close as possible to an exact copy of the patient’s mouth. This means that an accurate and undistorted registration of the clinical situation is requisite, whether using a conventional or digital technique.

1.1 Fixed full-arch implant rehabilitation

1.1.1 Prosthetic materials in fixed implant rehabilitation

Numerous types and combinations of materials have been employed for full-arch fixed implant-supported prostheses as mentioned in Bidra's classification.(3) The original hybrid prosthesis made of metal-acrylic resin is known for its reduced cost and easier reparability but also

for its high rate of prosthesis-related complications such as loosening/fracture of the screw, resin base, denture teeth and framework.(4)

Traditionally, the casting technique has been used for the fabrication of metal-based frameworks. However, the introduction of technologies such as computer-aided design/computer-aided manufacturing offered new alternatives for the fabrication of the prostheses, allowing dental technicians to overcome the procedural errors related to cast restorations. CAD/CAM technology allows the manufacturing of various materials, including zirconia in its yttria-stabilized tetragonal zirconia polycrystal (Y-TZP) form. The ability to create high-strength all-ceramic restoration along with the efficiency and cost-effectiveness of CAD/CAM technology, and favorable outcomes reported with screw-retained implant fixed implant-supported prostheses, have made zirconia the material of choice for monolithic and multilayer restorations in recent years.(5)(6)

Disadvantages of using zirconia in fixed implant-supported prostheses include low tolerance for minor inaccuracies in impression, which can result in the fracture of the prosthesis at the time of insertion.(3) As opposed to the workflow commonly employed for the metal-acrylic and metal-ceramic fixed implant-supported prostheses which allows more flexibility for the try-in of the framework, the passive fit of a zirconia framework relies solely on the accuracy of the impression and the poured model because it cannot be sectioned and soldered. A verification step which includes the fabrication of a jig is always required for those purposes.

1.1.2 Passive fit

Achieving a passive fit between the prosthetic structure and the supporting implants can ensure the long-term success of full arch implant-supported prostheses and prevent potential mechanical and even biological complications related to the structure. Although passive fit is still a difficult concept to define, it is commonly described as the minimum gap between the implant

or the abutment and the prosthetic framework that allows a connection without causing any stress when functional or parafunctional loads are not exerted on the prosthesis/abutment/screw/implant complex.(7)(8) Mechanical complications that can arise due to the tension, compression, and flexion forces resulting from a compromised fit include screw loosening and/or fracture, as well as prosthesis, abutment and implant fractures.(9)(10) Poor fit may also result in biological complications due to the existing gap between the prosthesis and the implant which can accumulate microorganisms that can affect the supporting tissues and cause peri-implant mucositis or peri-implantitis.(11)(12)

1.1.3 Tolerance and acceptable levels of misfit at the implant-abutment interface.

The mechanical, or machining tolerance between machined implant components, is the amount of horizontal shift possible between these paired components and can range from 22 to 100 μm according to a study conducted by Ma et al.(13) This machining tolerance can help make the passive fit achievable by minimizing the final distortion. From a biological standpoint however, the marginal opening should be smaller than the size of any periodontal bacteria that can cause harm, which is less than 2 μm.(14)

There has been no consensus over the years about the acceptable marginal opening. While some authors have stated that the maximum marginal discrepancy between the prosthesis and the implant or abutment should be 10 μm (15)(16), others have stated that a clinically acceptable gap should be 150 μm.(17) There has also been no agreement on the method that should be used to evaluate framework passivity.(16)

Since many steps are involved in the fabrication of implant-supported fixed restorations, especially in full-arch rehabilitations, achieving a 100% passive fit has been considered almost impossible.(18) Therefore, a passive framework fit not only requires a high level of laboratory

precision, but also clinical precision, beginning with a highly accurate registration of the intraoral situation.

1.2 Impression materials in fixed implant rehabilitation

1.2.1 Conventional impressions

To date, many clinical factors affect the accuracy of dental impressions, amongst them are (19)(20)(21):

- The tray type (standard or customized, metal or disposable)
- The impression technique (whether one or two steps)
- The impression material used (hydrophobic or hydrophilic characteristics, distortion, dimensional stability, elasticity, etc.)
- Mixing methods
- Impression disinfection
- Pouring methods
- Dental stone properties (expansion), etc.

For implant-supported fixed prostheses, impressions could be made at either the implant level or at the abutment level. The accuracy of the impressions may vary as a result of variations and combinations of different techniques such as open- or closed-tray impressions, splinted or non-splinted impression copings. According to the results of available systematic reviews (22)(23), elastomers are the recommended materials to be used for implant impressions, and higher accuracy is shown when the splinted pickup technique was used for four or more implants.(19)(24)(25) Therefore, the splinted open-tray impression technique is recommended for fixed full-arch implant-supported prostheses and provides acceptable results. However, this impression technique often requires complicated procedures, is considered time-consuming and is uncomfortable to the

patient. In addition, the master model's accuracy is influenced by the dimensional changes of the stone and machining tolerance of components.(26)(27)

1.2.2 Digital impressions: Intraoral Scan

Digital impression techniques have become more popular in implant dentistry with the surge of CAD/CAM technology.(28) Intraoral scanners equipped with a digital photo or video technology allows for data to directly capture images produced by a laser light reflecting off of the teeth and oral soft tissues.(7)

The concept of intraoral scanning relies on structured light. This active triangulation technique is based on projecting a sequence of different alternating dark and bright stripes onto the surface of an object and extracting the 3D geometry by monitoring the deformations of each pattern. The distance from the scanner to the object's surface is then calculated by examining the edges of each line in the pattern (Figure 1).

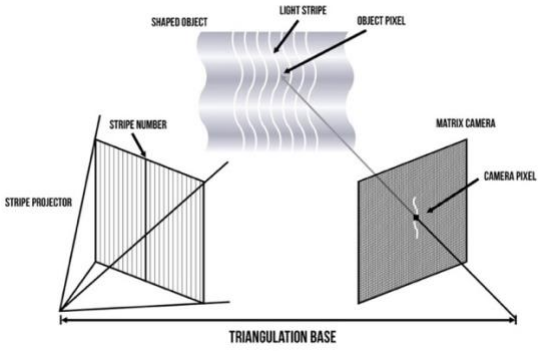

Figure 1. Diagram illustrating the principles of structured light measurement devices.(29)

Intraoral scanners (IOS) can obtain an STL file of all the intraoral structures by defining every new 3D point captured without a fixed reference to the rest of the points of the resulting STL file.(7)

The process of scanning implants relies on placing scan bodies over the implants or abutments to transfer the 3-dimensional implant positions into the digital system by capturing raw data as point clouds.(30) A point cloud is a set of data points in space where each point is defined by the X, Y and Z coordinates and corresponds to one position on the surface of a 3D shape or object.(31) Although intraoral scanning has many advantages, the amount of stitching involved in the scanning process produces an STL file with varying degrees of inaccuracy. The longer the span of the scan, the more stitching required which leads to more errors, especially if the arch is edentulous and lacks distinct anatomical landmarks or distinguishing features.(32)(33) This can explain the various reports of in vitro and in vivo studies demonstrating that the new generation of intraoral scanners do not produce reliable impressions of multiple implants when they are distributed along the whole arch.(34) IOS systems have a number of other limitations related to the patient, the optical system and the digital-data-processing software (35), which can include:

- Scanning technology and scanning strategy (36)

- Salivary flow and sulcular bleeding (Figure 2): which may distort part of the dental structures and negatively influence the systems of intraoral scanners.

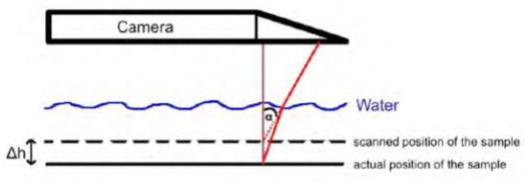

Figure 2. Illustration of possible errors when a layer of water is deposited on the tooth structure.(37)

- Accessibility of the camera: a limited mouth opening or a mandibular ramus close to the dental surfaces can limit or even prevent access of the camera in the posterior areas.

- Ambient light (38)

- Implant depth, implant angulation (33) and interimplant distance (39)

- Scan body design and material (40)

1.2.3 Photogrammetry

Since the early 1980s, photogrammetry has been employed extensively in fields like topography, naval engineering, and car manufacturing. The surge of photogrammetry technology was introduced to dentistry by Lie and Jemt in 1994 to analyze the distortion of implant frameworks.(41)

As the "science of making measurements from photographs," photogrammetry uses metric data to determine the geometric characteristics of objects, as well as their spatial arrangement extracted from 2D and/or 3D photographic images.(42)

In contrast to intraoral scanning, this system generates information from x,y and z points with a fixed relation to the rest of the points so that the data are interrelated and cannot be separated.(43) The STL file obtained contains information about the exact position of the implants

but does not contain any soft tissue information, and therefore requires a second STL file, which can be seen as a drawback for this technology.

Photogrammetry uses a passive triangulation technique. The pinhole camera model has a ray going from the center of perspective through the point in the image to the point on the object (Figure 3).

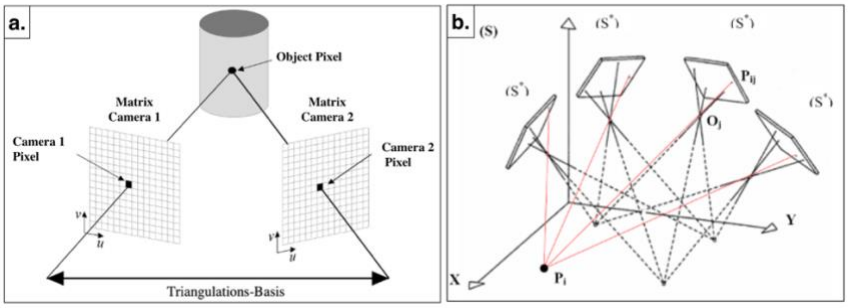

Figure 3. a. Single point triangulation (passive triangulation technique) (44) b. Multiple point triangulation (One camera, many pictures) (45).

The whole procedure is done quickly and is considered to be more comfortable for patients and easier for the operators than conventional or digital impression methods. A few studies have been done to assess the accuracy of photogrammetry systems, but the results are inconsistent.(46)(47)(48)

1.4 Trueness and precision

In order to measure the accuracy of a system, two terms are central to understanding metrology (49):

- Trueness: which relates to the closeness of a measured value to the true known value or the a standard value.

- Precision: which refers to the repeatability (testing under same conditions) and reproducibility (testing under different conditions) of the measured values to each other.

According to the International Organization for Standardization (ISO) 5725-1 (50), accuracy is defined as a combination of precision and trueness. Figure 4 illustrates the correlation between trueness and precision through a bullseye example. The center of the target represents the true value or the standard. Figure 4 (a) demonstrates results that has both low trueness and precision, whereas Figure 4 (d) shows a situation where the system is both true and precise; only in this case, the system is considered to be accurate.

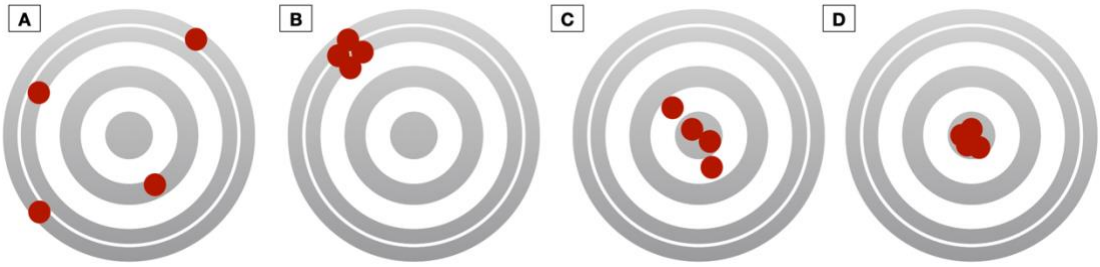

Figure 4. Illustration of the correlation between trueness and precision.(51)
a: Low trueness, low precision, b: Low trueness, high precision, c: High trueness, low precision, d: High trueness, high precision.

Precision should be verified first with a system. Only if a system is precise can it be made to be accurate, typically through calibration. Therefore, in the metrological nomenclature, the mean value and standard deviation would respectively be correlated to trueness and precision.

To evaluate the trueness and precision of impression techniques, different methods have been created. Most researchers used a master cast that has either been measured by a Computer Measuring Machine (CMM) or by a laboratory scanner to obtain reference data as a 3D virtual file. The master cast is then scanned by test scanners and the virtual models obtained are compared to the reference file.(32)(46)(47)(48)(51)(52)(53)(54)

1.5 Statement of Problem

When it comes to impression for an implant-supported full-arch prosthesis, both conventional and digital impression techniques reveal some inaccuracies, which in turn, affect the

fabrication of a passive framework. Since the photogrammetry technique is relatively new and has not been on the market for nearly as long as conventional or digital impressions, it is important to determine whether it is as a reliable alternative to the aforementioned techniques.

1.6 Purpose

The purpose of this in vitro study was to measure and compare the accuracy of the conventional impression, the intraoral scanner, and the photogrammetry techniques for full-arch implant-supported dental prostheses at the abutment level.

1.7 Null Hypothesis

The null hypothesis was that no significant differences exist between the different impression techniques in terms of accuracy in 3D deviations, global angular deviations, and cross-arch distance deviations.

1.8 Significance of the study:

Photogrammetry in dentistry is relatively new on the market and has been gaining popularity amongst treatment modalities that clinicians are using to treat edentulous patient with full-arch implant-supported prostheses due to their convenience and fewer office visits. Although there have been some in-vitro studies that were done regarding the accuracy and several clinical case reports, the results are still sparse. It is important to determine whether this is a reliable technology and if the verification step of full-arch implant-supported prostheses can be eliminated, without compromising the fit of the framework, and therefore, avoiding any mechanical or biological related complications.

Chapter 2: MATERIALS AND BACKGROUND STUDIES

2.1 Materials

All equipment, tools, and materials used in this study are listed in Table 1, 2 and 3.

Table 1. List of Devices, Equipment, & Machinery.

Description	Model (Manufacturer)
Cone Beam Computed Tomography (CBCT) Scanner	iCAT Next Generation Dental Imaging System (Imaging Sciences International, USA)
Dental Laboratory Scanner	• inEOS X5 (Dentsply Sirona, Germany) • 3Shape D1000 (3Shape, Copenhagen, Denmark)
5-Axis Milling Machine	MC X5 (Dentsply Sirona, Germany)
Implant Drill Unit (Motor)	OsseoSet 300 (Nobel Biocare, USA)
LED Curing Light	SmartLite Focus (Dentsply DeTrey GmbH, Germany)
Photogrammetry system	ICam 4D Generation 3 photogrammetry system with 4 cameras (Imetric, Switzerland)
Intraoral Scanner device and software	Trios 3; 3shape, Copenhagen, Denmark
CAD software for STL conversion of Scan body	Exocad DentalCAD; Darmstadt, Germany
Spatial Fit software	IScan3D Dental Version 9.1.104 (Imetric, Switzerland)
CAD software for custom tray fabrication	3Shape CAD software (3shape, Copenhagen, Denmark)
CAD software for Mesh refinement	Meshmixer 3.5.474, Autodesk, Inc.
3D Inspection software	• IScan3D Dental Version 9.1.104 (Imetric, Switzerland) • IScan4D Dental Version 9.1.104 (Imetric, Switzerland) • Geomagic Control X 2020.1; 3D Systems

3D Printer	Formlabs Form 3, Preform

Table 2. List of Materials and Components (Restorative, Implant).

Commercial Name	**Generic Name**	**Size**	**Shade**	**REF Number**	**Lot Number**
Z-Dupe, Henry Schein	Addition-Vulcanizing Duplication Silicone (Base & Catalyst)	N/A	N/A	1026526	
Multilayer PMMA Disc, Dentsply Sirona	Multi-layered Polymethyl Methacrylate (PMMA) Disk	98.5×20mm	A2	8071120	162053
Elos Accurate® Multi-unit Scan Body	Intraoral and Laboratory Scan Body for Multi-unit (compatible with Nobel Biocare Multi Unit)	RP/NP multi-unit	N/A	IO 2C-A	160943
Elos Accurate® Scan Body Driver	Driver for Intraoral and Laboratory Scan Body for Multi-unit	N/A	N/A	C13485	161099
NobelReplace® Conical Connection RP, Nobel Biocare	Titanium Bone Level Tapered Implant, TiUnite Surface	4.3×10 5.0×11.5	N/A N/A	36705 36712	12187180 13121110
NobelReplace® Multi-Unit abutments	Titanium Multi-Unit abutment	RP 2 mm	N/A	29200	
NobelReplace® Multi-unit Abutment Plus Replica	Titanium Laboratory Analog for Multi-unit Abutment	RP	N/A	38918	161809
NobelReplace® Impression Copings for Multi Unit Abutments	Impression coping open tray Multi-Unit	RP	N/A	29089	162616
ICamBodies MU-RP 1.4 mm	Photogrammetry Scan Body for Multi-unit (compatible with Nobel Biocare Multi Unit)	RP	N/A	MURP2112-111	N/A
Screwdriver for ICamBody MU-RP	Driver for Photogrammetry Scan Body for Multi-unit	N/A	N/A		

Pattern Resin LS; GC	Pattern Resin	N/A			
Silky Rock	Type IV Stone WhipMix				
Model Resin	Model Resin (FormsLab 3)	1 L	V2	RS-F2-DMBE-02	
Impregum	Impregum Polyether Impression Material; 3M ESPE				

Table 3. List of Rotary Tools & Instrument Kits.

Name	**Manufacturer**	**Reference number**
inLab MC X5 - miller for PMMA plastics: Bur PMMA (2.5, 1.0, 0.5)	Dentsply Sirona, Germany	64 78 098 64 78 106 64 78 114
Implant Drill Kit - Nobel Replace CC Guided Pureset	Nobel Biocare, USA	301164
Implant Prosthetic Kit - Prosthetic PureSet Basic	Nobel Biocare, USA	301233

2.2 Background studies: Methodology

2.2.1 Specimen Preparation: Master Model

A real patient demonstration case involving a maxillary edentulous arch restored with digital dentures (AvaDent Digital Dental Solutions, Global Dental Science, AZ, USA) was provided by the Prosthodontics Division of the Restorative Sciences & Biomaterials Department of Boston University Henry M. Goldman School of Dental Medicine. Only the maxillary arch was used for this study. The pre-existing STL file of the maxillary model for this case was previously modified by filling in the palate and buccal vestibule and increasing the base height in order to create a stronger model designed to fit the milling criteria of a CAD/CAM disk with a diameter of 98.5 mm and a height of 20 mm. The pre-existing STL file of the maxillary digital denture was converted to a full contour digital wax up where all flanges and palatal coverage were removed and was then merged to the modified edentulous maxillary model STL using a third-party CAD software (Meshmixer 3.5.474, Autodesk, Inc.). Two STL files were produced, the modified edentulous maxillary model and a full contour wax up model (Figure 5).

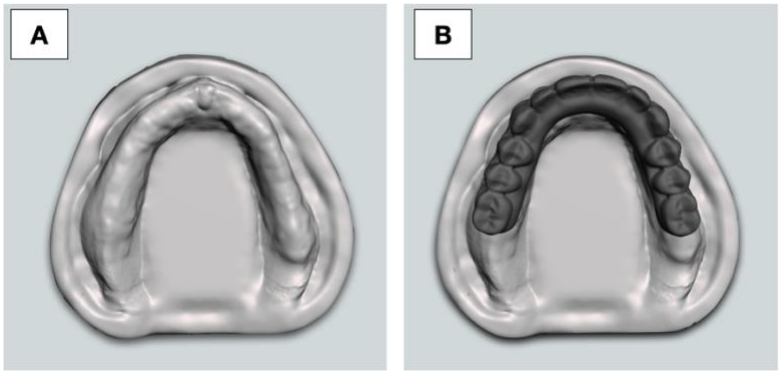

Figure 5. Digital models obtained of a clinical case of an edentulous patient and denture modified for the purposes of this study.
A: Modified STL of edentulous maxilla (occlusal view); B: STL of full-contour digital wax up (occlusal view)

The modified STL file of the edentulous model was then imported into a CAM software (inLab CAM SW 20.0.1, Dentsply Sirona, Germany) and milled using a multilayer polymethyl methacrylate (PMMA) CAD/CAM disk (Multilayer PMMA Disc, Dentsply Sirona, Germany) to serve as a radiographic model and as the implant placement model. Once milled, the maxillary model was separated from the disk and the sprue areas were smoothed (Figure 6).

Figure 6. Milled Maxillary Edentulous Model.
A: Edentulous model milling template; B: Milling Machine (Sirona MCX5); C: Milled Model in Multilayer PMMA

The milled model was scanned with a Cone Beam Computed Tomography (CBCT) scanner (iCAT Next Generation Dental Imaging System, Imaging Sciences International, USA) for implant planning purposes and the DICOM file obtained was imported into a digital implant planning software (DTX Studio™ Implant, Nobel Biocare, USA). The STL file of the milled maxillary edentulous model was used as the dental scan and was merged to the CBCT through the software's SmartFusion™ feature. The STL file with the full-contour wax-up was then merged to the dental scan and used to plan the implant positions (Figure 7). Six tapered bone-level titanium implants (NobelReplace® Conical Connection, Nobel Biocare, USA) were planned at the sites of #3, #5, #7, #10, #12 and #14 simulating an "all-on-six" treatment. 4.3 x 10 mm implants were planned for #5, #7, # 10 and #12 and 5.0 x 13 mm implants were planned for #3 and #14. Implants were planned as parallel as possible (Figure 8). For the purposes of this study, angled implants were

avoided to simplify the measurements. A 3D-printed surgical template (NobelGuide®, Nobel Biocare, USA) was then fabricated based on the implant plan.

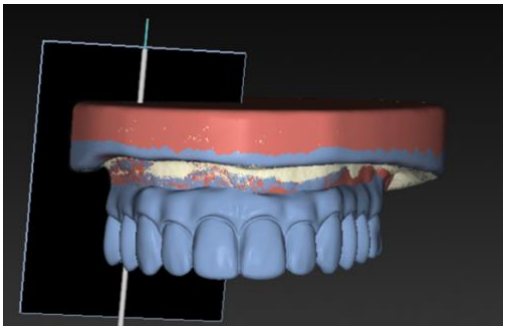

Figure 7. SmartFusion™ of edentulous model and wax-up model to CBCT.

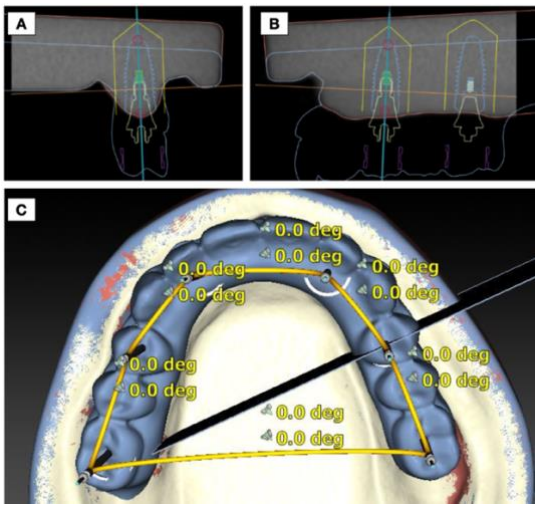

Figure 8. Different views of planned implants.

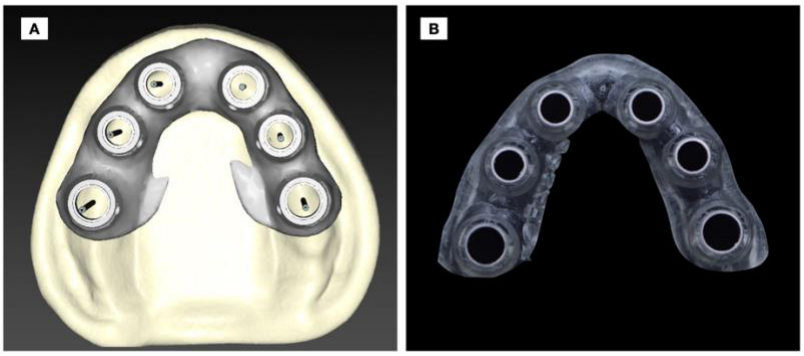

Figure 9. A: surgical guide design; B: 3D printed surgical guide

The surgical guide's fit was verified on the milled model (Figure 9). Drilling sequence for Nobel Replace Conical connection according to the manufacturer's instructions was followed for fully guided procedure using an implant motor (OsseoSet 300, Nobel Biocare, USA) and the appropriate implant drills (Nobel Replace CC Guided Pureset, Nobel Biocare, USA) (Figure 10).(55)

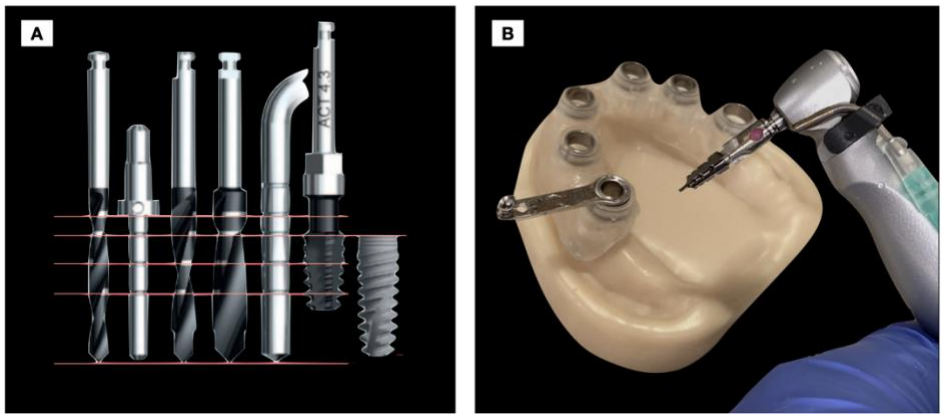

Figure 10. Placement of implants into restorative model.
A: drilling protocol; B: guided implant placement in restorative model.

Once the implants were placed in the prepared sites as planned, the multi-unit abutments (NobelReplace Multi-Unit abutments, Nobel Biocare, USA) were torqued in at 35 Ncm according to the manufacturer's recommendations (Figure 11a).

Since the surface character of the acrylic resin model prevents proper digitization, a dental Type IV stone replica (Silky Rock, WhipMix) was fabricated to act as the master model. Prior to duplication, autopolymerizing acrylic resin (Super T Crown & Bridge Resin, Henry Schein, USA) was added with a bead brush technique to increase the thickness of the material around the implant platforms where some threads were exposed. The PMMA model was also modified by creating internal notches with an acrylic bur and external markers with wax on the edges of the model as well as on the palatal area to allow an easier merge of future STL files for the study. To duplicate this model into dental stone, multi-unit impression copings (NobelReplace® Impression Copings

for Multiunit Abutments, Nobel Biocare, USA) were connected to the multi-unit abutments and were splinted with dental floss and low-shrinkage pattern resin (Pattern Resin LS; GC). After complete polymerization, the PMMA resin was cut with a diamond disc and was reconnected with PMMA resin to minimize distortion due to shrinkage.(56)(57) This splint was used to transfer the implant positions from the PMMA model to the stone model (Figure 11b).

Wax sticks (Boxing Wax Sticks, Kerr Dental, USA) were placed over the impression copings screws to create extension channels to be able to access the screw through the duplication mold (Figure 11c). Addition-vulcanizing duplication silicone (Z-Dupe, Henry Schein, USA) was then poured around the PMMA model, and the impression copings splinted by GC Pattern were presented in a way that the wax extensions would be visible. Once the silicone material was fully set, the wax extensions were removed allowing for the screw channels to be accessed (Figure 11d). A hex screwdriver was used to unscrew the now embedded GC-Pattern Splint from the PMMA model (Figure 11e). Six multi-unit abutment replicas (NobelReplace® Multi-unit Abutment Plus Replica, Nobel Biocare, USA) were then fixed to the multi-unit impression copings within the mold. The multi-unit abutment replica was chosen for the stone model because it is a one-piece component, combining the implant and the abutment, instead of having the implant and the multi-unit as two separate pieces. Dental stone was then poured with a scannable low expansion Type IV stone (Silky Rock, WhipMix) and was allowed to set for 24 hours.(58) The hex screwdriver was used to unfasten the stone model from the mold. The stone model which contained 6 multi-unit abutment analogs served as the master model for the entire study (Figure 11f).

Taking into consideration the probable dimensional changes stone can have over time, the relative humidity and the temperature of the storage area were recorded every day (40±10%, 22±2°C) and the entire study was conducted within the same week. (26)

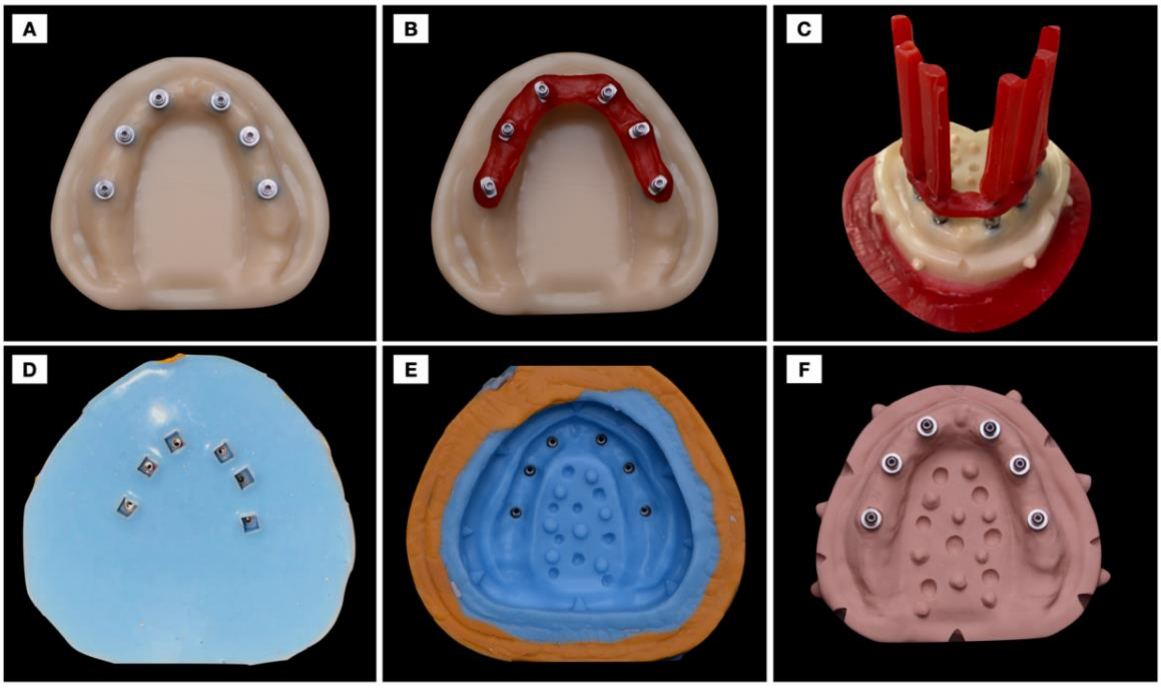

Figure 11. Fabrication of a duplicate implant model made of Type IV Stone.
A: PMMA model with implants and multi-unit abutments torqued in; B: Multi-unit impression copings placed over the multi-unit abutments and splinted with dental floss and low-shrinkage pattern resin; C: Wax stick extensions placed upright over screw access channels; D: Wax stick extensions were removed after polymerization of silicone to access impression copings screw holes; E: Intaglio view of duplication mold with indexed implant positions; F: Duplicate stone model with multi-unit implant analogs separated from the mold.

2.2.2 Laboratory Scanner: selecting the Reference STL for control

To measure the trueness of a system, a “reference” or “control” STL file needs to be acquired. Previous studies have shown different methods of obtaining that virtual 3D file that included a high precision laboratory scanner, an industrial optical scanner, or a coordinate measuring machine.(46)(47)(48)(51) Laboratory scanners, also known as extraoral scanners, are recognized for their higher accuracy registration. These scanners work by using lasers or structured light and contrary to intraoral scanners, do not have a limited field of view or inhibiting factors such as reflections from scanned surfaces or lens wetting. In this case, a laboratory scanner was

used to obtain reference data. Two laboratory scanners were tested in a pilot study in order to use the best one.

The two laboratory scanners in the pilot test were 3Shape D1000 (Trios, 3Shape) and inEOS X5 (Denstply Sirona) scanners. According to the manufacturers, the accuracy of a 3Shape D1000 scanner is 5-8 μm (59) and inEOS X5 scanner is 2.1 μm (60). The accuracy of those systems was then verified by the following pilot study.

Scan bodies (ELOS Accurate, IO-2C-A, Denmark) were fastened to the multi-unit abutment replicas of the master stone model. Two subgroups were created, the "Same Position" and "Remounted" subgroups. The "Same Position" subgroup tested repeatability, where the scan body position remained unchanged between each scan, and the "Remounted" subgroup tested reproducibility, where the scan bodies were changed in different random positions after each scan (Figure 12). The scanners were calibrated prior to every group scan. Scan bodies were fastened on the implant abutment replicas on the master cast by hand tightening each time and five scans of the master model were taken for each group (Figure 13 and Figure 14).

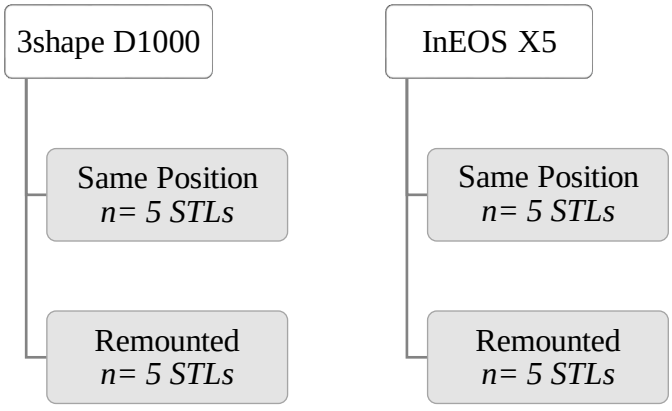

Figure 12. Pilot study design to compare different laboratory scanners

Figure 13. Scan workflow using 3ShapeD1000 (3Shape Trios) Laboratory Scanner
A: 3ShapeD1000 Machine; B: Model with Scan bodies being scanned; C: Acquisition of STL file on 3Shape software.

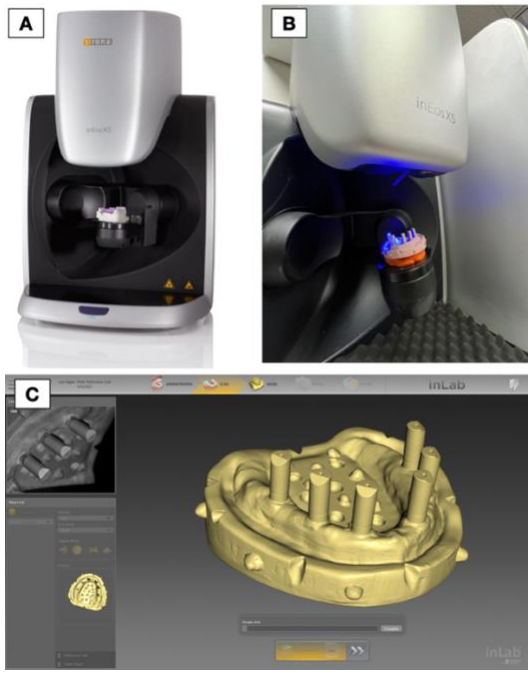

Figure 14. Scan workflow using inEOS X5 (Dentsply Sirona) Laboratory Scanner
A: InEOS X5 Machine; B: Model with Scan bodies being scanned; C: Acquisition of STL file on InLab CAD/CAM software.

Once all the STL files were acquired, an inspection software (Geomagic; 3D systems) was used to create a template for each group and subgroup, resulting in a total of four different templates that correspond to the following: 1. 3ShapeD1000 Same SB position; 2. 3ShapeD1000 Remounted SB position; 3. InEOS X5 Same SB position; 4. InEOS X5 Remounted SB position. The template STL file, labeled scan ID number 1, was chosen at random for each group in this case to act as the "reference". Each template STL file was refined in a way to get segmented regions to obtain results, which are optimized on the desired surfaces of comparison (Figure 15). The scan bodies were isolated from the whole scan.

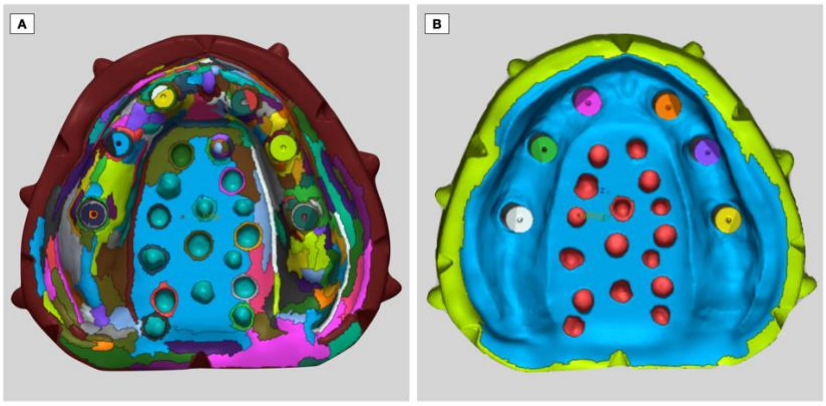

Figure 15. Template fabrication on the reverse engineering software (Geomagic; 3D systems). A: Template before segmentation of regions; B: Template after segmentation of regions.

Since the scan body's overall shape is conical, it was segmented in a way to have two separate regions - a conical body and a flat angled surface on each scan body (Figure 16).

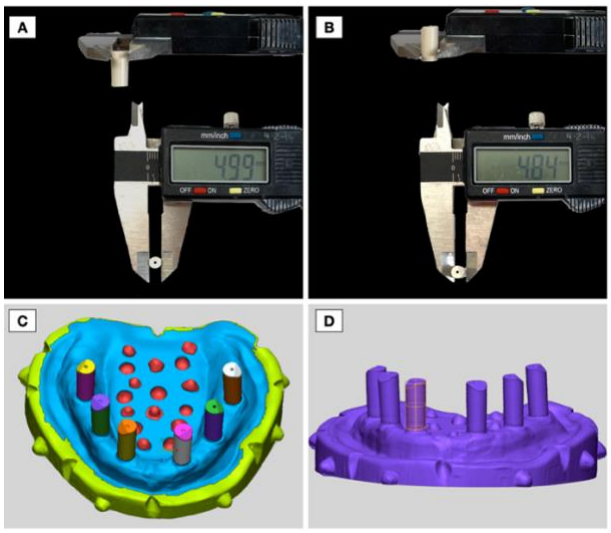

Figure 16. Scan body geometry

A and B: Physical measurement of the diameter at two ends of the scan body to a confirm conical geometry using a digital caliper; C: Resegmentation on Geomagic software to separate the conical body from the flat angled scan body head; D: Conical geometry detected on the inspection software.

The next step included adding each STL for comparison. The principle was to overlap the template STL file with the tested one so that they are locked in space. An initial alignment is needed to calculate how the two STL models fit together primarily and then a “best fit alignment” is done (Figure 17). The process utilized for this software relies on overlapping regions through an iterative closest point algorithm (ICP) which detects the transformation between a point cloud and other point clouds through minimizing the square errors between the correlated points.(61)

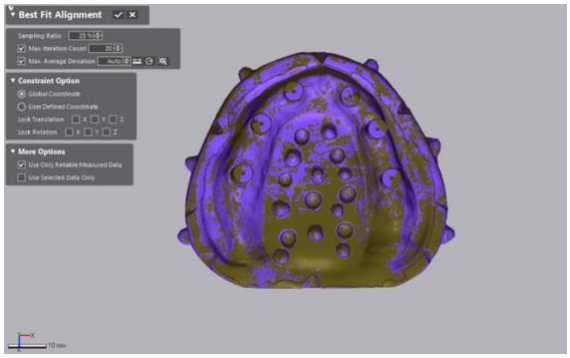

Figure 17. Best fit alignment

2.2.2.1 Geomagic testing

Three different tests were run at this point:

2.2.2.1.1 3D comparison

The "3D compare" feature was used to calculate the 3D deviations of the scan body regions. Only the conical geometry of the scan bodies was selected and a surface tolerance of 50 µm was chosen for the minimum and maximum range.(62)(63) This test was done at two specific tolerance values which were 5 µm and 20 µm. This method allows to understand the percentage of points that have a gap distance within the defined tolerance (the in-tolerance percentage) and outside the defined tolerance (the out-tolerance percentage). A colorimetric map was then generated for the immediate visualization of the results. The root means square (RMS) values, which is a measure of the magnitude of all deviation values, were obtained (Figure 18).

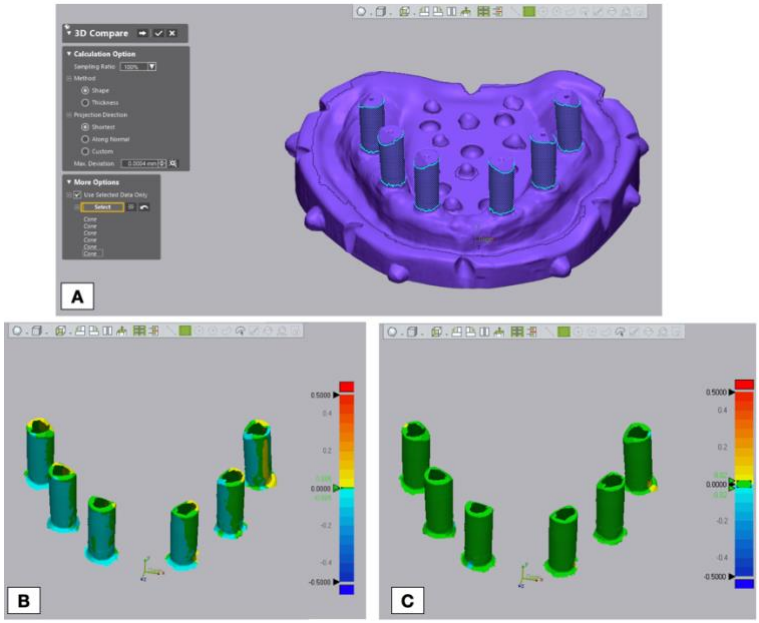

Figure 18. 3D comparison test
A: Selection of the scan body's conical geometry for 3D comparison; B: Comparison at 5 µm tolerance; C: Comparison at 20 µm tolerance.

2.2.2.1.2 Angular deviation

The “geometrical deviation” feature was used to measure the angular deviation that detects any clear geometrical shape, which was identified to be conical for the scan bodies in this study (Figure 19). The delta angle measurement obtained represents the angular deviation of each scan body from the test STL file to the reference STL file. A mean measurement of all six delta angle was done and was referred to as the global angular deviation.

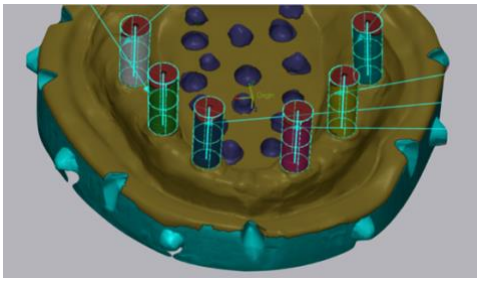

Figure 19. Angular deviation of conical geometry from the scan body

2.2.2.1.3 Linear deviations from cross-arch distances

The “point comparison” feature was used to obtain cross-arch distances (Figure 20) and to measure the linear deviations.

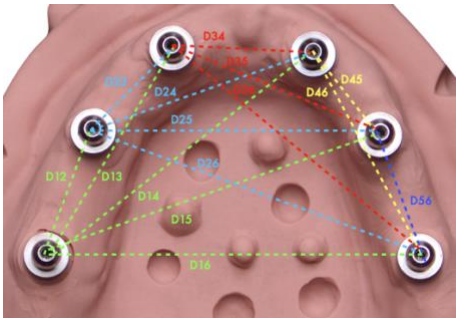

Figure 20. Representation of cross-arch distances used to measure linear deviations

Three comparison points were placed at random around each scan body (Figure 21). The reference coordinates and the test file coordinates were then exported onto an excel sheet where the distances and deviations were measured and calculated.

The Euclidean formula used to calculate the absolute linear distances between paired points (x_a, y_a, z_a) and (x_b, y_b, z_b) was the following:

$$D = \sqrt{(x_a - x_b)^2 + (y_a - y_b)^2 + (z_a - z_b)^2}$$

Equation 1. Euclidean formula to calculate absolute linear distances

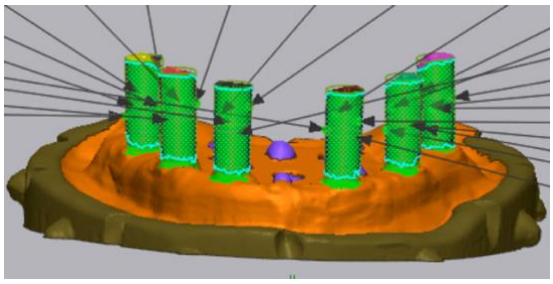

Figure 21. Point comparison for linear deviations

The formula used to calculate the absolute distance deviations from the experimental STL file to the reference STL file was the following:

$$Absolute\ deviation = |Distance_{Reference} - Distance_{Measured}|$$

Equation 2. Formula to calculate absolute distance deviations

2.2.2.2 Results of the background study

Table 4. RMS from 3D Compare test on the Scan body surface

	RMS, mm		
Source	**N**	**Mean**	**Std Dev**
3Shape D1000 - Same SB Position	4	0.0143	0.0138
3Shape D1000 – Remounted SB Position	4	0.0307	0.0304
inEos X5 - Same SB Position	4	0.0062	0.0012
inEos X5 - Remounted SB Position	4	0.0246	0.0033

Table 5. Angular deviation from conical geometry deviation test from the scan body surface

	Delta Angle, Degree		
Source	**N**	**Mean**	**Std Dev**
3Shape D1000 - Same SB Position	24	0.129	0.043
3Shape D1000 – Remounted SB Position	24	0.173	0.093
inEos X5 - Same SB Position	24	0.020	0.014
inEos X5 - Remounted SB Position	24	0.161	0.090

Table 6. Cross-arch distance deviations from Point comparison test from the Scan body surface

	Cross-arch distance deviations, mm		
Source	**N**	**Mean**	**Std Dev**
3Shape D1000 - Same SB Position	45	0.0055	0.0054
3Shape D1000 – Remounted SB Position	45	0.0213	0.0154
inEos X5 - Same SB Position	45	0.0036	0.0032
inEos X5 - Remounted SB Position	45	0.0161	0.0145

The results obtained in Table 4, 5 and 6 revealed the following:

- When comparing scan body positions only, the 3Shape D1000 and inEOS X5 same scan body position groups both showed improved accuracy over the remounted scan body position groups
- When comparing the 3Shape D1000 scanner to the inEosX5 scanner, inEOS X5 showed to have better results regardless of the scan body position in terms of RMS, cross-arch distances and angular deviations.

For the following steps of the baseline studies, the inEOS X5 scanner will be used and the 3Shape D1000 will be dismissed due to its lower accuracy.

2.2.3 Baseline studies for standardization of testing methodology for all comparison groups:

2.2.3.1 STL file standardization

Since this study aims to compare three different impression techniques, it is important to find a uniform geometry for comparison purposes. Considering that the scan bodies' geometries vary between techniques, it was decided to convert the scan body STL files into virtual abutment analog STL files. The objective of the following baseline studies was to validate the use of abutment analog STL files and verify if a correlation exists with the results found with the scan body STL files. Different inspection software were tested and used for the calculation of those results.

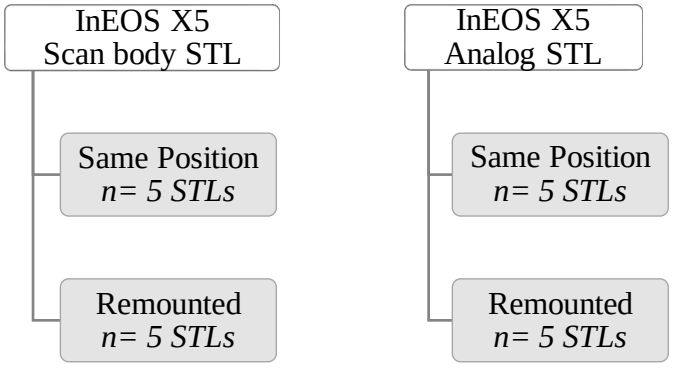

Figure 22. Pilot study design to compare different STL file data

The pilot study focused on evaluating the inEOS X5 in the two following groups from the abutment analog surface: inEOS X5 Same SB position and inEOS X5 Remounted SB position (Figure 22). The scan body STL files for each group were imported to a dental CAD software (Exocad DentalCAD; Darmstadt, Germany); and scan bodies from the digital library were used to merge to the scan bodies from the scanned STL file (Figure 23a). The merge was verified through a colorimetric map provided in the software (Figure 23b and 23c) and then the virtual scan body

was converted to implant abutment replicas (a multi-unit implant analog) through the virtual library from ELOS Accurate which corresponded to the physical analog on the master cast (Figure 24).

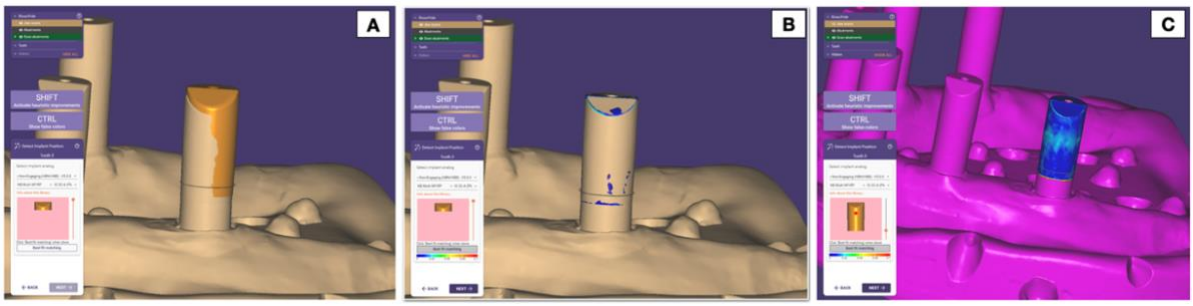

Figure 23. Scan body merged from virtual library with scanned STL using a CAD software (Exocad).
A: Initial "best fit matching" between the virtual and scanned scan body done using only the upper third data of the scan body for vertical position recognition; B: Verification of initial merge using colorimetric map; C: Second "best fit matching" done using the entire scan body surface for best fit.

The palate with the markers was preserved for merging purposes (Figure 24c). To facilitate measurement, all scan images, except implant abutment analogs and the cropped palate, were hidden in the digital model and saved as an STL file. These procedures were repeated 5 times to fabricate 5 digital models.

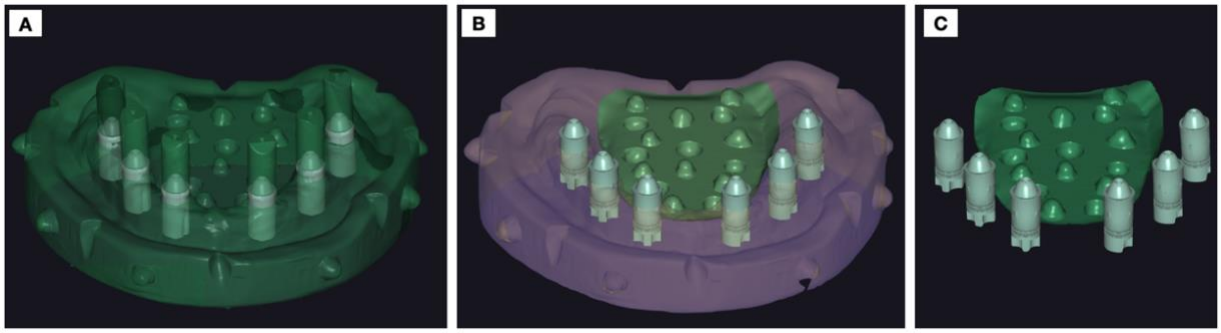

Figure 24. Fabrication of the Analog STL file with palatal surface markers preserved for merging purposes.
A: Full view of the STL file with scan body and virtual analogs; B: View with hidden scan bodies and cropped palatal surface with markers; C: Final STL obtained containing only the analog positions and the palatal area.

2.2.3.2 Inspection software testing:

2.2.3.2.1 Geomagic Control X

The new updated STL files were imported to the inspection software (Geomagic Control X; 3D systems). The same STL files in the scan body versions (scan ID number 1), that were used as templates in the previous baseline study, served as the templates in their analog versions for this section of the study. In this scenario, two templates were created for the following Analog groups: 1. InEOS X5 Same SB position_Analog; 2. InEOS X5 Remounted SB position_Analog. Each reference STL file was imported as a "CAD STL" instead of a "Scan STL" and was segmented into regions to obtain results which was specific to the desired surfaces of comparison (Figure 25).

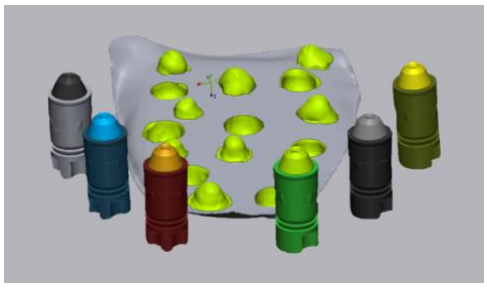

Figure 25. Implant abutment analog reference CAD STL file shown in Geomagic Control X

The two STL files were superimposed by using "initial alignment" and then the "best fit alignment" (Figure 26). Similar tests were done in terms of 3D comparison, linear deviations from cross-arch distances and angular deviations. Inconsistent results were found using CAD STLs on this software compared to the scanned STLs previously used in terms of 3D deviations and cross-arch distances deviations. It was therefore decided to conduct those tests on other inspection software and study if there was a correlation with the results found from the scanned data's scan body surfaces on Geomagic (Geomagic Control X 2020.1; 3D Systems).

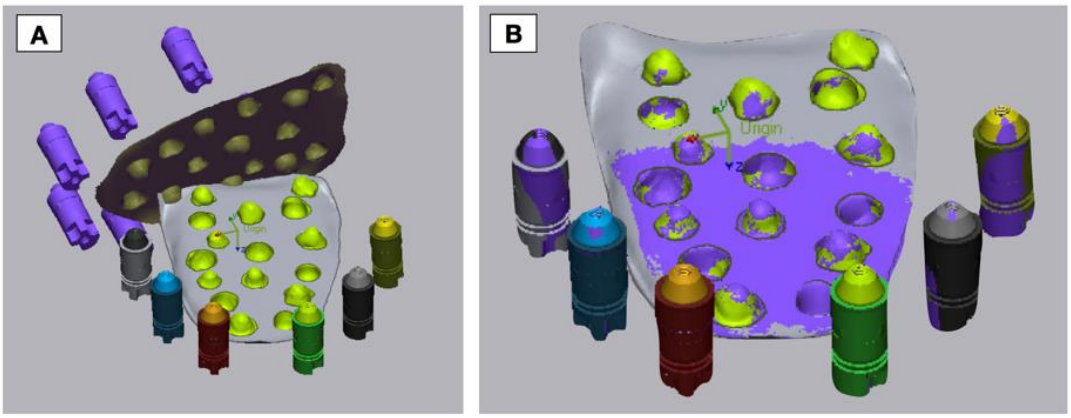

Figure 26. Surperimposition of 2 STL files using Geomagic Control X.
A: Before alignment; B: After best fit alignment

The angular deviation test was evaluated using the "geometry deviation" feature from the inspection software on the virtual analogs. The test was done on two different surfaces with different geometries to compare and see if the results obtained were correlated regardless of the surface chosen. The first surface being the screw access hole which was recognized by the software as a cylinder, and the second surface being the conical surface of the analog which was recognized by the software as a cone (Figure 27). The results obtained are shown in Table 7.

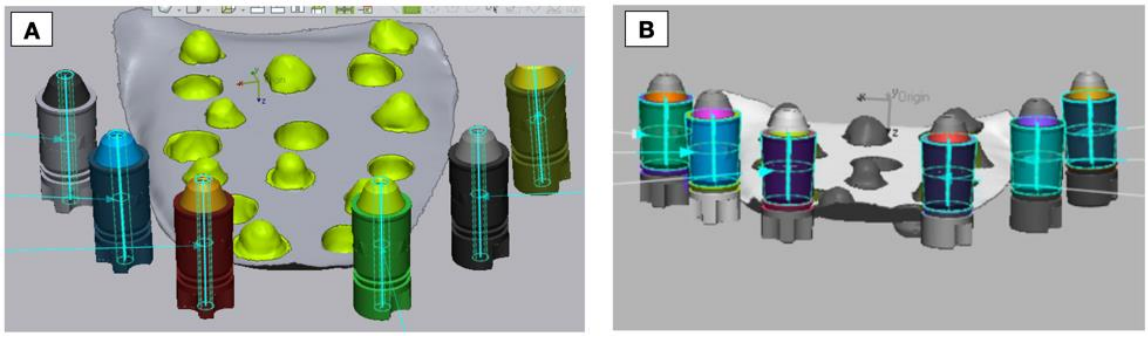

Figure 27. Angular deviation on the analog surface
A: Analog screw access hole cylinder geometry; B: Analog surface cone geometry

Table 7. Angular deviation results from Geometry deviation test from the Analog surface

	Delta Angle, Degree		
Source	**N**	**Mean**	**Std Dev**
inEos X5 - Same SB Position_ScrewHole_Cylinder	24	0.022	0.015
inEos X5 - Remounted SB Position_ScrewHole_Cylinder	24	0.055	0.041
inEos X5 - Same SB Position_AnalogSurface_Cone	24	0.027	0.015
inEos X5 - Remounted SB Position_ AnalogSurface_Cone	24	0.065	0.033

This baseline study revealed that the angular deviation test obtained similar results whether it was assessed from the scanned data of the scan body STL files or from the CAD data of the virtual analog STL files and regardless of the scan body positions. This study also helped in determining the final protocol for measuring the angular deviation's data uniformly between all the groups from an Analog STL standpoint.

2.2.3.2.2 IScan3D Dental

The IScan3D Dental (Version 9.1.104, Imetric, Switzerland) CAD and inspection software was provided with the photogrammetry unit. It allows for the photogrammetry data to get captured and for the coordinates of each implant center to get extracted in an X,Y,Z coordinate format called the "Origin" point. It also provides a spatial fit analysis through a 3D spatial similarity transformation platform incorporated which is based on the Helmert transformation concept. Helmert transformation is a geometric transformation method within a 3D space which transforms a set of points that are similar into one another by rotation, scaling, and translation (64). In this software, the spatial similarity transformation is computed using the origin points of 2 different sets of coordinates and allows the obtention of RMS values. This is referred to in this study as the "Origin" data, representing the center of the implant abutment interface (Figure 28).

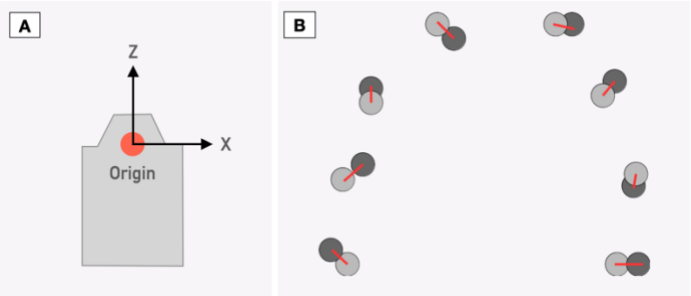

Figure 28. Spatial similarity transformation
A: Representation of the origin of the abutment interface; B: Representation of spatial similarity transformation between 2 different sets of origins (2 STLs being compared)

Another feature included in the spatial fit analysis allows the comparison of 2 different sets of coordinates using the origin point as X and Y. In this case, the Z coordinate is referred to as the "Axis point" projected at 10 mm from the Origin in the same direction as the implant. This is referred to in this study as the "Origin+Z" data.

A 3D comparison between the STLs using the "Origin" and "Origin+Z" RMS data was performed to evaluate if any correlation existed with the RMS obtained from the 3D compare using the scan body scanned STL files on the other inspection software (Geomagic Control X 2020.1; 3D Systems). The step-by-step process included importing each STL with the scan bodies from the following groups: 1. InEOS X5 Same SB position; 2. InEOS X5 Remounted SB position.

Once everything was aligned in the same coordinate system, the reference STL of each group, which was labeled as scan ID number 1, was chosen in a similar way as the previous baseline study for consistent results. All coordinates were imported into the spatial similarity transformation platform and transformations were computed (Figure 29). The "Origin" and "Origin+Z" RMS data were obtained (Table 8). If there is no significant difference between the "Origin" and "Origin+Z" RMS values, then there is no significant angular deviation.

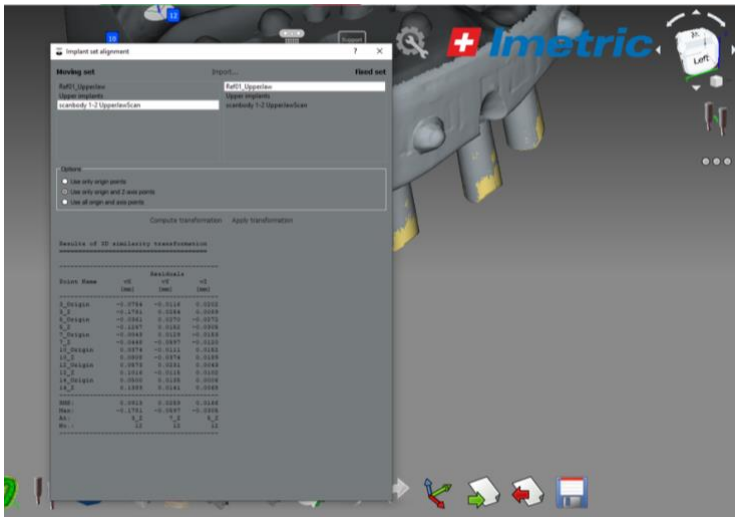

Figure 29. Spatial similarity transformation platform

Table 8. RMS results from 3D Compare test using spatial similarity transformation on IScan3D Dental

	RMS, mm				
	METHOD				
		Imetric Origin		Imetric Origin + Z	
SOURCE	**N**	**Mean**	**Std Dev**	**Mean**	**Std Dev**
inEos X5 - Same SB Position	4	0.0017	0.0003	0.0017	0.0003
inEos X5 - Remounted SB Position	4	0.0186	0.0047	0.0190	0.0047

In terms of cross-arch deviations, all coordinates were exported onto an excel sheet where the distances and deviations were measured and calculated. In contrast to the previous test on Geomagic (Geomagic Control X 2020.1; 3D Systems) where 3 points were used per implant, in this case only one point was used. This was the “Origin” point on the abutment interface (Figure 30). The mean cross-arch distances values were then obtained (Table 9).

Figure 30. Origin points on abutment interfaces

Table 9. Cross-arch distances deviations using Origin coordinates extracted from IScan3D Dental

	Cross-arch distance deviations, mm		
SOURCE	**N**	**Mean**	**Std Dev**
inEos X5 - Same SB Position	60	0.0028	0.0022
inEos X5 - Remounted SB Position	60	0.0293	0.0209

2.2.3.2.3 IScan4D Dental

The IScan4D (Version 9.1.104, Imetric, Switzerland) inspection software relies on overlapping regions through an iterative closest point algorithm (ICP). Analog STLs were added for comparison. The test scans were overlapped to the chosen reference STL labeled as scan ID number 1 in both groups. A “mesh alignment” was performed using the markers on the palate to compute the initial merge followed by a “fine mesh alignment” to get the best fit between the 2 STL files (Figure 31). The palatal area was sectioned out after merge and a visual inspection of the virtual analogs was done at a tolerance value of 50 μm. The RMS values were then obtained (Table 10).

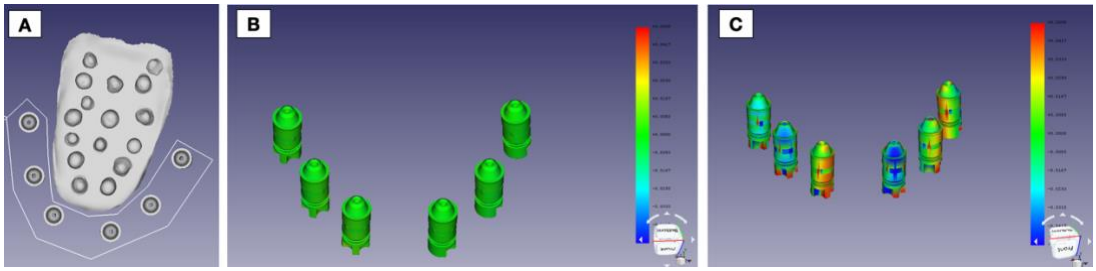

Figure 31. Iscan4D inspection software

A: The palatal area cropped out after merge; B: Colorimetric map of same scan body position group; C: Colorimetric map of remounted scan body position group.

Table 10. RMS results from 3D Compare test from the virtual analog surface with IScan4D Dental

	RMS, mm		
SOURCE	**N**	**Mean**	**Std Dev**
inEos X5 - Same SB Position	4	0.0036	0.0011
inEos X5 - Remounted SB Position	4	0.0229	0.0013

2.2.3.3 Correlation of results for RMS values:

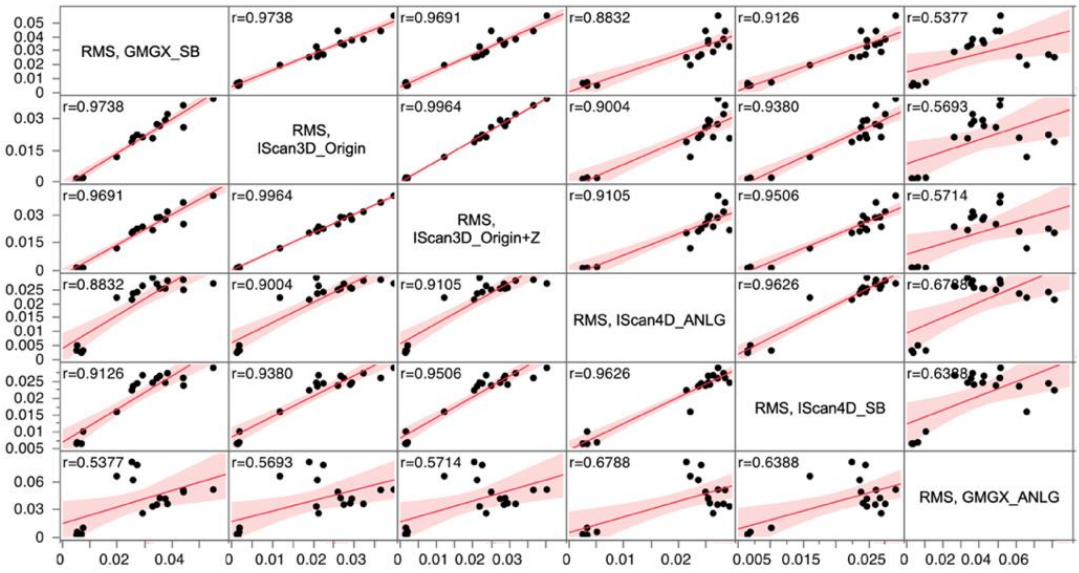

Figure 32. Scatterplot matrix for multivariate linear regression showing the correlation of RMS data amongst different inspection methods using STL data obtained by inEOS X5 scanner

Different methodologies can lead to different values of deviations observed in edentulous arches with implants for implant-supported prostheses. It is important for this reason to understand the source of the results and examine the correlation between the different software.

Looking at Figure 32, the RMS data from Geomagic analog surface showed poor correlation with all the other methods, including the Geomagic scan body data ($r = 0.5377$). The RMS data from Iscan4D analog surface showed a very good correlation with the RMS data from the Iscan4D scan body surface ($r = 0.9626$). The best correlation was found between the Geomagic scan body data and the IScan3D Origin ($r = 0.9738$) followed by Origin+Z data ($r = 0.9691$).

Remounting the scan body position between each scan was found to increase the deviations found by the 3D comparison test, the angular deviation test, and the cross-arch deviations test. Taking this into consideration, the final methodology involved a standardized protocol of remounting the scan body position between scans as this process would be unavoidable for the digitization of the casts in the conventional impression group (see Chapter 3). This would also allow testing the reproducibility of the different registration techniques as opposed to the repeatability.

Chapter 3: FINAL METHODOLOGY

3.1 Materials

Refer to chapter 2 section 2.1.

3.2 Study Design: Phase 1

3.2.1 Specimen preparation

Refer to chapter 2 section 2.2.1.

3.2.2 Digitization of the master cast: reference STL

The entire physical portion of the study was conducted on the stone master model within one week to take into consideration the possible but negligeable dimensional changes of Type IV dental stone over time. The cast was stored in similar conditions. Humidity and temperature were evaluated throughout the study (40±10%, 22±2°C).

Scan bodies (ELOS Accurate, IO-2C-A, Denmark) were hand-tightened over the multi-unit abutment replicas. The dental stone master model was then digitized using a previously calibrated extraoral scanner with a 2.1 μm accuracy (inEOS X5, Dentsply Sirona, Germany). A reference STL file was obtained and served as the control.

Three groups of digital models were compared to the acquired reference STL file: the intraoral scanning group (Group 1: IOS), the photogrammetry group (Group 2: PTG), and the conventional impression group (Group 3: CNV) (Figure 33).

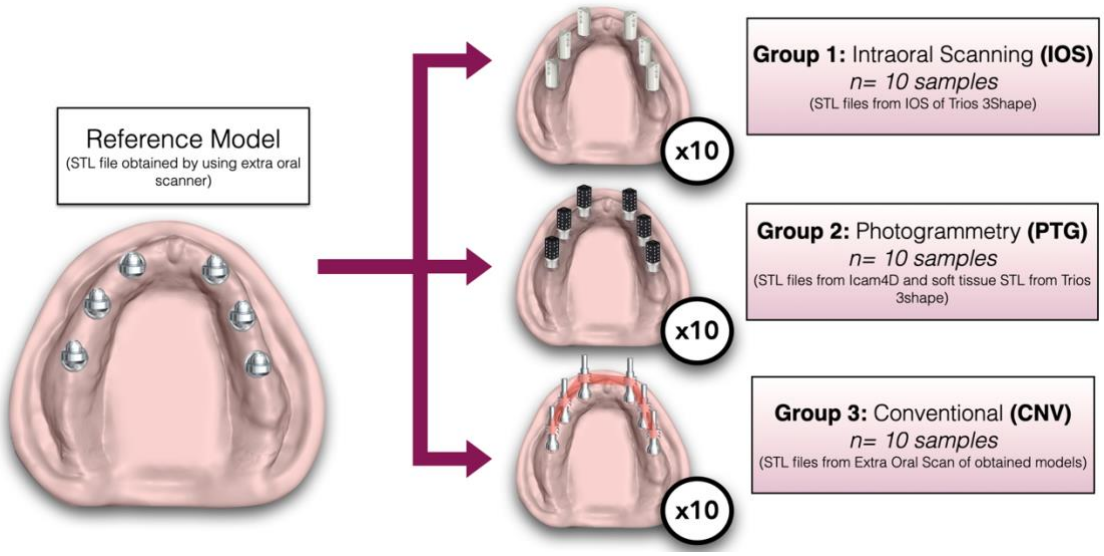

Figure 33. Phase 1 study design, grouped by test and impression technique

3.2.3 Group 1: Intraoral scan (IOS)

For the intraoral scanning group, an intraoral scanner (Trios 3, 3Shape) previously calibrated per the manufacturer's instructions was used. Abutment level scan bodies (ELOS Accurate, IO-2C-A, Denmark) were fastened to the multi-unit abutment replicas on the dental stone master model by hand tightening each time by the same operator. The model was placed in a box during the scan to get the same lighting conditions amongst all scans. The utilized scanning technique followed manufacturer recommendations to scan the arch form first with the scan bodies always present, and then altering around each scan body in curved paths before finally scanning the palate.(65) A standardized scan path was performed with one continuous stroke of the occlusal surface, followed by the buccal surface and finally the palatal surface. Ten scans were taken, and scan bodies were remounted between each scan (Figure 34).

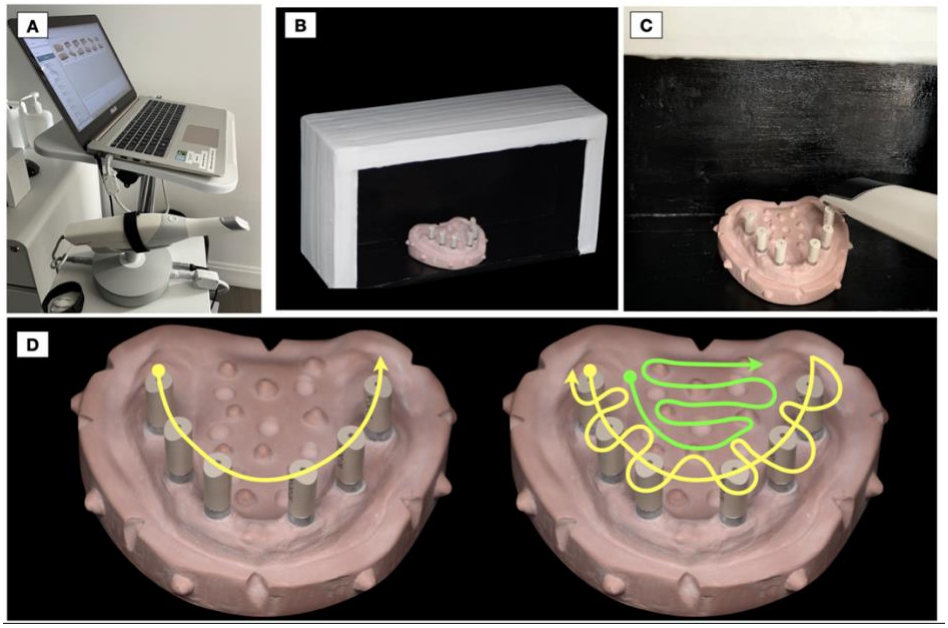

Figure 34. Intraoral scanning procedure (Trios3, 3shape)

A: Trios3 3Shape Intraoral Scanner used; B: Scan bodies hand tightened on the stone master model and model inserted in the black box to control lightning conditions; C: Scanning around the scan body with the intraoral scanner; D: Scan path which includes primarily (on the left side) to do one continuous stroke over the scan bodies and then (picture of the right) to go around each scan body (in yellow) before scanning the palate (in green).

Once all the data was exported as scan body STL files, they were imported into a CAD software (Exocad DentalCAD; Darmstadt, Germany) and were converted into virtual abutment analog STL files. The palate with the markers was preserved for merging purposes for all the STLs (Figure 35).

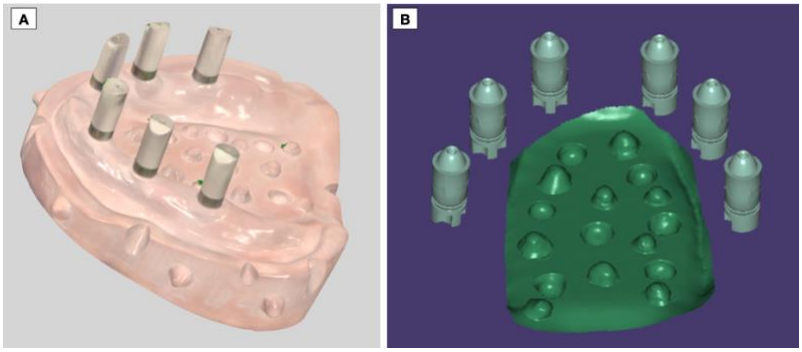

Figure 35. IOS STL files.

A: IOS Scan body STL file on the 3shape Software; B: IOS converted scan body to abutment analog virtual library with palatal markers STL files

3.2.4 Group 2: Photogrammetry (PTG)

For the photogrammetry group, a photogrammetry system with 4 cameras (Icam4D, Imetric) was used to record the implant positions (Figure 36). Abutment-level photogrammetry scan bodies (ICamBodies MU-RP 1.4 mm, Imetric, Switzerland) were fastened to the multi-unit abutment analogs on the stone master model using the specific screwdriver provided for ICamBody MU-RP. The ICamBodies were placed so that the edge of the square shaped ICamBody points to the front, to be able to capture two surfaces of the scan body during the measurements (Figure 37).

Figure 36. Photogrammetry system with 4 cameras (ICam4D, Imetric, Switzerland)

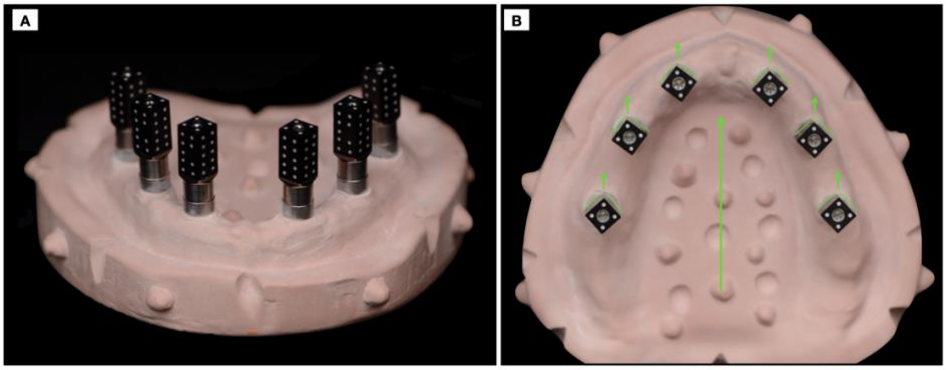

Figure 37. Photogrammetry scan body placement (ICamBody, Imetric, Switzerland) A:Frontal view of ICamBodies placed over the multi-unit implant abutment analogs; B:Occlusal view of ICamBodies positioned to follow the big arrow to capture two faces of the scan body during the measurements.

The model was once again placed in a box during the scanning process to get the same lighting conditions amongst all scans. The ICam4D was consistently calibrated with a calibration plate immediately before the measurement procedure: as soon as a measurement begins, the software directs the operator into the calibration mode. The ICam4D is first placed further away from the calibration plate and is slowly maneuvered towards it. The red rectangle appearing on the software indicates 5 zones where enough data of the calibration plate must be captured. Once all those zones turned green, the software was automatically placed into the "ICamBody measurement mode" (Figure 38).

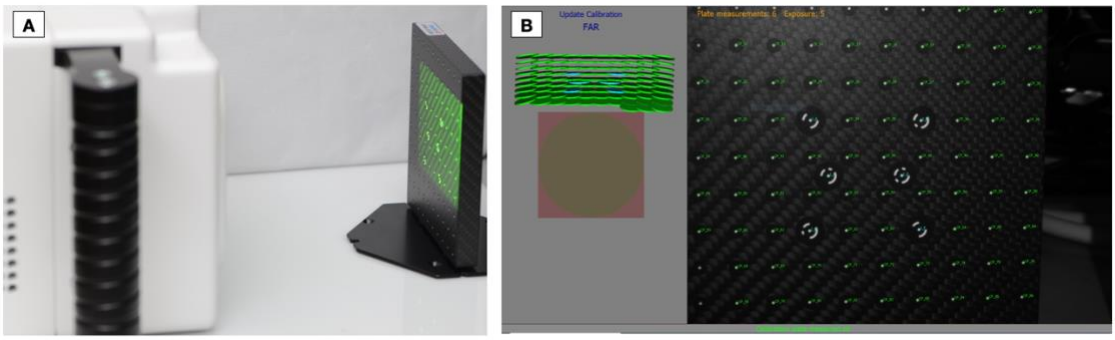

Figure 38. Photogrammetry system calibration prior to scan body measurement (ICam4D, Imetric, Switzerland)
A: ICam4D camera placed in front of the calibration plate; B: Screen during calibration with the 6 coded targets.

The distance maintained between the ICam4D and the master stone model was such that the complete model was shown on the screen and that the left side of the screen indicated a green area, representing the optimum distance for the ICamBody measurements. The scanning protocol instructed by the manufacturer's was to start at one side of the model and to slowly move to the other side to improve the "triangulation angle". The ICamBodies on the screen first appeared in red, meaning only one side was measured. They are then turned yellow once two sides of them have been measured but the software does not consider the measurement precise enough. Once the

ICamBodies turned green, the software considered the measurement precise enough. The number of views or captures indicated at the top of the screen reached at least about 30 views for optimal accuracy for each measurement taken (Figure 39).

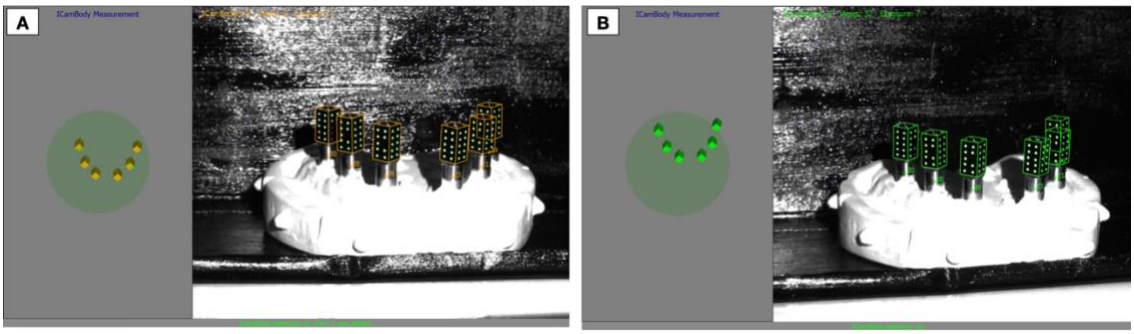

Figure 39. Screen during measurement of ICamBodies
A: Screen showing on the left green circle indicating optimum distance and on the right the view from the camera during measurement. ICamBodies are yellow at this stage of capture; B: ICamBodies are green at this stage of capture with 32 views.

Once the capture is completed, the ICamBodies geometry was converted into the virtual multi-unit implant abutment analogs (Figure 40). The output STL contains the palate with the markers and the virtual analogs. The process was repeated 10 times while remounting the ICamBodies in different positions between each scan.

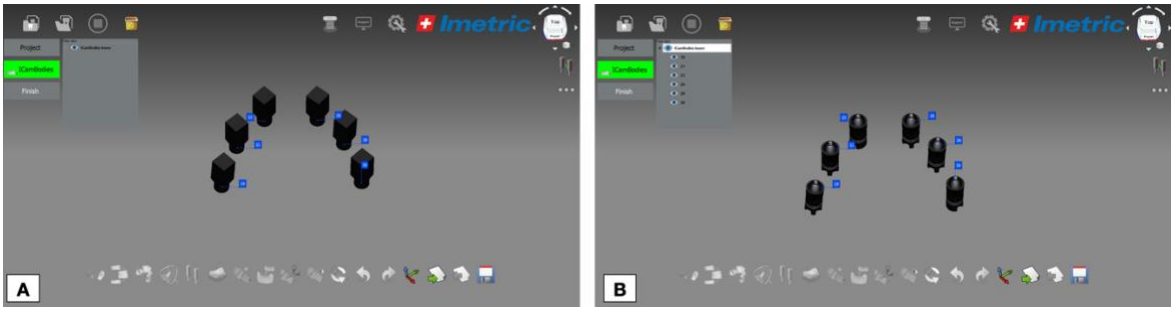

Figure 40. Virtual conversion of ICamBodies into Multi unit implant abutment analogs
A:ICamBodies measurement obtained from capture ; B: ICamBodies converted into Multi unit implant abutment analogs using the “change geometry” feature in the software.

3.2.5 Group 3: Conventional impressions (CNV)

3.2.5.1 Splint fabrication

A splinted open impression tray technique was chosen for the conventional group in this study. First, a template splint was fabricated in the following manner. Multi-unit open tray impression copings were fastened on the multi-unit abutment analogs and splinting was done using dental floss and auto polymerizing acrylic resin (Pattern Resin LS; GC Intl). This template was fabricated to have an overall height of 3 to 3.5 mm for a stronger splint and left to set for 17 minutes to achieve complete polymerization (Figure 41).(56)(66)(67)

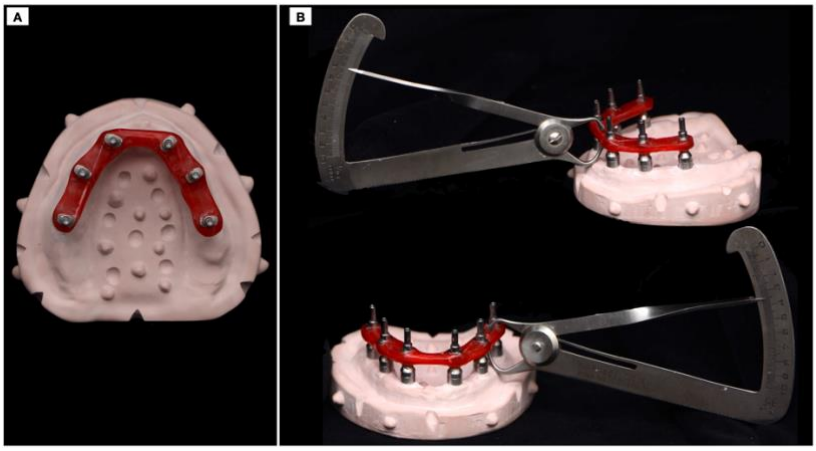

Figure 41. Splinted impression copings template fabrication.
A: Splinted Impression Copings with Floss and Pattern Resin; B: 3-3.5mm overall height of splint

To standardize the splints for each 10 samples in the group, a jig was fabricated using additional PVS (Figure 42) to replicate the template splint.

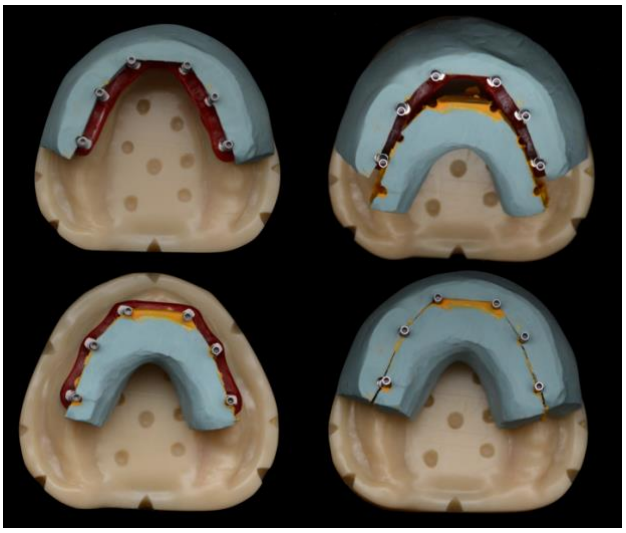

Figure 42. Jig fabrication for Splinted impression copings template

Once the putty index was set, 6 impression copings for each sample were screwed to the multi-unit abutments on the PMMA model (Figure 43).

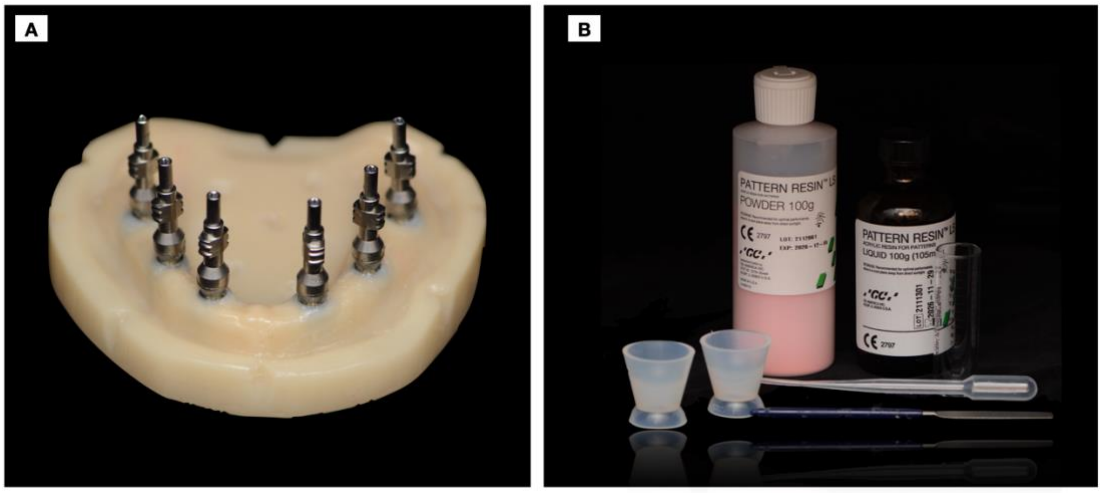

Figure 43. Splint for impression copings duplication process
A: 6 open tray multi-unit impression copings placed over the multi-units; B: Auto polymerizing material used the splint fabrication.

The manufacturers of GC Pattern Resin do not provide recommended powder-to-liquid ratios but only describe a bead brush technique. According to previous literature (68) which conducted a study on the comparison of polymerization shrinkage of pattern resins, the recommendation to obtain a clinically manageable consistency with this specific auto

polymerizing acrylic resin (Pattern Resin, GC) was to use a ratio of 0.5g to 0.3 ml. Each of the 10 splints were fabricated using 3.2g measured on an electronic scale (Ohaus SPX1202 Scout Portable Balance) of acrylic resin and 2 mL of monomer and mixed for 20 seconds (Figure 44).

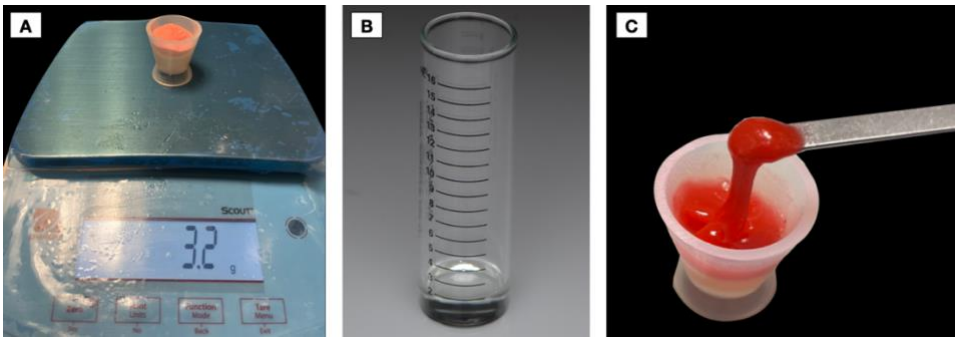

Figure 44. Mixture preparation of auto polymerizing acrylic resin for standardized splint fabrication.
A: 3.2 g of power of acrylic resin; B: 2 ml of monomer of acrylic resin; C: mixture for 20 seconds to obtain clinical manageable consistency.

Figure 45. Ten splints duplicated using the putty index

All 10 splints were left to set for 24 hours (Figure 45). To minimize polymerization shrinkage and strain, the resin splint was sectioned using a disk and reconnected. The reconnected resin acrylic was left to set for 17 minutes prior to impression making (Figure 46).(56)(57)

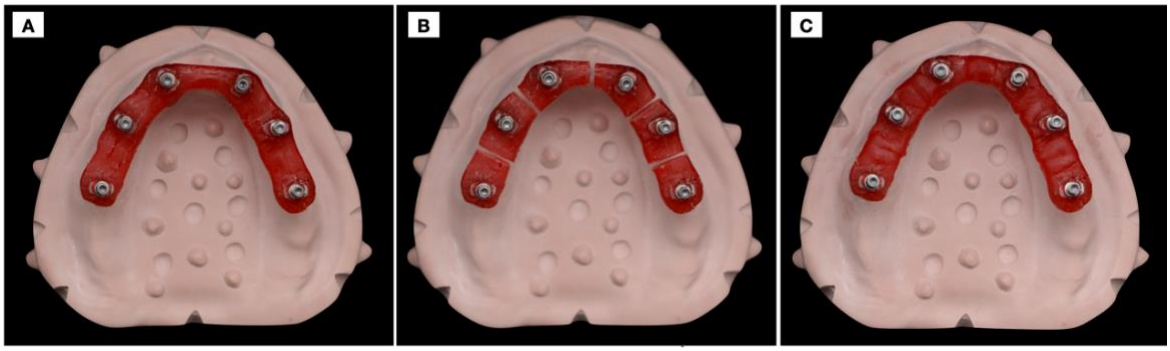

Figure 46. Resin splint sectioning and reconnecting
A: Resin splint left to set for 24 hours; B: Resin splint sectioned using a disk; C: Resin splint rejoined and left to set for 17 minutes.

3.2.5.2 Custom tray fabrication

To fabricate the custom trays, a spacer was created around the splinted impression copings and was sprayed with CAD/CAM powder (CEREC® Optispray, Dentsply Sirona) to aid with the digitization of the spacer (Figure 47).

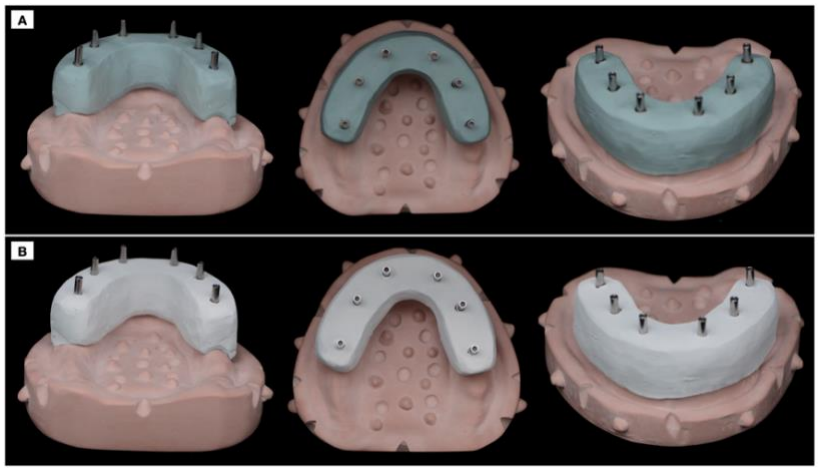

Figure 47. Spacer made around the splinted impression copings for custom tray fabrication.
A: Spacer made using PVS putty; B: Spacer sprayed with CAD/CAM spray for scanning purposes.

The dental stone master model and spacer around the splinted impression copings were scanned using a high accuracy extraoral scanner (inEOS X5, Dentsply Sirona, Germany) and the STL file was imported into a CAD software (3Shape software). The custom tray was designed to

have a 1.50mm of spacer and 2.50 mm of thickness. Four of the notches around the model were engaged for standardized positioning and seating of the custom tray. Finally, holes were designed around the impression copings to allow adequate screw access (Figure 48).

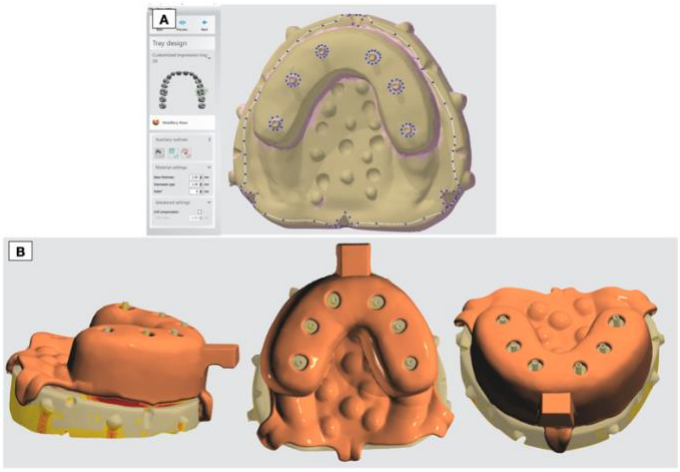

Figure 48. Digital custom tray fabrication
A: Marked outline for design; B: Digital design of the custom tray in different views.

Ten standardized custom trays were then fabricated using a 3D printer (Formlabs 3, Preform) (Figure 49). The 3D printing resin used was the model resin to achieve 50 μm layers of accuracy. The fit of each 3D printed custom tray was verified on the stone master model prior to any impression (Figure 50).

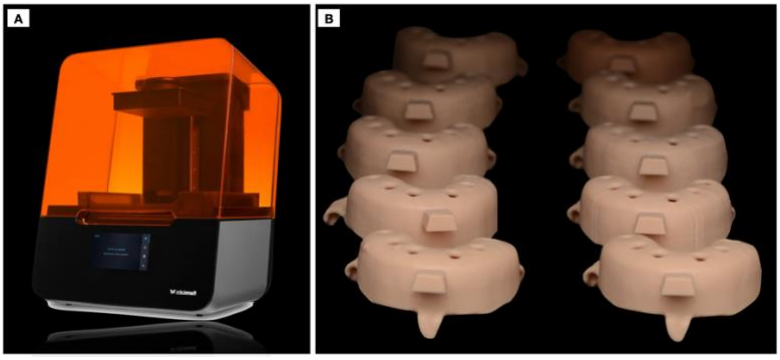

Figure 49. Digital custom tray 3D print.
A: Form Labs 3 3D Printer; B: 10 standardized Custom trays 3D printed.

Figure 50. Verification of custom tray fit on the stone master model in different views.

3.2.5.3 Conventional impression and digitization

Impression boxing followed before dental stone pouring. Polyether tray adhesive was applied on the custom tray and polyether medium body material (Impregum Penta Soft; 3 M ESPE) was used for the final impressions. Once the impression material's polymerization was completed, it was recovered from the master model and multi-unit implant analogs were connected to the impression copings (Figure 51). Type IV dental stone (Silky Rock, WhipMix) was mixed according to the manufacturer's instructions and poured into the impression to fabricate a definitive cast. The dental stone was left to set for 24 hours prior to separating the impression and impression copings from the definitive cast to avoid any delayed dimensional changes.(26)(58)

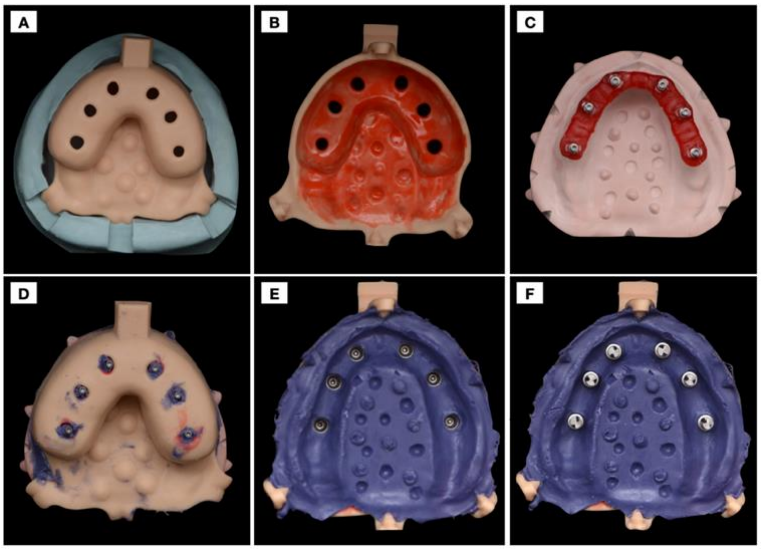

Figure 51. Conventional impression step-by-step.

A: Boxing was done to pour the impressions in; B: Polyether adhesion placed on the tray; C: Reconnected splinted impression copings (left to set for 15 minutes); D: Medium body polyether impression taken and allowed to set for 5 minutes; E: Impression copings unscrewed from the model and impression was recovered; F: Multi-unit implant analogs connected to the impression copings before pouring the impression.

The process was repeated 10 times and 10 definitive casts were fabricated using this conventional splinted open tray implant abutment procedure (Figure 52).

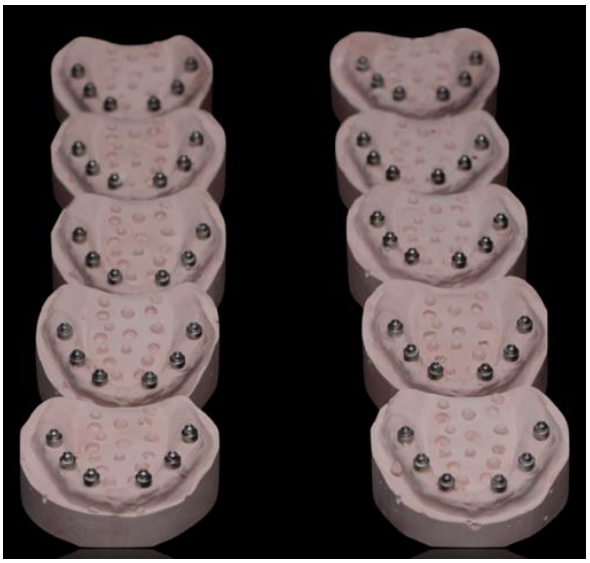

Figure 52. 10 definitive casts from conventional impression technique

Each model was numbered and labeled from 1 to 10 and scan bodies (ELOS Accurate, IO-2C-A, Denmark) were hand tightened over the multi-unit implant replicas for each model. All 10 models were then digitized using a previously calibrated extraoral scanner (inEOS X5, Dentsply Sirona, Germany) and 10 STL files with scan bodies were obtained. Once all the data was exported as scan body STL files, they were imported into a CAD software (Exocad DentalCAD; Darmstadt, Germany) and were converted into virtual analog STL files with preservation of the palate that contained the markers for merging purposes (refer to Chapter 2, section 2.2.3.1).

3.3 Study Design: Phase 2

Phase 2 of the study design focused on the three different comparison tests:

- A 3D comparison test (IScan3D Dental Version 9.1.104 and Iscan 4D Dental Version 9.1.104)
- An angular deviation test (Geomagic Control X 2020.1; 3D systems).
- A cross-arch distance test (IScan3D Dental Version 9.1.104)

3.3.1 3D Comparison test

Two inspection software were used (IScan3D and Iscan 4D) to perform a 3D comparison test which allowed to calculate the 3D deviations of the implants.

3.3.1.1 Inspection software #1

On the first inspection software (Iscan 4D, Imetric, Switzerland), the reference STL was initially imported and the test group STLs were overlapped to it using a best fit an initial "mesh alignment" with the markers on the palate to compute the initial merge followed by a "fine mesh alignment" to get the best fit between the 2 STL files. The palatal area was sectioned out after merge and a visual inspection of a colorimetric map was then generated for the immediate visualization of the results (Figure 53). The root mean square (RMS) values were obtained.

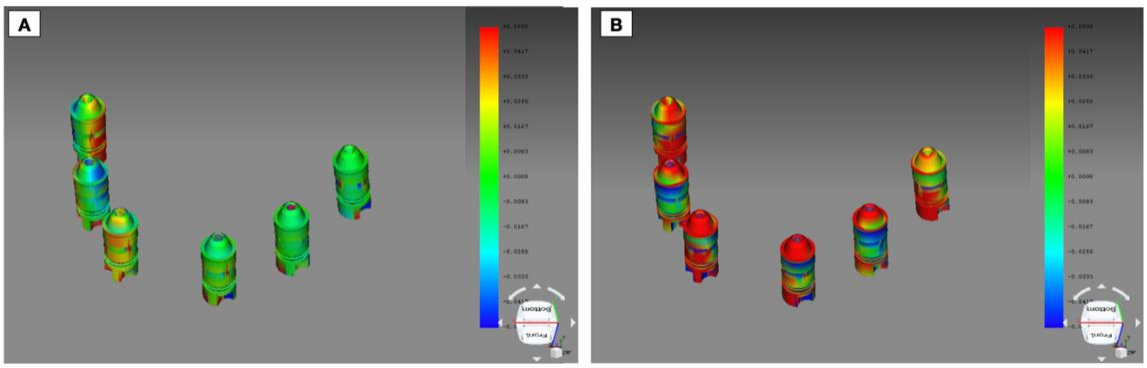

Figure 53. Iscan4D inspection software using best fit algorithm
A: Comparison of PTG to the Reference STL; B: Comparison of CNV to the Reference STL

3.3.1.2 Inspection software #2

The transformation points from the reference STL in the X Y Z coordinate system were first imported as the “Fixed set” into the second inspection software’s 3D spatial similarity transformation platform (IScan3D Dental Version 9.1.104, Imetric, Switzerland). The test files’ transformation points were then added as the “Moving sets”. Each test file was compared to the reference file with the “compute transformation” feature (Figure 54). This spatial fit analysis was done using the “Origin” points (total of 6 points) and the “Origin+Z” points (total of 12 points) for each comparison group. The “Origin” and “Origin+Z” RMS data were obtained.

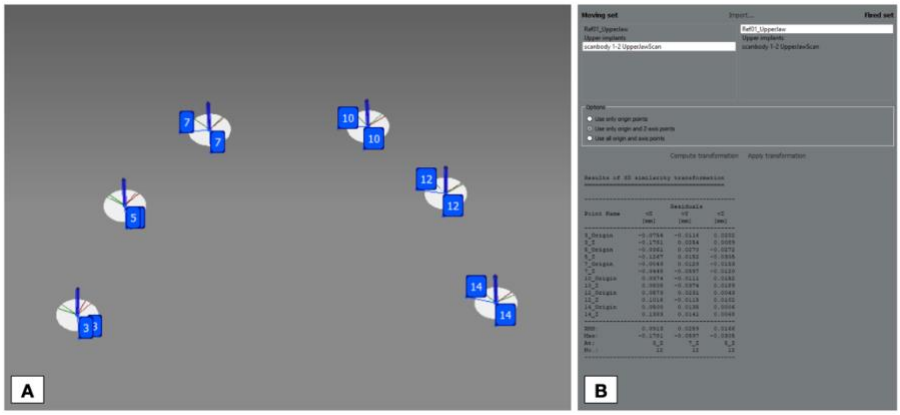

Figure 54. Spatial similarity transformation platform on Iscan3D

3.3.2 Angular deviation test

The reference STL file was imported to a third inspection software (Geomagic Control X 2020.1; 3D systems) and was used as a template where the regions were refined and segmented to obtain results which are specific to the desired surfaces of comparison (Figure 55).

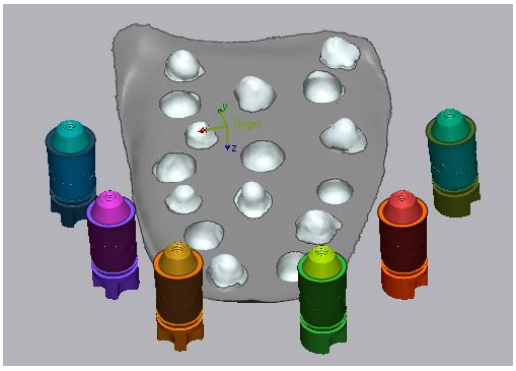

Figure 55. Analog STL Template fabrication on the inspection software (Geomagic Control X 2020.1 ;3D systems).

STL files from the test groups were superimposed to the reference STL file by using an "initial alignment" and then doing a "best fit alignment". The "geometrical deviation" feature was then used to measure the global angular deviation of the conical geometry shape of the analog surface (Figure 56).

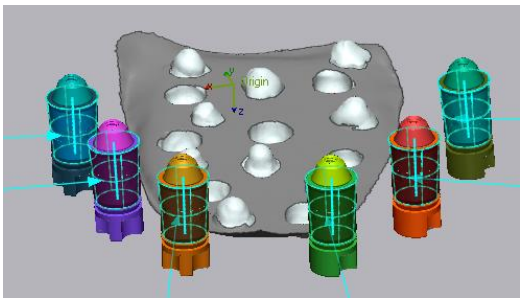

Figure 56. Angular deviation test on cone surface of the analog.

A correlation test between the data extracted from the RMS values of "Origin" and "Origin+Z" was also used to determine if there were any angular deviations in the studied groups.

3.3.3 Overall deviations and cross arch distances

To measure the overall linear deviations and cross-arch distances, the "Origin points" coordinates (Figure 57) obtained from the inspection software (IScan3D Dental Version 9.1.104)

of each abutment from the reference and test files were exported to a spreadsheet where the absolute linear distances were calculated.

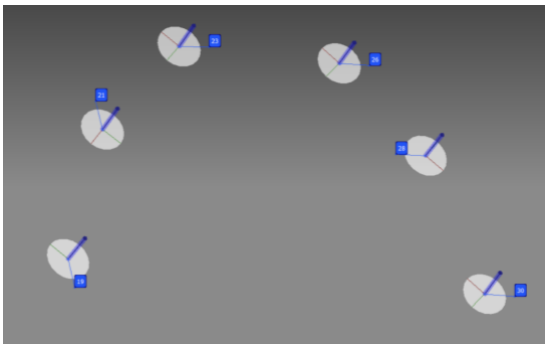

Figure 57. Origin points

The deviations of all possible combinations of interimplant distances were analyzed for each scan.

3.4 Statistical analysis

All calculations were performed on Microsoft Excel (Version 2016, MS Office 2016, Microsoft, USA). All statistical analyses were performed using JMP® Pro (Version 15.2.0 SAS Institute Inc., Cary, NC, USA). Both software were used to produce graphical representations of the results. Table 11 summarizes the factors, outcomes, and statistical methods used for each phase.

Table 11. Summary of factors, outcomes, and statistical methods by tests.

Test	**Factors**	**Outcomes**	**Statistical Method**
Test 1: 3D Comparison	• Root mean square values	• Precision • Trueness	• One-Way ANOVA • Two-Way ANOVA • Tukey-Kramer HSD post hoc • Student's t-test
Test 2: Angular deviation	• Delta Angle	• Trueness	• One-Way ANOVA • Two-Way ANOVA

Test	Factors	Outcomes	Statistical Method
			• Tukey-Kramer HSD post hoc • Equivalence test
Test 3: Cross-arch distances and linear deviations	• Deviations of the mean of all cross-arch distances using the center point of each implant (named "origin point"). • Absolute deviations in cross-arch distances. • Absolute deviations in XYZ coordinates of each implant.	• Precision • Trueness	• One-Way ANOVA • Two-Way ANOVA • Tukey-Kramer HSD post hoc • Student's t-test

Quantitative results were summarized as means and standard deviations (SD). One-way ANOVA test was used to compare the means amongst the different groups for continuous outcomes such as precision and trueness. Two-way ANOVA and least squares regression models were utilized to study the effects of multiple factors on outcomes such as precision and trueness. Tukey-Kramer HSD post hoc test and student's t-test were utilized to determine interactions between factors. The level of significance was set at $\alpha = 0.05$.

The assessment of trueness was conducted using statistical analysis with the 95% significance one-way ANOVA. All the measurements were compared with the coordinates obtained from the inEos X5 (Dentsply, Germany) STL reference values.

Chapter 4: RESULTS

4.1 3D Comparison test

4.1.1 Baseline studies

In this baseline part of the study, the focus was on determining if any correlation existed between the different software and methods of comparison for the different registration techniques using all possible scenarios for the scan body positions. The IOS group (Group 1) contained three different subgroups according to the scan body positions labeled in the following way:

- **Group 1a : "Same-Same"**

Same*-Same**: the 1st "*" is the scan body position between X5 (reference STL) and the experimental group. "Same" meant that the scan bodies were kept the same between the scanning of the model with the X5 and the IOS scans. The 2nd "**" indicated if the scan body position was changed or stayed the same within each scan in the experimental group. In this case, the position of the scan body remained the same between each scan of the experimental group.

- **Group 1b : "Diff-Same"**

Diff*-Same**: the 1st "*" is the scan body position between X5 (reference STL) and the experimental group which was "Diff": this meant that the scan bodies were remounted between the scanning of the model with X5 and with the experimental group (IOS in this case). The 2nd"**" indicated that the scan body was the "Same", unchanged, between each scan of the experimental group.

- **Group 1c : "Diff-Diff"**

Diff*-Diff**: the 1st "*" is the scan body position between X5 (reference STL) and the experimental group which was "Diff": this meant that the scan bodies were remounted between the scanning of the model with X5 and with the experimental group (IOS in this case). The 2nd"**"

indicated that the scan body was the “Diff”, so remounted between each scan of the experimental group.

The PTG group (Group 2) contained two different subgroups according to the scan body positions labeled in the following way.

- **Group 2a : “Diff-Same”**
- **Group 2b: “Diff-Diff”**

A “Same-Same” group could not be made in this case since the photogrammetry scan bodies (Icam4D scan bodies) are different from the scan bodies used for scanning with the X5 laboratory scanner (ELOS Accurate).

Finally, the CNV group (Group 3) contained only one subgroup according to the scan body positions since digitization was done on 10 different casts in which a remount of the scan body is inevitable.

Since the previous baseline study that the scan body position affects the scanning precision, all scenarios were considered (Figure 58).

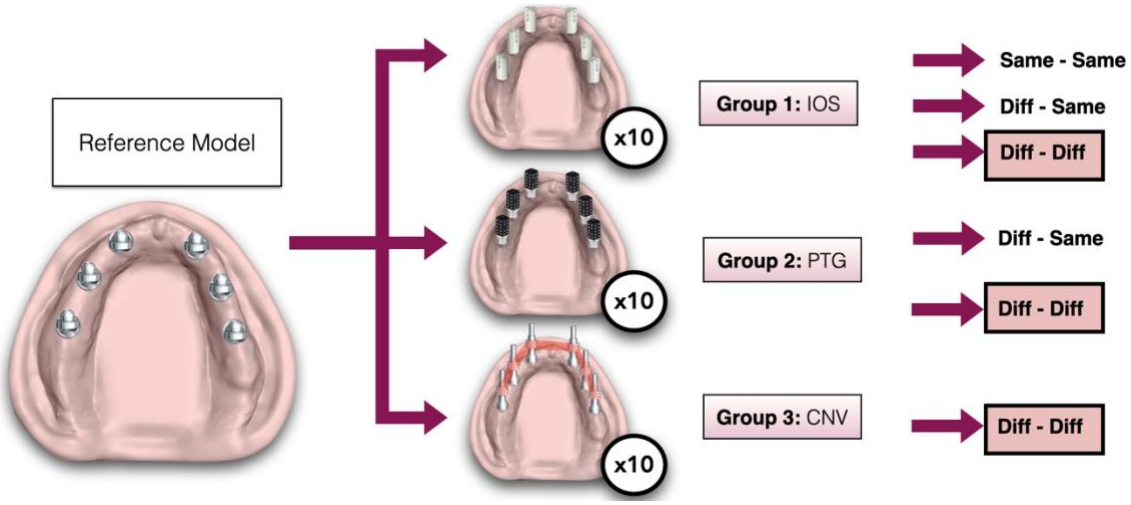

Figure 58. Study design with groups and subgroups.

The data was summarized in Table 12 and a multivariate linear regression model for correlation was done (Figure 59).

Table 12. Summarized 3D comparison deviation RMS data from different inspection software and methods of comparison with all scan body position scenarios

			RMS (mm)		
Registration technique	**Scan body Position**	**Method of Comparison**	**N**	**Mean**	**Std Dev**
CNV	Diff-Diff	GMGX_ANLG	10	0.0404	0.0084
		GMGX_SB	9	0.0391	0.0225
		IScan3D_Origin	10	0.0289	0.0060
		IScan3D _Origin+Z	10	0.0293	0.0057
		Iscan4D_ANLG	10	0.0269	0.0015
		Iscan4D_SB	10	0.0260	0.0017
IOS	Diff-Diff	GMGX_ANLG	10	0.0499	0.0067
		GMGX_SB	10	0.0528	0.0049
		IScan3D_Origin	10	0.0236	0.0029
		IScan3D _Origin+Z	10	0.0366	0.0039
		Iscan4D_ANLG	10	0.0272	0.0013
		Iscan4D_SB	10	0.0279	0.0006
	Diff-Same	GMGX_ANLG	10	0.0524	0.0040
		GMGX_SB	10	0.0582	0.0059
		IScan3D_Origin	10	0.0263	0.0030
		IScan3D _Origin+Z	10	0.0423	0.0068
		Iscan4D_ANLG	10	0.0288	0.0005
		Iscan4D_SB	10	0.0278	0.0010
	Same-Same	GMGX_ANLG	10	0.0332	0.0044
		GMGX_SB	10	0.0410	0.0049
		IScan3D_Origin	10	0.0152	0.0058
		IScan3D _Origin+Z	10	0.0312	0.0061
		Iscan4D_ANLG	10	0.0276	0.0013
		Iscan4D_SB	10	0.0264	0.0007
PTG	Diff-Diff	GMGX_ANLG	10	0.0640	0.0069
		IScan3D_Origin	10	0.0206	0.0039
		IScan3D _Origin+Z	10	0.0232	0.0039
		Iscan4D_ANLG	10	0.0232	0.0016

	Diff-Same	GMGX_ANLG	10	0.0588	0.0005
		IScan3D_Origin	10	0.0243	0.0004
		IScan3D _Origin+Z	10	0.0252	0.0002
		Iscan4D_ANLG	10	0.0247	0.0005
X5	Diff-Diff	GMGX_ANLG	4	0.0718	0.0093
		GMGX_SB	4	0.0246	0.0033
		IScan3D_Origin	4	0.0186	0.0047
		IScan3D _Origin+Z	4	0.0190	0.0047
		Iscan4D_ANLG	4	0.0229	0.0013
		Iscan4D_SB	4	0.0216	0.0038
	Same-Same	GMGX_ANLG	4	0.0058	0.0035
		GMGX_SB	4	0.0062	0.0012
		IScan3D_Origin	4	0.0017	0.0003
		IScan3D _Origin+Z	4	0.0017	0.0003
		Iscan4D_ANLG	4	0.0036	0.0011
		Iscan4D_SB	4	0.0075	0.0017

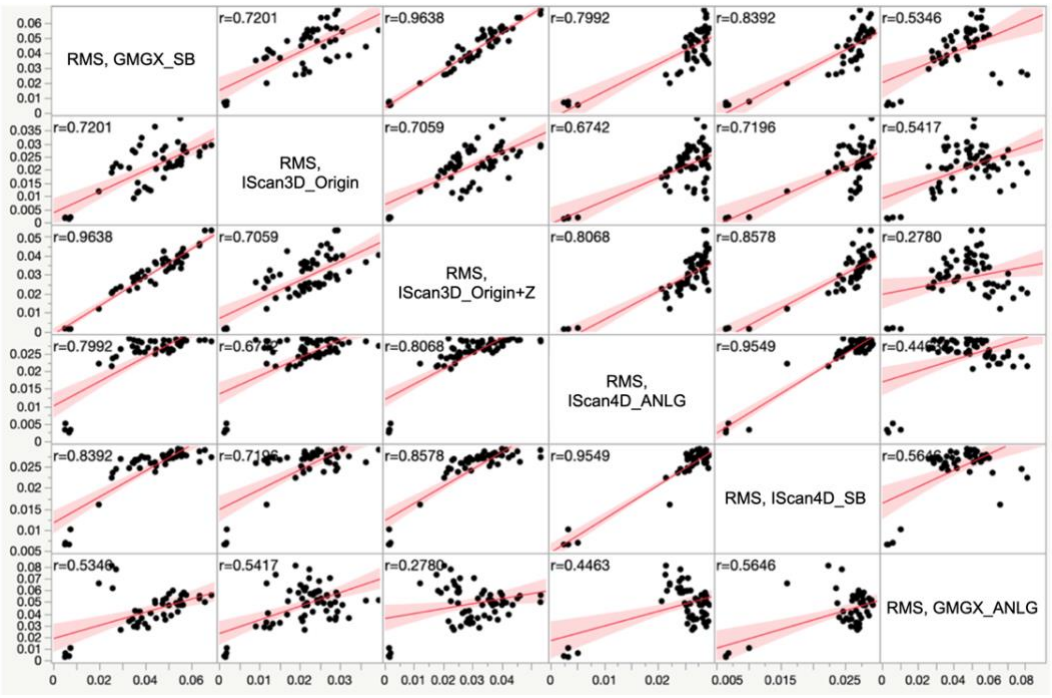

Figure 59. Scatterplot matrix for multivariate linear regression showing the correlation of RMS data between different inspection methods

The best correlation was found between the Geomagic scan body data and the IScan3D Origin+Z data (r=0.9638). The second-best correlation was found between the Geomagic scan body data and Iscan4D analog surface data (r=0.7992).

The RMS data from Geomagic analog surface showed poor correlation with all methods, including the Geomagic scan body data (r=0.5346). The RMS data from Iscan4D analog surface showed a very good correlation with the RMS data from the Iscan4D scan body surface (r=0.9549).

It is important to note however that an outlier variable was identified during the 3D comparison test of the CNV group using Geomagic on the scan body surface. It was decided that this variable should be excluded from the correlation analysis.

4.1.2 3D Comparison test for final study model:

The RMS data from Iscan3D's Origin+Z and the Iscan4D analog surface data was summarized in Table 13 for "Diff-Diff" scan body subgroups of each registration technique.

Table 13. Summarized 3D comparison deviation RMS data selected

		RMS (mm)			
Registration technique	**Method**	**N**	**Mean**	**SD**	**P-value**
Group 1: IOS	**Iscan4D**	10	0.0272	0.0013	< 0.0001*
	Iscan3D Origin+Z	10	0.0366	0.0039	
Group 2: PTG	**Iscan4D**	10	0.0232	0.0016	0.9683 **
	Iscan3D Origin+Z	10	0.0232	0.0039	
Group 3: CNV	**Iscan4D**	10	0.0269	0.0015	0.2204 **
	Iscan3D Origin+Z	10	0.0293	0.0057	

P< .05 statistically significant; assessed by test of difference in two population means
P> 0.05 no statistical significance; assessed by test of difference in two population means

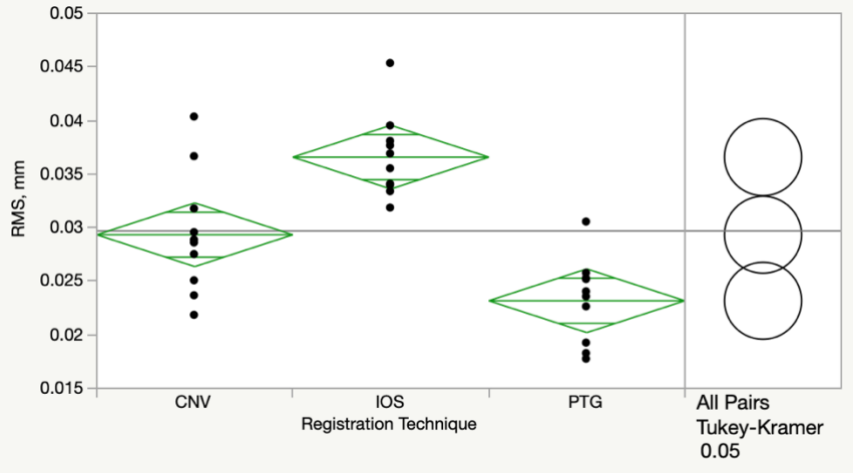

Figure 60. Oneway Analysis of RMS by registration technique using IScan3D Origin + Z data

Table 14. Tukey-Kramer HSD, connecting-Letters Report of RMS between different registration techniques using IScan3D Origin+Z data

Level		Mean
IOS	A	0.0366
CNV	B	0.0293
PTG	C	0.0232

Levels not connected by the same letter are significantly different.

Table 15. Ordered differences report of RMS between different registration techniques using IScan3D Origin+Z data

Level	- Level	Difference	Std Err Dif	Lower CL	Upper CL	p-Value
IOS	PTG	0.0134	0.0021	0.0083	0.0185	<.0001*
IOS	CNV	0.0072	0.0020	0.0022	0.0123	0.0041*
CNV	PTG	0.0062	0.0021	0.0011	0.0113	0.0151*

Tukey-Kramer HSD post hoc test was used to identify significant differences between registration groups and RMS registered with IScan3D Origin+Z data (Figure 60). There was a significant difference in RMS between IOS and PTG (p<.0001), and IOS and CNV (p=0.0041), and CNV and PTG (p=0.0151) with the RMS from IScan3D Origin +Z (Table 14 and 15).

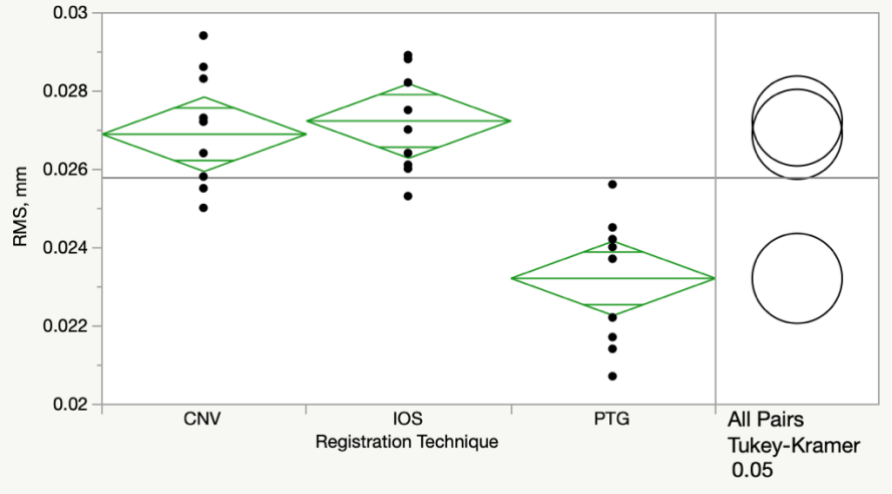

Figure 61. Oneway Analysis of RMS by registration technique using IScan4D data

Table 16. Comparison of RMS between different registration techniques using Iscan4D data

Level	Sig. *	Mean
IOS	A	0.0272
CNV	A	0.0269
PTG	B	0.0232

**Levels not connected by the same letter are significantly different by Tukey-Kramer HSD*

Table 17. Ordered differences report of RMS between different registration techniques using IScan4D data

Level	- Level	Difference	Std Err Dif	Lower CL	Upper CL	p-Value
IOS	PTG	0.0040	0.0007	0.0024	0.0056	<.0001*
CNV	PTG	0.0037	0.0007	0.0021	0.0053	<.0001*
IOS	CNV	0.0003	0.0007	-0.0013	0.0020	0.8626

Tukey-Kramer HSD post hoc test was used to identify significant differences between registration groups and RMS registered with Iscan4D (Figure 61). There was a significant difference in RMS between IOS and PTG ($p<.0001$), and CNV and PTG ($p<.0001$). CNV and IOS were not statistically different ($p=0.8626$) with the RMS from IScan4D (Table 16 and 17).

4.2 Angular deviation test:

4.2.1 Baseline studies

In this part of the baseline studies, the focus was on determining if any correlation existed between the scan body STL files and converted analog STL files in terms of angular deviations for the different registration techniques using all possible scenarios for the scan body positions. The delta angles were collected for each group following the methodology described in Chapter 2 section 2.2.3.

The data for the angular deviation was collected on the scan body surface and analog cone surface and was summarized in Table 18. A multivariate linear regression model for correlation was done (Figure 62).

Table 18. Summarized Angular deviations data from different registration techniques and different STL surfaces of comparison with all scan body position scenarios

			ΔAngle (Degree)		
Surface	**Registration technique**	**SB Position**	**N**	**Mean**	**Std Dev**
Analog Cone	CNV	Diff-Diff	60	0.129	0.070
	IOS	Diff-Diff	60	0.398	0.118
		Diff-Same	60	0.487	0.131
		Same-Same	60	0.440	0.119
	PTG	Diff-Diff	60	0.133	0.059
		Diff-Same	60	0.126	0.059
	X5	Diff-Diff	24	0.065	0.033
		Same-Same	24	0.027	0.015
SB Cone	CNV	Diff-Diff	60	0.217	0.102
	IOS	Diff-Diff	60	0.555	0.163
		Diff-Same	60	0.518	0.125
		Same-Same	60	0.468	0.110
	X5	Diff-Diff	24	0.161	0.090
		Same-Same	24	0.020	0.014

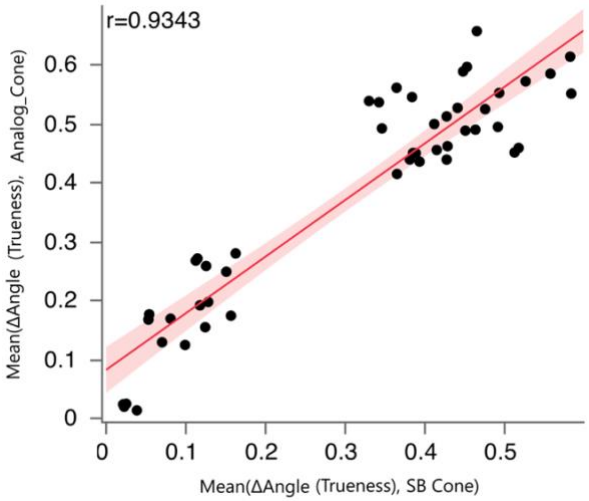

Figure 62. Bivariate plot with linear regression showing the correlation of the implant axis angular deviation between different comparison software

The bivariate linear regression models in Figure 62 show that the values of the delta angle obtained on the scan body cone surface versus on the analog cone surface via X5, CNV (digitized by X5) and IOS was strongly correlated (r=0.9343). That indicates the comparison results of the delta angle from the analog cone surface would be strongly correlated to those using the delta angle from scan body cone surface. Therefore, delta angle from the analog cone surface can be utilized to compare the angular deviation of implant scan body.

4.2.2 3D Angular deviation test for final study model:

Since the analog shape and the "Diff-Diff" scan body positions were standardized amongst all groups, the results for angular deviations were shown in Table 19 and Figure 64.

Table 19. Summarized Angular deviation data from different registration techniques

		ΔAngle (Degree)		
Registration technique	**SB Position**	**N**	**Mean**	**Std Dev**
CNV	Diff-Diff	60	0.129	0.070
IOS	Diff-Diff	60	0.398	0.118
PTG	Diff-Diff	60	0.133	0.059

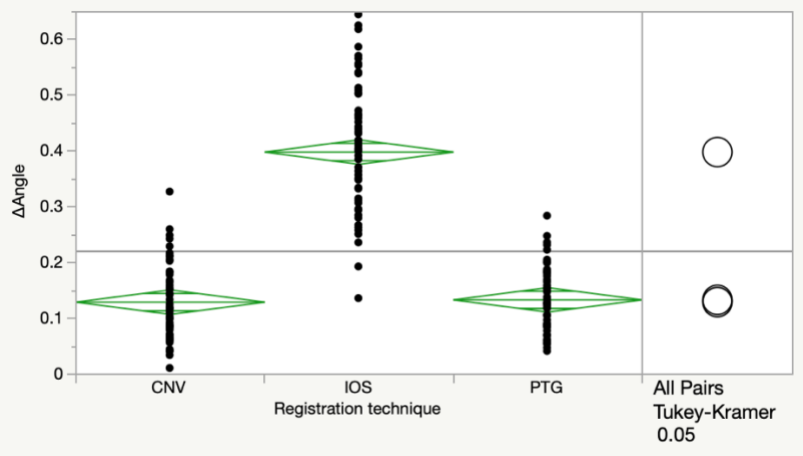

Figure 63. Oneway Analysis of ΔAngle by registration technique

Table 20. Connecting-Letters Report of Angular deviations between different registration techniques compared by Tukey-Kramer HSD

Level		Mean
IOS	A	0.399
PTG	B	0.1333
CNV	B	0.1292

Levels not connected by the same letter are significantly different.

Table 21. Ordered differences report of Angular deviations between different registration techniques.

Level	- Level	Difference	Std Err Dif	Lower CL	Upper CL	p-Value
IOS	CNV	0.2693	0.0157	0.2382	0.3003	<.0001*
IOS	PTG	0.2652	0.0157	0.2341	0.2962	<.0001*
PTG	CNV	0.0041	0.0157	-0.0270	0.0351	0.9636

Tukey-Kramer HSD post hoc test was used to identify significant differences of angular deviations between registration groups (Figure 63). There was a significant difference in angular deviation between IOS and PTG ($p<0.0001$), and IOS and CNV ($p<0.0001$). CNV and PTG were not statistically different from each other ($p=0.9636$) (Table 20 and 21).

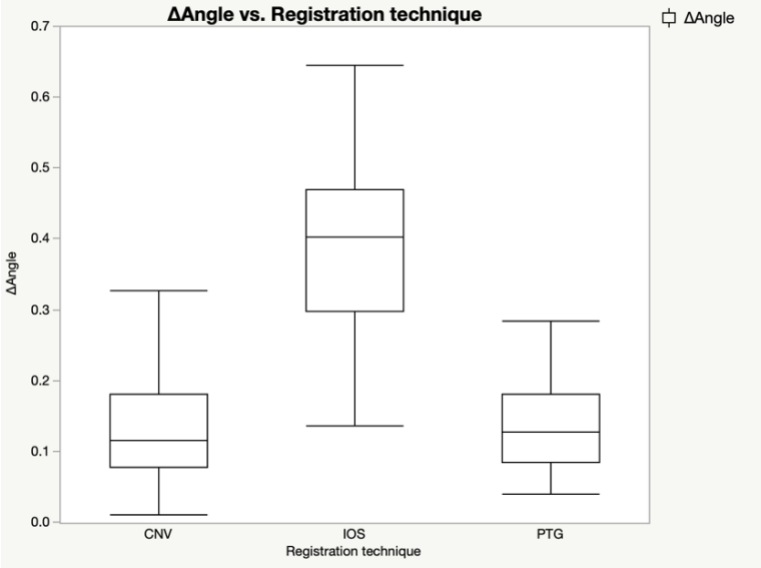

Figure 64. Box plot representation of angular deviation by registration techniques.

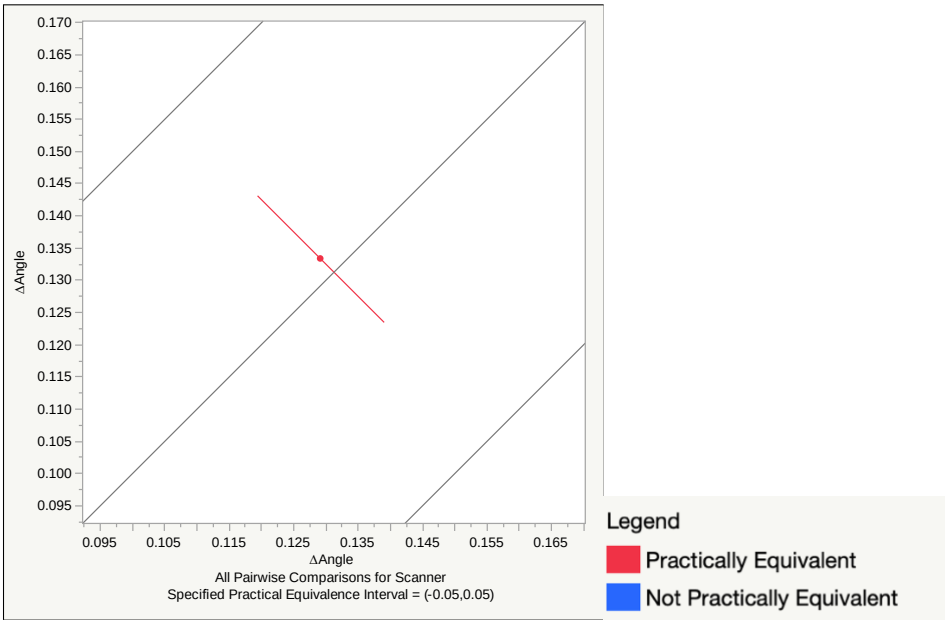

Figure 65. Equivalence Tests Scatterplot of Delta Angle between CNV and PTG with α level=0.05 and specified practical equivalence interval set at 0.05.

The equivalence test of CNV and PTG with a specified practical equivalence tolerance of 0.05 degree showed that the two groups were practically equivalent in terms of angular deviations (p=0.9636) (Figure 65).

4.3 RMS values of Origin and Origin+Z to understand angular deviation:

4.3.1 Baseline studies

This study intended to collect deviation RMS data from Iscan3D Origin and Origin + Z for all 3 groups and their subgroups when compared to the reference STL file. These comparison groups were labeled "To ref" since they were compared to the reference STL file to obtain trueness measurements. In the comparison groups labeled "Internal", the STL files within each experimental group were compared to an STL file selected at random from each group to obtain measurements that would reflect on the precision of the system. The data were summarized in Table 22 and a multivariate linear regression model for correlation was done (Figure 66).

Table 22. Summarized RMS data for "To ref" and "Internal" groups

		Internal RMS_Origin		Internal RMS_Z+Origin		To ref RMS_Origin		To ref RMS_Z+Origin	
Registration technique	**Scan body position**	**Mean**	**Std Dev**	**Mean**	**Std Dev**	**Mean**	**Std Dev**	**Mean**	**Std Dev**
CNV	Diff-Diff	0.0207	0.0050	0.0220	0.0055	0.0289	0.0060	0.0293	0.0057
IOS	Diff-Diff	0.0215	0.0042	0.0258	0.0040	0.0236	0.0029	0.0366	0.0039
	Same-Same	0.0126	0.0042	0.0161	0.0032	0.0207	0.0073	0.0367	0.0085
PTG	Diff-Diff	0.0183	0.0034	0.0206	0.0027	0.0206	0.0039	0.0232	0.0039
	Same-Same	0.0015	0.0004	0.0013	0.0003	0.0243	0.0004	0.0252	0.0002
X5	Diff-Diff	0.0186	0.0047	0.0190	0.0047	0.0186	0.0047	0.0190	0.0047
	Same-Same	0.0017	0.0003	0.0017	0.0003	0.0017	0.0003	0.0017	0.0003

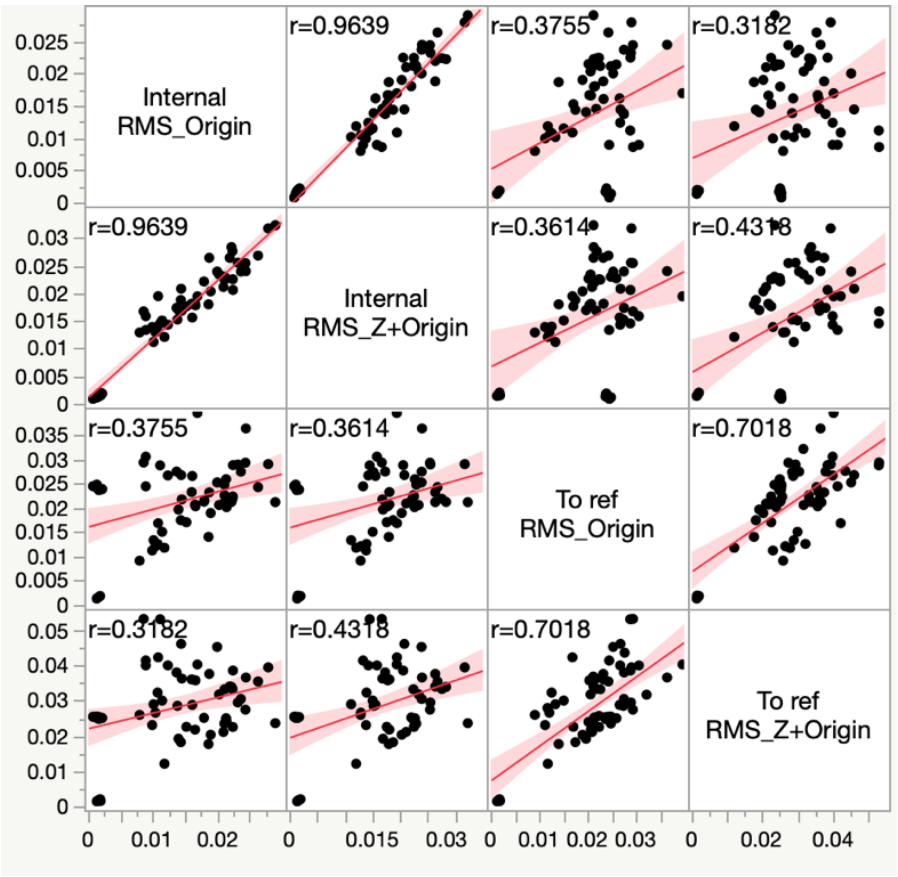

Figure 66. Scatterplot Matrix for Multivariate linear regression showing the correlation between RMS obtained from Origin vs Origin+Z in “Internal” and “To ref” groups.

The linear correlation of different registration techniques when comparing Origin to Origin+Z within each group (Internal) was well fit with r = 0.9639 and p-value < 0.0001 .

The correlation coefficient decreased (r=0.702) between Origin and Origin+Z when studying the different groups compared to the reference STL file from the inEOS X5 scanner.

A bar chart representation of Origin and Origin+Z RMS for comparison method and comparison group with all scan bodies scenarios was done (Figure 67).

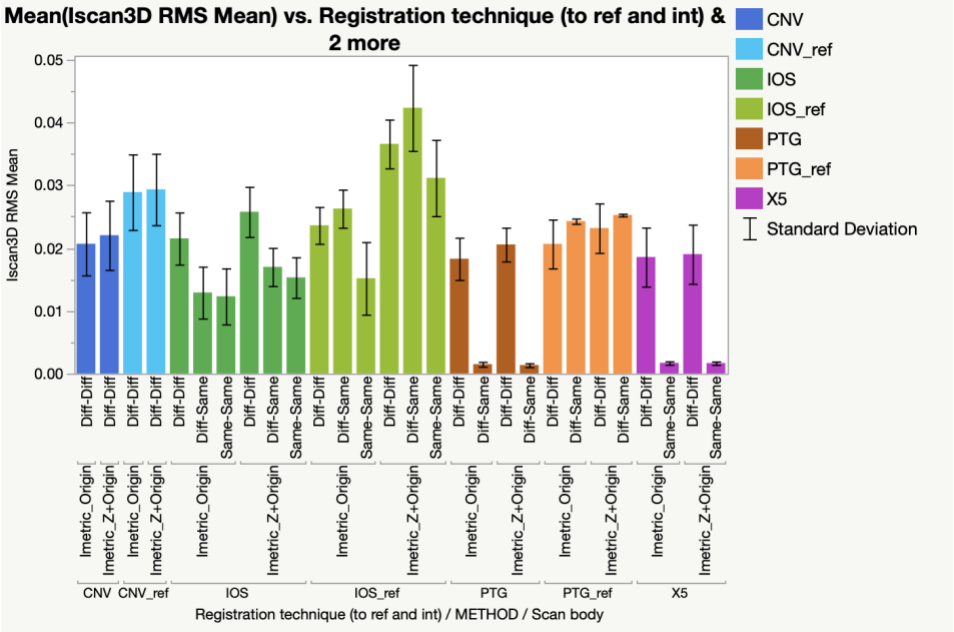

Figure 67. Bar chart of Origin and Origin+Z RMS for comparison method and comparison group with all scan bodies scenarios.

Comparison method used was Iscan3D's Origin and Origin + Z. Comparison group were: 1)"To Ref" which represents the comparison of experimental group to Reference STL file from inEOS X5. 2)"Internal": Within each experimental group.

4.3.2 Comparison of the RMS values considering the Z vector

Table 23. Summarized RMS data for "To ref" and "Internal" groups with Diff-Diff scan body positions

		RMS (mm)			
Registration technique	**Method**	**N**	**Mean**	**SD**	**P value**
CNV_To ref	Imetric_Origin	10	0.0289	0.0060	0.8713**
	Imetric_Z+Origin	10	0.0293	0.0057	
CNV_Internal	Imetric_Origin	9	0.0207	0.0050	0.5917**
	Imetric_Z+Origin	9	0.0220	0.0055	
IOS_To ref	Imetric_Origin	10	0.0236	0.0029	< 0.0001*
	Imetric_Z+Origin	10	0.0366	0.0039	
IOS_Internal	Imetric_Origin	9	0.0215	0.0042	0.0421*
	Imetric_Z+Origin	9	0.0258	0.0040	
PTG_To ref	Imetric_Origin	10	0.0206	0.0039	0.1670**
	Imetric_Z+Origin	10	0.0232	0.0039	
PTG_Internal	Imetric_Origin	9	0.0183	0.0034	0.1337**
	Imetric_Z+Origin	9	0.0206	0.0027	

**P< .05 statistically significant; assessed by test of difference in two population means*
***P> 0.05 no statistical significance; assessed by test of difference in two population means*

The RMS data for “To ref” and “Internal” groups with Diff-Diff scan body positions was summarized and assessed by test of difference in two population means (Table 23). The IOS_To ref and IOS_Internal groups revealed statistically significant differences ($p < 0.05$), confirming a significant angular deviation existed. The PTG_To ref, PTG_Internal, CNV_To ref and CNV_Internal did not show any statistical significance ($p > 0.05$). Studying the RMS from Origin vs Origin+Z achieved from spatial similarity transformation software can help assess if any angular deviations exist in a system. A bar chart representation of Iscan3D RMS Mean vs Comparison group & Method of Comparison with “Diff-Diff” Scan body was also done (Figure 68) to aid in the visualization of the results.

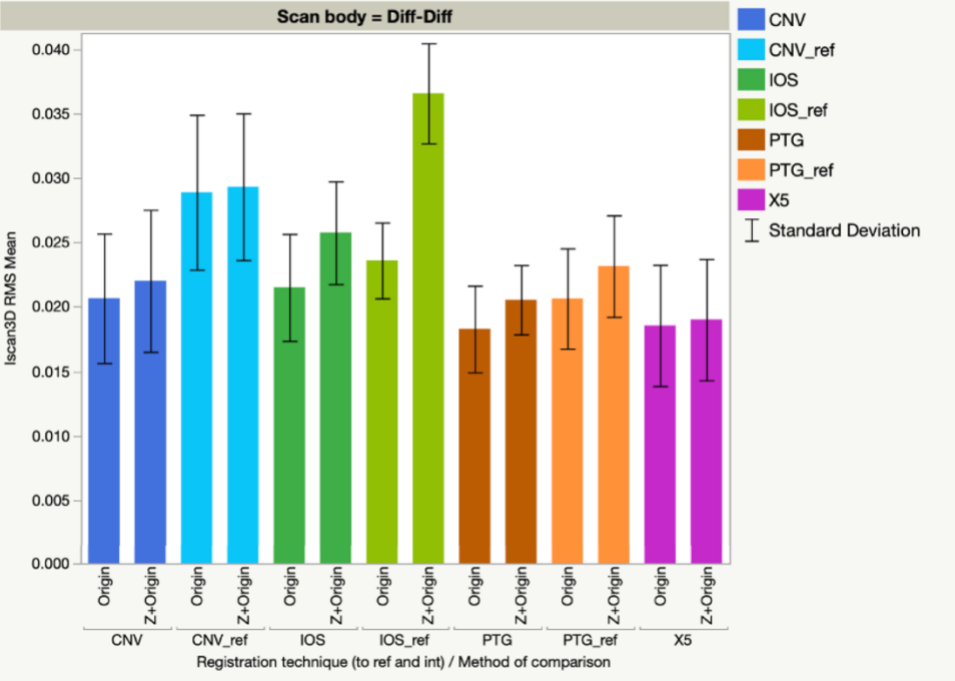

Figure 68. Iscan3D RMS Mean vs. Comparison group & Method of Comparison with “Diff-Diff” Scan body

4.3.3 RMS values: trueness and reproducibility versus registration technique

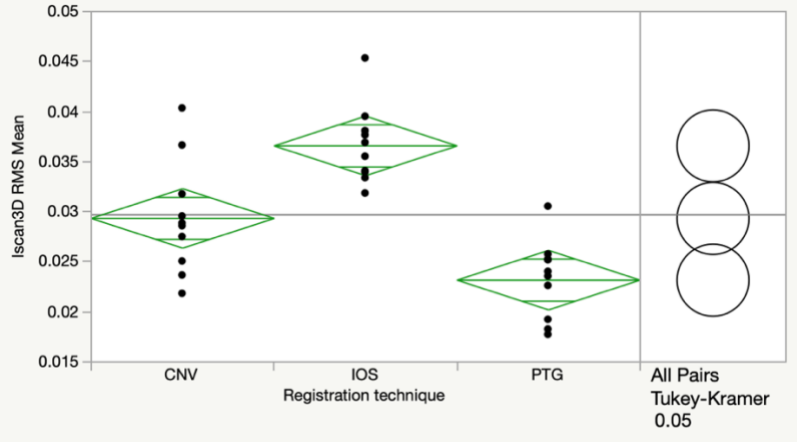

Figure 69. Oneway Analysis of Iscan3D RMS Mean using Iscan3D Origin+Z By Registration technique "To Ref"

Table 24. Connecting-Letters Report of RMS Mean using Iscan3D Origin+Z by Registration technique "To Ref"

Level	Sig.*	Mean
IOS	A	0.0366
CNV	B	0.0293
PTG	C	0.0232

**Tukey-Kramer HSD; Levels not connected by the same letter are significantly different.*

Table 25. Ordered differences report of RMS Mean using Iscan3D Origin+Z by Registration technique "To Ref"

Level	- Level	Difference	Std Err Dif	Lower CL	Upper CL	p-Value
IOS	PTG	0.0134	0.0021	0.0083	0.0185	<.0001*
IOS	CNV	0.0073	0.0021	0.0022	0.0123	0.0041*
CNV	PTG	0.0062	0.0021	0.0011	0.0113	0.0151*

Tukey-Kramer HSD post hoc test was used to identify significant differences between registration techniques in terms of 3D deviations trueness using the Origin+Z RMS data ("To ref") (Figure 69). There was a significant difference in RMS between IOS and CNV ($p = 0.0041$), IOS and PTG ($p<0.0001$) and CNV and PTG ($p = 0.0151$) (Table 25). The best results were found in the PTG group (Table 24)

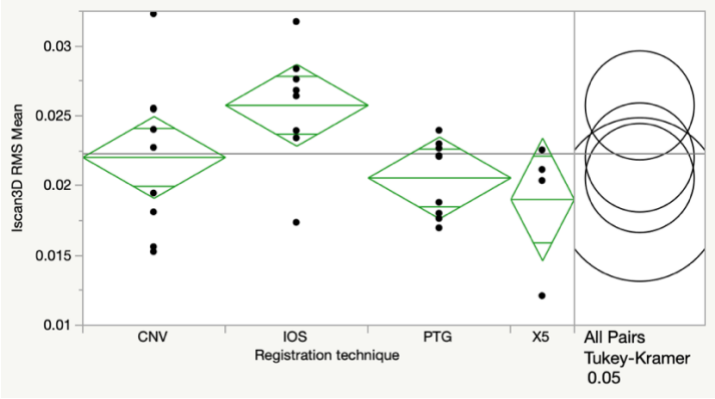

Figure 70. Oneway Analysis of Iscan3D RMS Mean using Iscan3D Origin+Z By Registration technique "Internal".

Table 26. Connecting-Letters Report of RMS Mean using "Diff-Diff" Iscan3D Origin+Z data by Registration technique "Internal"

Level		Mean
IOS	A	0.0258
CNV	A	0.0220
PTG	A	0.0206
X5	A	0.0190

Tukey-Kramer HSD; Levels not connected by the same letter are significantly different.

Table 27. Ordered differences report of RMS Mean by Registration technique "Internal" using Iscan3D Origin+Z RMS

Level	- Level	Difference	Std Err Dif	Lower CL	Upper CL	p-Value
IOS	X5	0.0068	0.0026	-0.0003	0.0138	0.0639
IOS	PTG	0.0052	0.0020	-0.0003	0.0107	0.0702
IOS	CNV	0.0037	0.0020	-0.0018	0.0093	0.2731
CNV	X5	0.0030	0.0026	-0.0040	0.0101	0.6496
PTG	X5	0.0015	0.0026	-0.0055	0.0086	0.9312
CNV	PTG	0.0015	0.0020	-0.0041	0.0070	0.8847

Tukey-Kramer HSD post hoc test was used to identify significant differences between registration techniques in terms of 3D deviations precision using the Origin+Z RMS data ("Internal") (Figure 70). There was no significant difference in RMS between the different registration techniques ($p>0.05$) (Table 26 and 27).

4.4 Cross-arch measurements:

4.4.1 Baseline studies: Correlations

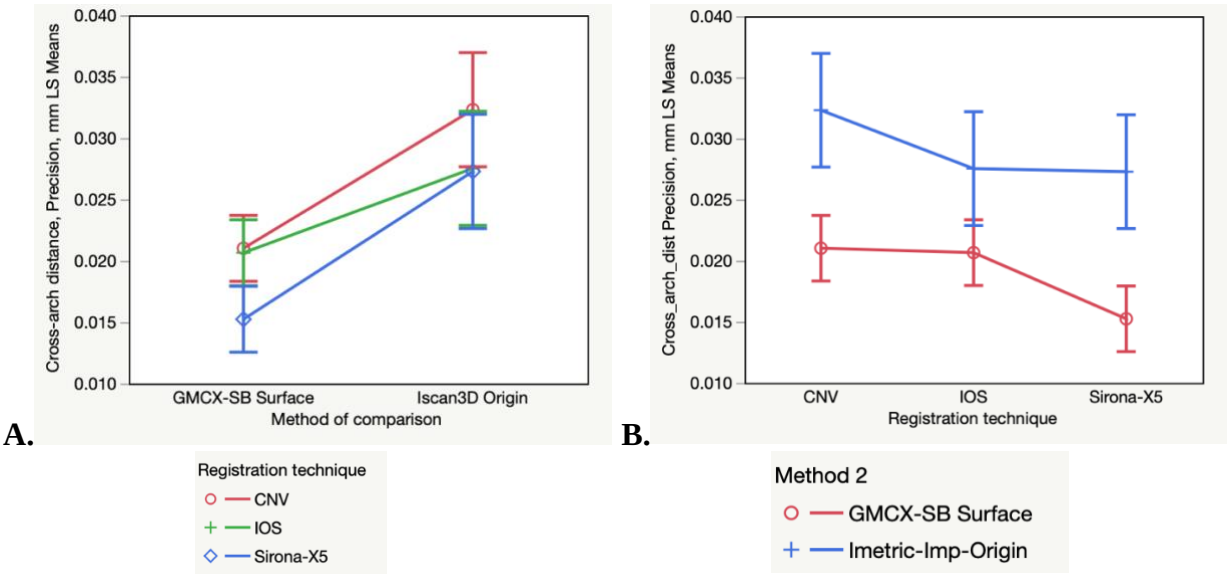

Figure 71. Least squares mean plot of registration technique by method of comparison in response to absolute distance deviation precision values.

When looking at the precision values of absolute distance deviation from different registration techniques using different methods of comparison, a general trend exists between the results obtained on Geomagic (with the coordinates on the scan body surface) and Iscan3D (with the Origin points (Figure 71). The results from X5 were always the lowest, followed by the results from the IOS group and finally the CNV group. The method of comparison may vary the values obtained; however it does not change the final results. It is difficult to determine which method of comparison remains the best. Since the photogrammetry group does not contain the same scan body geometry as the IOS group, CNV group or X5 reference STL, it is not feasible to do the study with the scan body surface using Geomagic. Therefore, the rest of the study was conducted using the Iscan 3D origin points.

4.4.2 Absolute distance deviations: trueness and precision

4.4.2.1 Trueness

The data for cross-arch distances trueness using the Iscan3D Origin coordinates is summarized in Table 28.

Table 28. Comparison of Cross-arch distance trueness vs. registration technique using the Iscan3D Origin coordinates.

	Cross-arch distances Trueness, mm		
Registration technique	**N**	**Mean**	**Std Dev**
CNV	150	0.0488	0.0391
IOS	150	0.0385	0.0269
PTG	150	0.0353	0.0251
inEOS X5	60	0.0293	0.0209

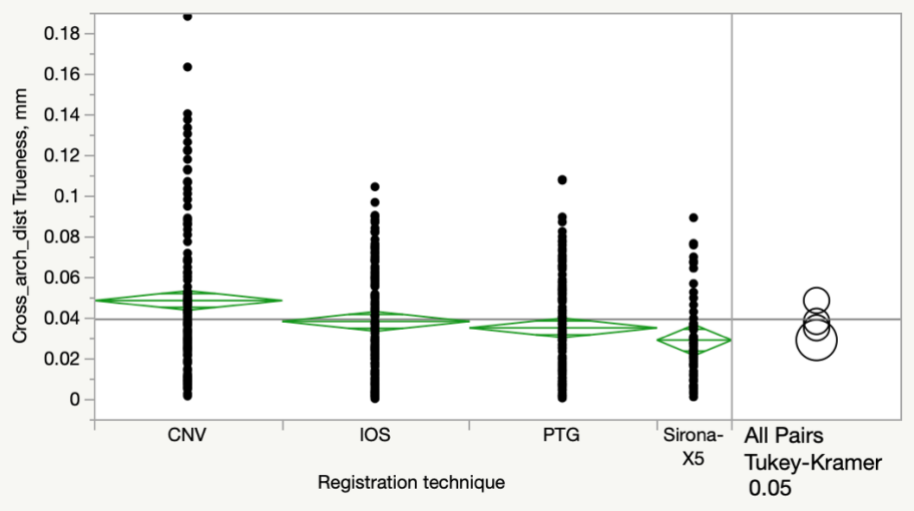

Figure 72. Oneway Analysis of Cross-arch distance (trueness) mean using Iscan3D Origin coordinate by Registration technique.

Table 29. Connecting-Letters Report of Cross-arch distance (trueness) mean using Iscan3D Origin coordinate by Registration technique.

Level		**Mean**
CNV	A	0.0488
IOS	B	0.0385
PTG	B	0.0353
Sirona-X5	B	0.0293

Tukey-Kramer HSD; Levels not connected by the same letter are significantly different.

Table 30. Ordered differences report of Cross-arch distance (trueness) mean using Iscan3D Origin coordinate by Registration technique.

Level	- Level	Difference	Std Err Dif	Lower CL	Upper CL	p-Value
CNV	Sirona-X5	0.0195	0.0046	0.0077	0.0313	0.0001*
CNV	PTG	0.0135	0.0035	0.0045	0.0224	0.0007*
CNV	IOS	0.0103	0.0035	0.0014	0.0192	0.0164*
IOS	Sirona-X5	0.0092	0.0046	-0.0026	0.0210	0.1859
PTG	Sirona-X5	0.0060	0.0046	-0.0058	0.0178	0.5538
IOS	PTG	0.0032	0.0035	-0.0058	0.0121	0.7951

Tukey-Kramer HSD post hoc test was used to identify significant differences between registration techniques in terms of cross-arch distance trueness using the Origin points as the coordinates (Figure 72). There was a significant difference in cross-arch deviations between CNV and PTG (p = 0.0007), CNV and IOS (p=0.0164). IOS and PTG were not statistically different from each other (p = 0.7951). (Table 29 and 30).

4.4.2.2 Precision

The data for cross-arch distances precision using the Iscan3D Origin coordinates is summarized in Table 31.

Table 31. Summarized Cross-arch distances precision using the Iscan3D Origin coordinates.

	Cross-arch distances Precision, mm		
Registration technique	**N**	**Mean**	**Std Dev**
CNV	15	0.0323	0.0069
IOS	15	0.0275	0.0070
PTG	15	0.0230	0.0064
inEOS X5	15	0.0273	0.0091

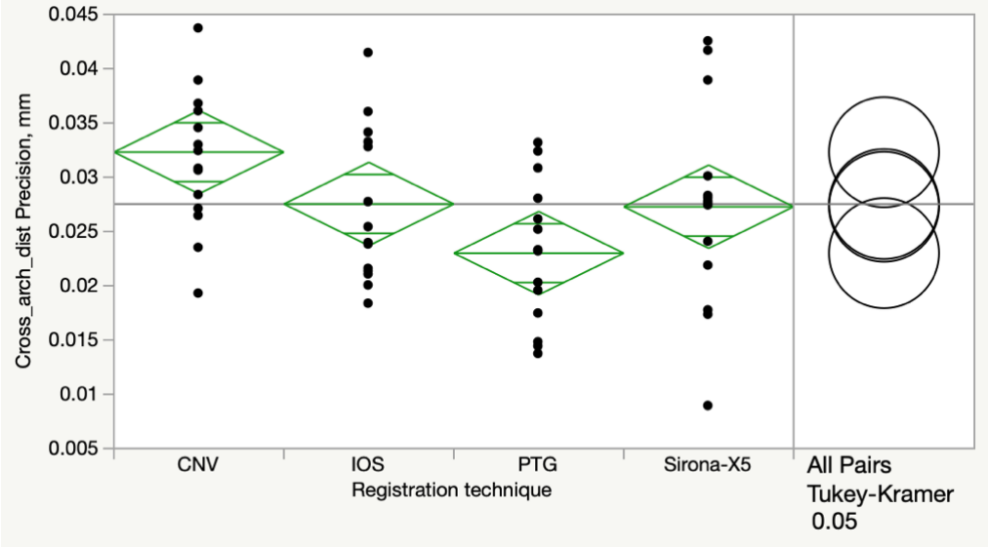

Figure 73. Oneway Analysis of Cross-arch distance (precision) mean using Iscan3D Origin coordinate by Registration technique**.**

Table 32. Connecting-Letters Report of cross-arch distances mean (precision) using Iscan3D Origin coordinates

Level			Mean, µm
CNV	A		0.0323
IOS	A	B	0.0275
Sirona-X5	A	B	0.0273
PTG		B	0.0230

Tukey-Kramer HSD; Levels not connected by the same letter are significantly different.

Table 33. Ordered differences report of Cross-arch distance (precision) mean using Iscan3D Origin coordinate by Registration technique.

Level	- Level	Difference	Std Err Dif	Lower CL	Upper CL	p-Value
CNV	PTG	0.0093	0.0027	0.0021	0.0165	0.0060*
CNV	Sirona-X5	0.0050	0.0027	-0.0021	0.0122	0.2586
CNV	IOS	0.0048	0.0027	-0.0024	0.0120	0.3010
IOS	PTG	0.0045	0.0027	-0.0026	0.0117	0.3475
Sirona-X5	PTG	0.0043	0.0027	-0.0029	0.0115	0.3975
IOS	Sirona-X5	0.0003	0.0027	-0.0069	0.0074	0.9997

Tukey-Kramer HSD post hoc test was used to identify significant differences between registration techniques in terms of cross-arch distance precision using the Origin points as the

coordinates (Figure 73). There was a significant difference in the precision of cross-arch deviations between CNV and PTG (p = 0.0060). IOS and PTG (p=0.3475) and IOS and CNV (p = 0.3010) were not statistically different from each other (Table 32 and 33).

4.4.3 Cross-arch deviations: understanding distance deviation

In this study, starting from the maxillary right posterior, all six scan bodies were numbered from 1 to 6. Distance (D) is expressed by scan body numbers: D12, D13, D14, D15, D16, D23, D24, D25, D26, D34, D35, D36, D45, D46, D56 (Figure 20).

Table 34. Connecting-Letters Report of cross-arch distances deviation (trueness) using Iscan3D Origin coordinates by A. Distance B. Registration technique

A.

Level							Least Sq Mean
D26	A						0.0674
D16	A	B					0.0584
D45	A	B					0.0545
D56	A	B	C				0.0516
D36	A	B	C	D			0.0481
D25		B	C	D	E		0.0423
D12		B	C	D	E		0.0412
D35			C	D	E	F	0.0330
D13				D	E	F	0.0290
D15				D	E	F	0.0284
D24					E	F	0.0251
D46					E	F	0.0243
D34					E	F	0.0239
D14					E	F	0.0224
D23						F	0.0196

B.

Level			Least Sq Mean
CNV	A		0.0488
IOS		B	0.0385
PTG		B	C 0.0353
Sirona-X5			C 0.0293

Tukey-Kramer HSD; Levels not connected by the same letter are significantly different.

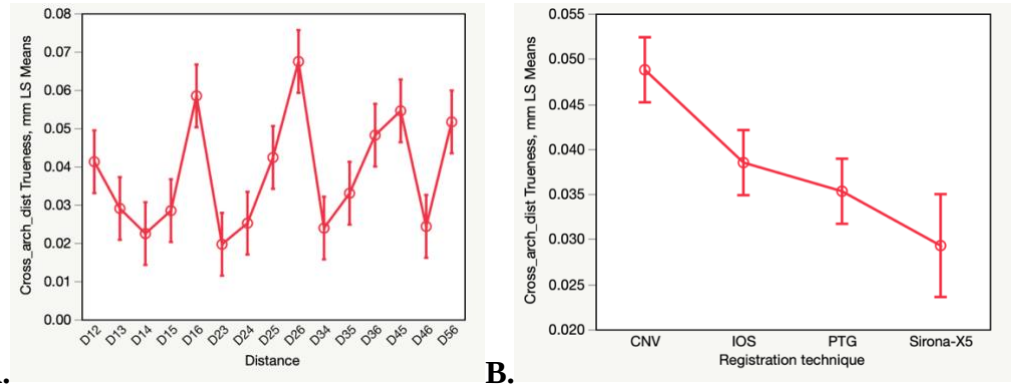

A. **B.**

Figure 74. Least squares mean plot of cross-arch distances mean (trueness) using Iscan3D Origin coordinates by A. Distance B. Registration technique

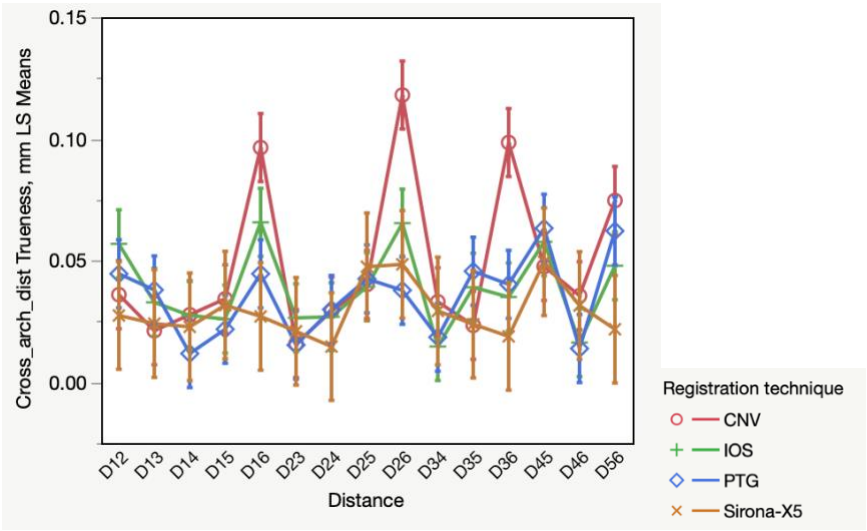

Figure 75. Least squares mean plot of registration technique by distance in response to cross-arch distance deviation values (Trueness)

Overall, the CNV group presented the highest deviations in terms on cross-arch distances trueness values, followed by the IOS group and finally the PTG group (Table 34). The graphs above (Figure 74 and 75) demonstrates that distance D26 (implant #2 to implant #6) had the highest deviations in all three groups and the lowest deviation was revealed in D23 (implant #2 to implant #3) in all groups.

4.4.4 Deviations in the X, Y and Z coordinates.

The absolute deviation data in the X, Y and Z coordinates using the Iscan3D Origin coordinates is summarized in Table 35 and an effect summary of registration technique, implant ID, and registration technique × implant ID is presented (Table 36).

Table 35. Overall effect summary of compared point absolute deviations and x, y z deviations

	Abs_Dev_X			Abs_Dev_Y			Abs_Dev_Z		
Registration technique	**N**	**Mean**	**Std Dev**	**N**	**Mean**	**Std Dev**	**N**	**Mean**	**Std Dev**
CNV	60	0.0339	0.0244	60	0.0289	0.0182	60	0.0167	0.0137
IOS	60	0.0244	0.0180	60	0.0377	0.0247	60	0.0251	0.0123
PTG	60	0.0191	0.0159	60	0.0229	0.0126	60	0.0041	0.0032
inEOS X5	24	0.0201	0.0139	24	0.0236	0.0139	24	0.0037	0.0024

Table 36. Effect summary of registration technique, implant ID, and registration technique*implant ID

Source	LogWorth	PValue
Registration technique	29.450	0.00000
Implant ID	7.279	0.00000
Registration technique*Implant ID	5.443	0.00000

Table 37. Connecting-Letters Report of Absolute deviations mean using Iscan3D Origin coordinates by A. Registration technique. B. Implant ID

A.

Level		Least Sq Mean
IOS	A	0.0569
CNV	A	0.0536
inEOS X5	B	0.0343
PTG	B	0.0332

B.

Level		Least Sq Mean
IMP 2	A	0.0522
IMP 6	A	0.0521
IMP 5	A	0.0507
IMP 3	B	0.0377
IMP 1	B	0.0375
IMP 4	B	0.0367

Tukey-Kramer HSD; Levels not connected by the same letter are significantly different.

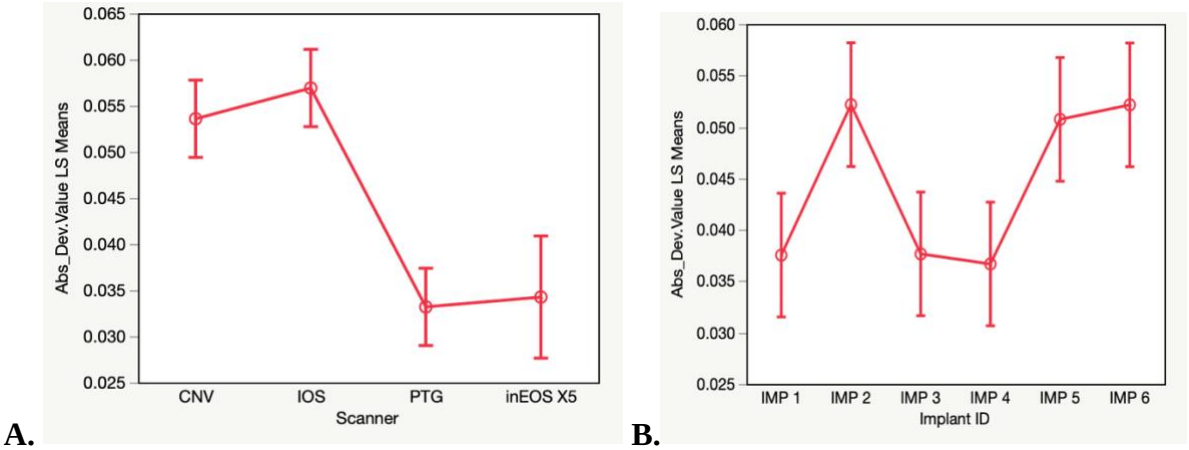

Figure 76. Least squares mean plot of Absolute deviation values (in XYZ coordinates) by A. Registration technique; B. Implant ID

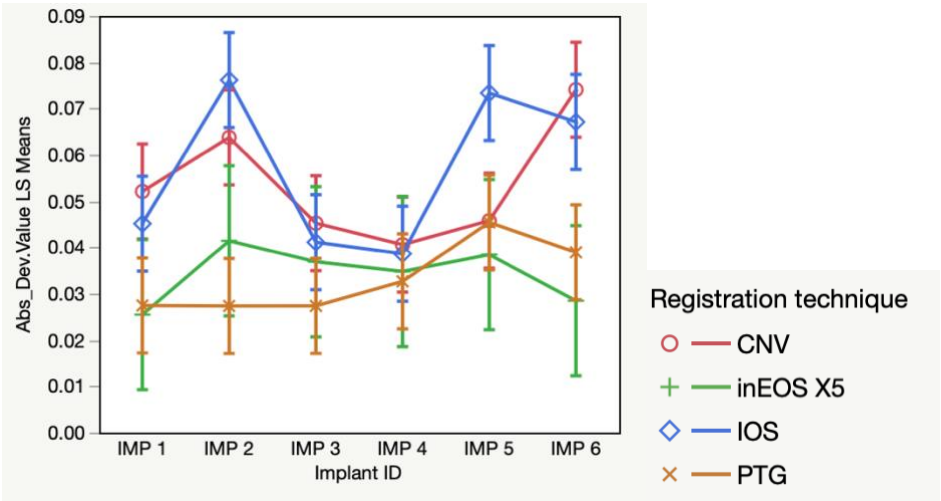

Figure 77. Least squares mean plot of registration technique by implant ID in response to Absolute deviation values (in XYZ coordinates)

Overall, the IOS group presented the highest deviations in the X, Y, Z coordination system, followed by the CNV group and finally the PTG group (Table 37). The graphs above (Figure 76 and 77) showed that implant #2, #5 and #6 had the highest deviations in all three groups and the lowest deviation was observed on implant #4.

Table 38. Connecting-Letters Report of Absolute deviations mean of the X Coordinate using Iscan3D Origin coordinates by A. Registration technique. B. Implant ID

A.

Level		Least Sq Mean
CNV	A	0.0339
IOS	B	0.0244
inEOS X5	B	0.0201
PTG	B	0.0191

B.

Level		Least Sq Mean
IMP 6	A	0.0402
IMP 2	B	0.0251
IMP 5	B	0.0248
IMP 1	B	0.0214
IMP 4	B	0.0181
IMP 3	B	0.0166

Tukey-Kramer HSD; Levels not connected by the same letter are significantly different.

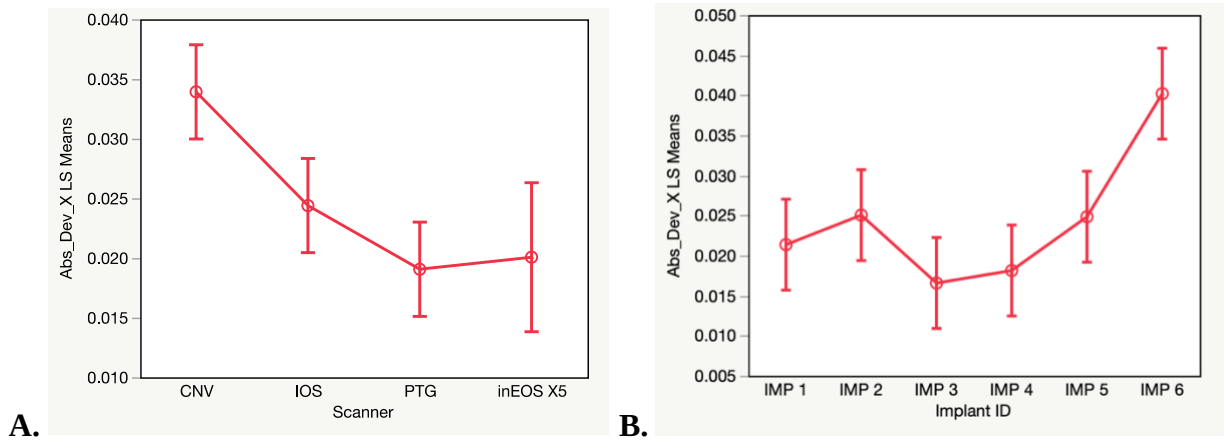

Figure 78. Least squares mean plot of Absolute deviation values X coordinate by A. Registration technique; B. Implant ID

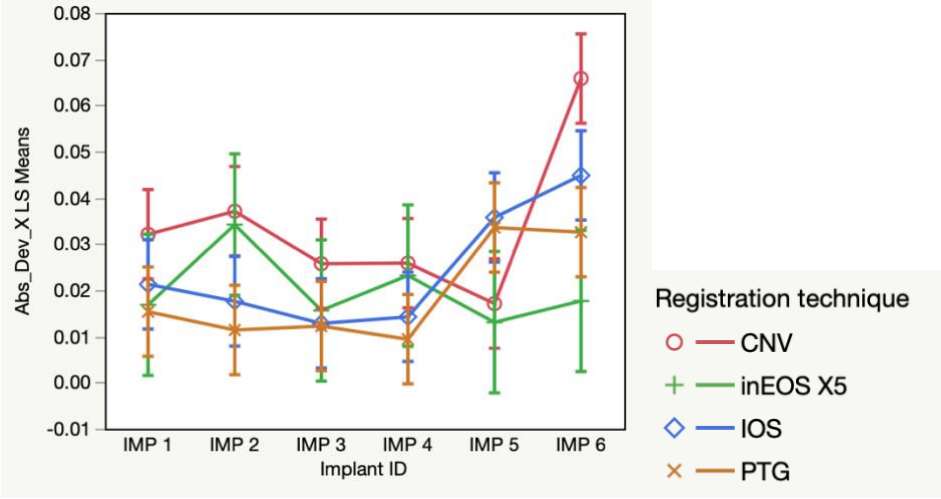

Figure 79. Least squares mean plot of registration technique by implant ID in response to Absolute deviation values in X coordinates**.**

In terms of deviations on the X axis of the coordinate system, the CNV group presented the highest deviations (Table 38). The graphs above (Figure 78 and 79) showed that implant #6 had the highest deviations in all three groups.

Table 39. Connecting-Letters Report of Absolute deviations mean of the Y Coordinate using Iscan3D Origin coordinates by A. Registration technique. B. Implant ID

A.

Level			Least Sq Mean
IOS	A		0.0377
CNV		B	0.0289
inEOS X5		B	0.0236
PTG		B	0.0229

B.

Level			Least Sq Mean
IMP 2	A		0.0387
IMP 5	A		0.0379
IMP 3	A	B	0.0280
IMP 4		B	0.0245
IMP 6		B	0.0236
IMP 1		B	0.0168

Tukey-Kramer HSD; Levels not connected by the same letter are significantly different.

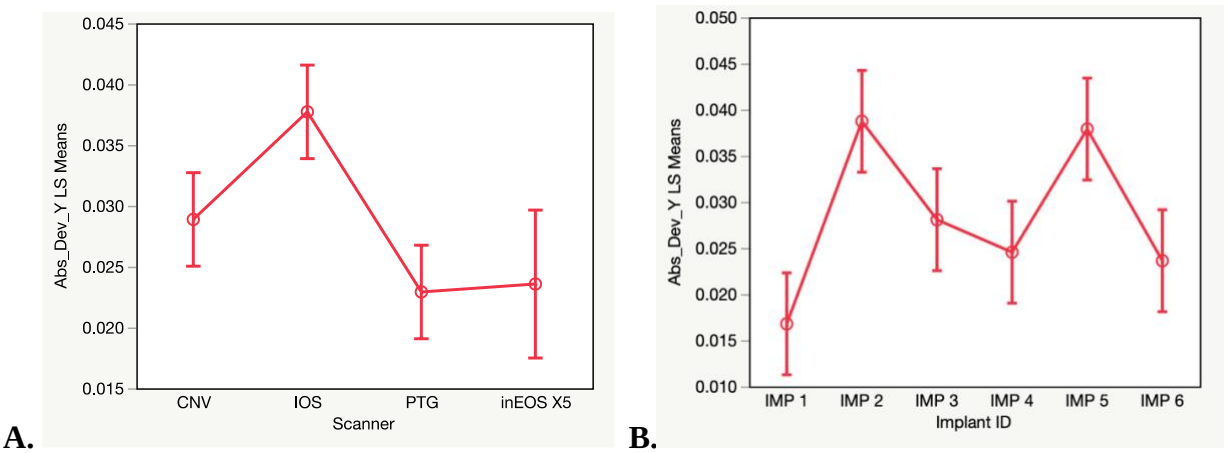

Figure 80. Least squares mean plot of Absolute deviation values Y coordinate by A. Registration technique; B. Implant ID

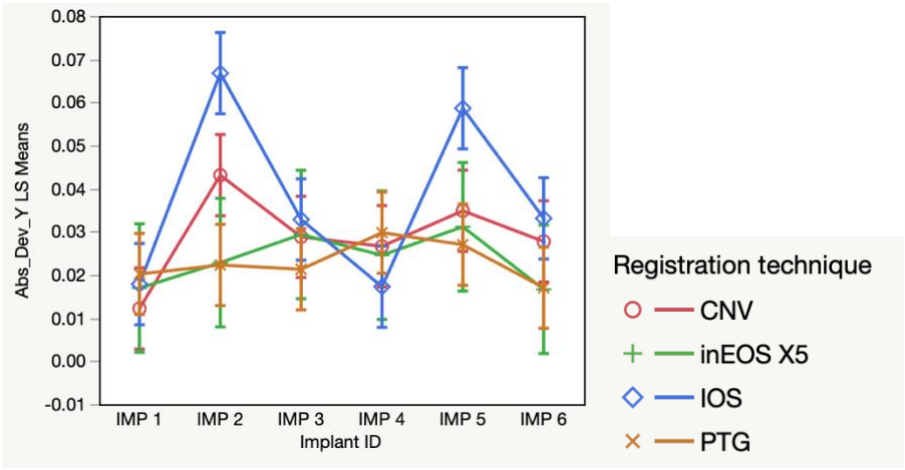

Figure 81. Least squares mean plot of registration technique by implant ID in response to Absolute deviation values in Y coordinates.

In terms of deviations on the Y axis of the coordinate system, the IOS group presented the highest deviations (Table 39). The graph above (Figure 80 and 81) demonstrated that implants #2 and #5 had the highest deviations in all three groups with implant #1 having the smallest**.**

Table 40. Connecting-Letters Report of Absolute deviations mean of the Z Coordinate using Iscan3D Origin coordinates by A. Registration technique. B. Implant ID

A.

Level				Least Sq Mean
IOS	A			0.0251
CNV		B		0.0168
PTG			C	0.0041
inEOS X5			C	0.0037

B.

Level			Least Sq Mean
IMP 1	A		0.0173
IMP 2	A	B	0.0142
IMP 6	A	B	0.0120
IMP 5	A	B	0.0108
IMP 4		B	0.0105
IMP 3		B	0.0095

Tukey-Kramer HSD; Levels not connected by the same letter are significantly different.

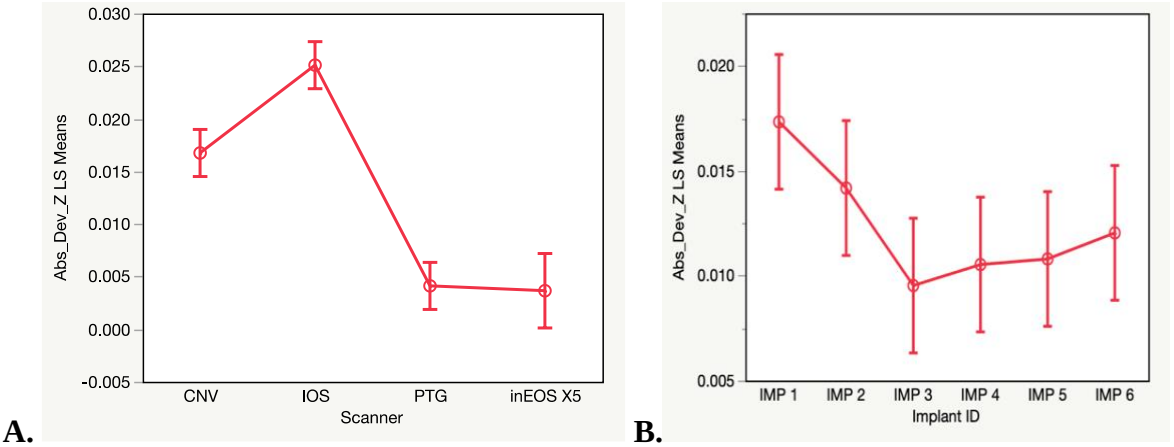

Figure 82. Least squares means plot of Absolute deviation values Z coordinate by A. Registration technique; B. Implant ID

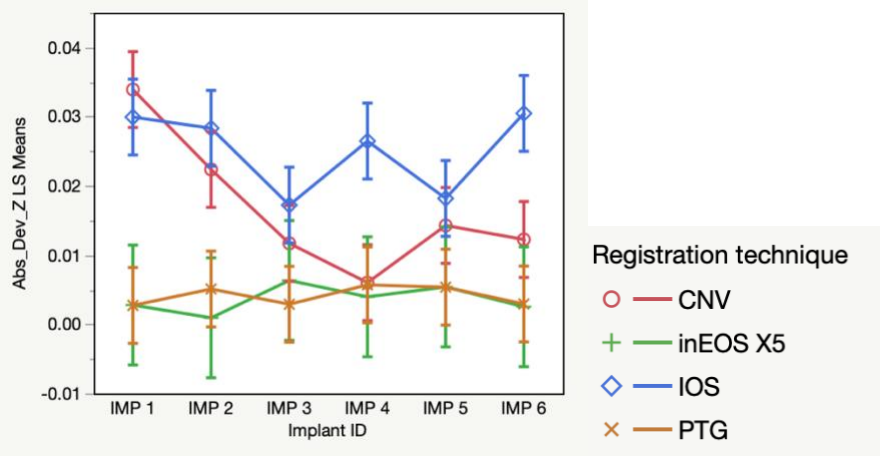

Figure 83. Least squares means plot of registration technique by implant ID in response to Absolute deviation values in Z coordinates.

In terms of deviations on the Z axis of the coordinate system, the IOS group presented the highest deviations, followed by the CNV and least in the PTG group (Table 40). The graph above (Figure 82 and 83) showed that implant #1 had the highest deviations overall in all three groups, while implant #3 had the smallest.

Chapter 5: DISCUSSION

The results of 3D deviations, global angular deviations, and cross-arch distance deviations led to reject the null hypothesis that no significant differences exist between the accuracy of IOS, PTG and CNV.

5.1 3D Comparison test and Angular deviation test

The photogrammetry technique showed the best results in terms of trueness and precision when analyzing the 3D deviations of the whole analog surface using one inspection software (IScan4D Dental), and the projected axis from the origin point using another inspection software for spatial similarity transformation (IScan3D Dental). The photogrammetry group was followed by the CNV group and finally the IOS group for this test.

According to the literature, the acceptable linear threshold is considered to be between 10 to 150 µm and the acceptable angular deviation is 0.2-0.5 degrees.(32)(69)(70) These levels of error, referred to as the mechanical tolerance, are considered to not cause technical or biological complications.(71)

In terms of global angular deviation, the conventional impression technique and the photogrammetry technique did not show statistical significance ($p=0.7955$) and presented equivalent results. The IOS group showed the most angular deviation and was statistically significant to the two other groups. This was also confirmed using the RMS values from Origin and Origin + Z as the graphs reveal the same pattern of results, showing the deviation in the PTG, IOS and CNV groups with IOS presenting the highest discrepancy between the Origin and Origin+Z values, validating the results obtained on the Geomagic inspection software. The results of this study are in accordance with those of Sallorenzo et al (54) which showed that the global

angular deviation for the IOS group was higher and that the PTG group met the clinically acceptable threshold.

The conventional impressions produced more accurate results in terms of trueness than the IOS group when comparing 3D deviations of the entire analog surface (Iscan4D Dental) and "Axis projection" (Iscan3D Dental), as well as comparing the global angular deviations. Although some studies have reported that the accuracy of intraoral scanner can be comparable to the conventional impression technique(46)(52)(72) or produce better results (28)(73), others showed that the conventional impression technique was still more accurate which was inconsistent with previous studies that reported that IOS produced better results.(39)(48) A consensus has not yet been reached despite numerous research comparing the accuracy of intraoral scanners in full arch implant rehabilitation to the traditional impression technique.

These results may be partially explained by the fact that the conventional impression group did not replicate the volumetric contraction linked to temperature difference between the oral cavity (37°C) and the room temperature (22±2°C), which can normally produce dimensional changes averaged more than 40 μm in the anterior region and less than 40 μm in the posterior region.(74) Although polyethers are not truly hydrophilic materials, research has shown that if humidity levels are increased, the accuracy may be affected by the dimensional changes.(75) In this study, the impressions were made and poured under controlled temperature and humidity conditions (22±2°C, 40±10%).

On the other hand, the operator experience and the scanning protocol recommended by the manufacturer were amongst the accuracy influencing factors that were controlled for the intraoral

scan groups. For both photogrammetry and intraoral scan group, the ambient lighting conditions were the same and controlled at 805±7 lux.(38)

This study was conducted on 6 implants all planned in nearly parallel positions. While one systematic review has reported no effect on implant angulation for IOS group (76), other studies have shown that the angulation of the implant can affect the precision and trueness as increased angulation might facilitate scan body imaging.(33)(52)(54)(77)(78)(79)(80)

The possible low accuracy results for the IOS group are probably due to its' 3D images which are generated by a stitching method in which case a longer scan pathway with a lack of stable landmarks on the mucosal surface and an environment which can cause interference with the images (saliva, blood, humidity) may lead to the accumulation of errors.(81) In vivo studies have shown that using markers to create more landmarks (73)(82) or even splinting the scan bodies (83) can significantly improve the accuracy of the intraoral scanner for edentulous full arch implant restorations. The photogrammetry system tested in this study seems to be overcoming these limitations, as it has four cameras with a larger scanning range and faster scanning speed. It also allows for image acquisition to be done outside the mouth, which reduces the influence the oral cavity environment has on the accuracy of the scanner.

The position of the implant abutments obtained in photogrammetry is based on a different concept than IOS. All data measured in each capture from the photogrammetry system generates vectors of the exact position of the scan bodies in relation to one another using reference points which makes it possible to calculate the locations of scan bodies without image superimpositions, ensuring better accuracy. However, this technology can only record the position of the implant abutments and therefore requires another file to capture the soft tissue data and align them.

While this study is in accordance with others in terms of photogrammetry accuracy (47)(48)(54), Revilla-León et al reported different outcomes regarding the photogrammetry technique, which was the least accurate.(46) The different outcomes for the results may be due to the different methodologies that were followed in both studies.

5.2 Cross-arch distance test

In terms of the accuracies of cross-arch distances, the photogrammetry group showed better results followed by the intraoral scanning group and then the conventional group.

Regarding cross-arch distances, D23, where the distance between implants was one of the shortest, showed that the distance deviation was the lowest regardless of the impression groups, followed by D14, D34, D46, D24. The deviation was detected the most where the distance between implants was higher as seen on D16 and D26. This may be related to the fact that the scanning sequence always started with implant #1 and ended on implant #6. Since this scanning path was the longest, it would require the most stitching. Another study by Gómez-Polo et al. has reported that the implant positioned in the dental arch where the intraoral scan was finished obtained a significantly higher distortion than the contralateral implant.(77)

Photogrammetry was the group that showed overall the least deviations. Conventional impressions showed smaller deviations than intraoral scans where the distances between scan bodies were short. Intraoral scans showed however smaller deviations than conventional impressions where the distance between the scan bodies was increased. These findings are inconsistent with previous studies that have compared the effects of interimplant distances on the accuracy of digital and conventional impressions. Those differences may be related to the different methodologies used and the study designs chosen, which included different implant angulations.

Some studies showed that a decreased distance between the implants increased the accuracy of the intraoral scan (84)(85). However, in line with this research, Schmidt et al revealed that the longer the scanning distance is, the more the deviation. (86) Pozzi et al suggested that the curve of the arch may also affect the accuracy of the IOS.(83) They state that a collapse of the curvature radius occurred more in the mandibular arch, which has a narrower arch form, than on the maxillary arch. The authors also pointed out that the palatal vault can serve as a landmark to aid in the connection of the posterior implants.

Considering the deviations on the 3 axes of each implant, the photogrammetry technique demonstrated a significant better accuracy on the X-axis, Y-axis, and Z-axis. Those favorable results on the longitudinal, lateral and vertical axes may be justified by the fact that the photogrammetry system can overcome the potential scanning issues related to interimplant distances, which the intraoral scan and conventional could not.

In the present study, the X-axis (longitudinal) showed the highest deviation for the CNV group, which may be related to dimensional changes of the master casts.(20)(24)(87) There was however no statistically significant difference between the IOS and PTG groups. Compared to the other axes, the deviations observed in the Y-axis were overall greater in magnitude in all the groups, which is in accordance to some findings in previous studies conducted on different conventional impression techniques, intraoral scanners and photogrammetry.(24)(46)(83)(87) The Y-axis (lateral) showed the highest deviation in the IOS group. Further investigation is needed to understand the reason for such increased distortions in the Y-axis. The Z-axis (vertical) also showed highest deviation using the IOS technique, followed by the CNV group and finally the PTG group which showed the least deviations. The differences relating to better results for the

CNV group than the IOS may be related to the rigidity of the splinting material used which aided in preventing vertical movements of the impression copings during the connection to the implant abutment analogs. Overall, the fit or misfit of a prosthesis may result from the collective error caused by deviations in all of the axes, even though significant differences might not be present in all of them. Clinical scenarios which involve different number of implants, with increased interimplant distance, different angulations and implants depth could lead to an increase of the system's accuracy.(46)(54)

5.3 Methodology

The lack of standardization in the methods utilized should be considered when comparing recent research to earlier ones. Contributing factors that vary amongst different methodologies can include the master model, the reference STL file, the scan body design and positions, inspection software, measurement of mesh overlap, presence or absence of fixed reference points, and anatomical landmarks in the oral mucosa.(32)

The objective of the current study was to assess the accuracy of a registration technique under repeatable conditions when scanning a fully edentulous arch with implants. In order to obtain a control virtual file from the master model, several studies relied on an extraoral desktop scanner to obtain the reference STL file.(28)(47)(48)(88)(89)(90) Other studies have used the coordinate measuring machine (CMM) (39)(46)(91) based on tactile computer metric measurements that only goes around specific landmarks (such as scan bodies or spheres placed on the model), making it possible to calculate only certain points in the scan instead of comparing thousands of cloud points. However, due to the spherical shape and size of its probe which cannot detect undercuts, the CMM becomes less accurate when evaluating freeform planes.(49)

Research on the accuracy of photogrammetry systems is still limited and the results are inconsistent. In accordance with the findings of this study, Tohme et al (47) and Ma et al (48) reported that the photogrammetry system was more accurate than intraoral scanners and conventional impressions when using “best-fit” alignment methods to compare the different groups. In contrast, Revilla-León et al. (46) found that the photogrammetry system evaluated had the least accuracy when compared to intraoral scanning and conventional impressions when using a coordinate measuring machine to compare the different groups. It could be suggested that the opposite results may be linked to different study designs involving different reference files and measuring techniques.

The second phase of the study included scanning and digitizing the same master model by test groups (PTG, IOS, CNV), obtaining virtual models which were measured and compared to the reference file acquired with an extraoral laboratory scanner.

The most common inspection software used in studies is Geomagic Control X.(47)(48)(61) Unlike other CAD programs that initially align the virtual library file to the flat angled surface of the scan body, this inspection software evaluates all the point clouds that are available. However, this software is not developed specifically for dental purposes. When conducting the study primarily on the scan body level instead of the analog level, the STL files from the reference scan (inEOS X5), the IOS and the CNV groups that were already resegmented, were still surrounded by more point clouds.(61) The lack of uniformity for all groups led to standardize all STL files by maintaining the palatal reference with the markers to aid with merging and converting all scan bodies into a standardized multi-unit virtual analogs. Once the STL files were merged, the palatal reference was cropped out to get an RMS value specific to the implant positions. Tohme et al (47)

conducted their study on the scan body level and did not crop any of the surrounding structures, while Ma et al (48) conducted theirs on the analog level and did not use any landmark markers to aid in the merge of the different STL files.

In this study model, a “best fit alignment” method was used based on the iterative closest point concept to assess full-arch scans with implants on two of the inspection software tested. The 3D compare feature obtained presented a color map data with threshold colors to visualize differences between two scans. The third inspection software (IScan3D Dental) relied on a spatial similarity transformation based on the Helmert transformation concept. To the author’s knowledge, this is the first study to describe the use of spatial similarity transformation for the comparison of implant abutment level positions from different registration techniques in full-arch implant-supported prostheses.

While the digital workflow seems to have less steps than the conventional, it is important to understand the different sources of errors when it comes to scan bodies. The STL created from a digital scan using an IOS or an extraoral scanner only shows the scan bodies and not the implants. The file is then imported into a dental software program where the implant positions are calculated by superimposing the scan bodies from the digital scan file with the specific scan body from the software program's implant library. Any deviation found in the scan body will have an impact on the superimposition of the virtual library files and, consequently, on the orientation of the implant that is being transferred. Chia et al. suggested that errors may arise from the digital conversion of a scan body to a virtual implant abutment replica if there is no perfect fit, coaxiality or perfect mating between the two physical components.(92) Additionally, they stated that scan body

positions revealed a machining tolerance of up to 7 μm and that the amount of tightening force had an impact on the scan body's vertical position. Overall, it is important to note that both PTG and IOS require only one connecting procedure, whereas the CNV group would require at least two connecting procedures (connection from the impression coping to the implant abutment, and a connection from the impression coping to the implant abutment analog).

The outcome of a scan can be influenced by the choice of a scan body design depending on the different scanner technology, a consideration which needs further investigation.(30)(93) It has been demonstrated that the density of the point clouds generated during scanning affects how accurately the virtual surface is recreated. If any point clouds are missing, it will be challenging to reconstruct the surface, which would lead to errors when attempting to register and align the scan body surface with the implant library.(94) This problem was generally encountered with the IOS group during this study. Another factor which can also affect point cloud density is the characteristics of the surface of the scan body: dull, smooth, and opaque surfaces are simpler to scan in a challenging environment where saliva tends to generate reflective surfaces.(37) Studies have also shown that scan bodies designed with deep, angled surfaces or undercuts were more difficult to scan and resulted in less accurate point clouds. In the case of the scan bodies (ELOS accurate) used in this study for the reference STL file, the IOS group and the digitization of the CNV group, the software application (Exocad DentalCAD; Darmstadt, Germany) relied on the flat angled surface as a reference point to overlap with the virtual library file. Any errors of merge at this point can impact how the implant position is determined and in turn, affect the passivity of the implant-supported fixed complete-arch prosthesis.(30)(40)(95)

In terms of scan body height, Gómez-Polo et al (96) revealed that the lowest clinical implant scan body height tested, which was 3 mm, had significantly higher linear and angular

measurement discrepancies amongst the different clinical implant scan body heights of 6 mm and 10 mm. In the present study, Iscan3D's Origin + Z axis point was a 10 mm projection from the center of the implant, which indicated the height of an ideal scan body. This allowed for the reliability on the measurement done which was correlated with Geomagic's analysis on the scan body surface.

Although this was not in the scope of the study, when comparing scan body positions, the results showed an increase in deviations if the scan bodies were repositioned between each scan. One study reported that scan bodies on laboratory analogs exhibited higher reproducibility of fit compared to original implants, suggesting that discrepancies exist in the machining tolerances between the components. The article stated that there was a production tolerance of about 15 μm that could go up to 25 μm.(97) Another study suggests that the machining tolerances between different implant components may vary from 22 to 100 μm.(13) The geometric design and size of most implant-abutment connections affect the rotational freedom of the positional index.(98) Semper demonstrated that, in case of rotational discrepancy, if implants are inserted parallel to each other, there won't be any horizontal shift. However, if the implants are angulated, the rotational misfit can cause a horizontal discrepancy.(99) Increased torque was also demonstrated to result in positional discrepancies of the scan bodies.(53) Since the present study represented a scenario where all implants were nearly parallel, the increased horizontal discrepancies in the CNV group and lateral discrepancies in the IOS group may have an impact on the fit of the final prostheses. Looking at the vertical axis, the Z-axis may not have a significant impact for the CNV group as much as it would on the IOS group where the absolute deviations were around 16.8 μm and 25.1 μm, respectively. It has been reported that a vertical gap of 50 to 100 μm can be compensated by turning the screw an extra half turn to connect the different components.(17)(100)

This technique however may not be applicable in all implant systems, since the prosthetic screws do not have the same designs.(17)(71)(101) However, in most clinical scenarios involving implant-supported full-arch prostheses, due to the inadequate amount of bone in the arch, implants are placed at different angulations and are rarely ever parallel to each other. It may be suggested in the scenario where the implants are angulated that the higher angular deviations found in the IOS group may in turn affect the horizontal discrepancies, and that the increased deviations in the X- and Y-axes found in the parallel scenario could lead to less tolerance and leeway for a passive fit.

When it comes to capturing information from the scan body over the implant, scanners and photogrammetry work in different ways. Photogrammetry uses a scan body that presents white markers called “targets” on its 4 surfaces. The scan body should be positioned so that the edge is facing the camera, and a minimum capture of three of targets on two surfaces is considered enough to measure the 3D position of the implant. However, scanning must capture at least 180 degrees of the intraoral scan body surface along with the top of the scan body in order to register the position of the implant (Figure 84). It is also important to mention that the photogrammetry system (ICam4D, Imetric4D Imaging Sàrl) uses a different scanning transfer for data formation and a different file output exported, which may explain why photogrammetry seems to get the best accuracy. The photogrammetry system also only records the implants’ position. Additional steps are required to obtain the soft tissue and occlusal relationship of the oral cavity which involves the superimposition of yet another STL file.

Figure 84. Photogrammetry vs IOS scan body design.
A: View from the top showing targets/surfaces that need to be scanned for proper registration for photogrammetry vs scanners; B: Scan bodies used in the study represented by scanning surface that is necessary for registration.

Amongst other factors which may affect the accuracy of digital scans with multiple scan bodies are the distance between them, the implant depth, and their location within the scan.(53)

5.4 Limitations of this study

This in vitro study did not fully replicate the conditions of the oral cavity and the complex interplay of biological and anatomical factors which could affect a system's accuracy, specifically with IOS where the impact of stitching images is greater.(102) This study aided in getting an optimal scan and ideal settings for making conventional impressions which did not account for volumetric contraction relating to different temperatures. In vivo studies have reported greater discrepancies and lower precision than in vitro studies.(103) In addition, the markers which were manually and purposely added on the palatal area of the master model to aid in merging two STL files for comparison did not reproduce a clinical situation but were necessary for the study design chosen.

Within the limitations of this study, the inspection software used which relied on a "best-fit" algorithm are likely to underestimate the size of the defect and errors that are available in the

data set.(61) The study was also conducted on implant abutment replicas, instead of implant abutments, or the implant interface. Connecting errors may exist between different components and should be accounted for.(27)

There is no ideal reference value for the implant position, and there is still no way to obtain the exact coordinates. The evaluation of trueness in this study was based on the decision to choose a reference from a desktop scanner as previous literature has shown. Determination of that decision was based on the company statements that the machine has an accuracy of 2.1 μm and on the pilot study to verify the precision of the system. The trueness of a system is even harder to evaluate in clinical studies as a "gold standard" is yet to be determined. In this case, the precision or repeatability of a system is more important than the trueness, and a more reliable measurement to look at.

Finally, regarding the scan bodies, the baseline studies showed that the scan body position between each scan can affect the repeatability and the reproducibility of the registration technique. To standardize the methodology in all the groups, the scan body positions were changed between each registration. This factor could have influenced the results of this study. In addition, in the present study, different scan body surfaces from one system to another prevented the use of the scanned STL files for comparisons and opted for the use of CAD files generated through a dental software. This was also done to standardize the object of comparison, which was the virtual multi-unit analog is this case. The generated files had less point clouds than the scanned STL files. The results obtained from the 3D comparison of the CAD files and scanned files on one of the inspection software (Geomagic Control X 2020.1; 3D Systems) used in this experiment did not get correlated values for the same scan IDs. However, the Iscan4D software had a great correlation between the CAD files and scanned files. This method of converting the scan bodies through the

dental software's implant library may also be considered as a way to replicate the entire CAD workflow before the CAM process which is used in everyday framework fabrication.

5.5 Recommendations for future studies

Further in vitro and clinical studies are required to confirm these results and explore their clinical relevance. Moreover, additional studies are needed to unravel the complexity of the methodology used for superimposition and comparison. A standardization of the methodology for the study of edentulous arches with implants for full-arch implant-supported prostheses should be made to compare results between each other.

The relevance of these deviations in each registration group should be physically interpreted by examining the passive fit and determining the misfit of the frameworks fabricated. The indication to conduct those measurements at a prosthetic level would also allow to obtain an idea of the entire CAD/CAM process involved with the IOS group and the PTG group.

A better understanding should be made on scanner technology and scan body digitization and improvement of machining tolerances. Variables such as the interimplant distance, number, angle and depth of the implants should also be further examined, and more studies should be done on the implant abutment level and on the implant level.

Finally, further research is needed to investigate the accuracy of different photogrammetry systems on the market.

Chapter 6: CONCLUSIONS

Based on the findings of this in vitro study, the following conclusions were drawn:

1- Whether tested through the spatial similarity method or through a best-fit alignment algorithm, the photogrammetry technique had the lowest 3D deviations and cross-arch distance deviations. It also showed the least deviations in the X-axis (horizontal axis), Y-axis (lateral axis) and Z-axis (vertical axis). Overall, the photogrammetry technique reported the best accuracy in terms of trueness and precision for complete-arch implant rehabilitation.

2- The angular deviation was equivalent for both the PTG group and the CNV group.

3- The IOS group showed the highest deviations in both 3D comparisons and angular deviations but had better accuracy than the CNV group in terms of cross-arch distances.

4- The IOS group exhibited the largest deviations in the Y-axis (lateral axis) and Z-axis (vertical axis) whereas the CNV group had the largest deviations in the X-axis (horizontal axis).

5- Different methodologies can lead to different values of deviations observed in edentulous arches with implants for implant-supported prostheses, and sometimes to different results. It is of crucial importance to understand how inspection software work and to conduct baseline studies in order to understand the results.

LIST OF ABBREVIATED JOURNAL TITLES

Abbreviation	Journal Title
Clin Oral Impl Res	Clinical Oral Implants Research
Dent Mater	Dental Materials
Eur J Oral Implantol	European Journal of Oral Implantology
J Clin Exp Dent	Journal of Clinical and Experimental Dentistry
J Dent	Journal of Dentistry
J Prosthet Dent	Journal of Prosthetic Dentistry

BIBLIOGRAPHY

1. The Glossary of Prosthodontic Terms: Ninth Edition. J Prosthet Dent. 2017 May;117(5S):e1-e105. doi: 10.1016/j.prosdent.2016.12.001. PMID: 28418832.

2. Bugugnani R, Landez C. Les empreintes en prothèse conjointe. Paris CdP. 1979;109–337.

3. Bidra AS RPGM. Clinical outcomes of full arch fixed implant-supported zirconia prostheses: A systematic review. Eur J Oral Implantol. 2017 Jan; 10(Suppl 1).

4. Aous A. Abdulmajeed KGLTONLFC. Complete-arch implant-supported monolithic zirconia fixed dental prostheses: A systematic review. J Prosthet Dent. 2016; 115.

5. Gonzalez J, Triplett RG: Complications and clinical considerations of the implant-retained zirconia complete-arch prosthesis with various opposing dentitions. Int J Oral Maxillofac Implants 2017;32:864-869.

6. Carames J, Marques D, Malta Barbosa J, et al: Full-arch implant-supported rehabilitations: a prospective study comparing porcelain veneered zirconia frameworks to monolithic zirconia. Clin Oral Implants Res 2019;30:68-78.

7. Pradíes G, Ferreiroa A, Özcan M, Giménez B, Martínez-Rus F. Using stereophotogrammetric technology for obtaining intraoral digital impressions of implants. J Am Dent Assoc. 2014 Apr;145(4):338-44. doi: 10.14219/jada.2013.45. PMID: 24686966.

8. Kioleoglou I, Pissiotis A, Michalakis K. Accuracy of fit of implant-supported bars fabricated on definitive casts made by different dental stones. J Clin Exp Dent. 2018 Mar 1;10(3):e252-e263. doi: 10.4317/jced.54603. Erratum in: J Clin Exp Dent. 2019 Jan 1;11(1):e104. PMID: 29721227; PMCID: PMC5923891.

9. Sahin, S.; Cehreli, M.C. The Significance of Passive Framework Fit in Implant Prosthodontics: Current Status. Implant Dent. 2001, 10, 85–92.

10. Tan, K.B. The Clinical Significance of Distortion in Implant Prosthodontics: Is There Such a Thing as Passive Fit? Ann. Acad. Med. Singap. 1995, 24, 138–157.

11. Jemt T, Lekholm U. Measurements of bone and framework deformations induced by misfit of implant superstructures. A pilot study in rabbits. Clin Oral Impl Res. 1998;9:272-280.

12. Spazzin AO, Dos Santos MB, Sobrinho LC, Consani RLX, Mesquita MF. Effects of horizontal misfit and bar framework material on the stress distribution of an overdenture-retaining bar system: a 3D finite element analysis. J Prosthodont. 2011;20:517-522.

13. Ma T, Nicholls JI, Rubenstein JE (1997) Tolerance measurements of various implant components. Int J Oral Maxillofac Implants 12:371–375.

14. Schüpbach P. Oral communication, panel discussion. Nobel Biocare Study Club Bern, Switzerland. 2016.

15. Brånemark PI. Osseointegration and its experimental background. J Prosthet Dent 1983;50:399–410.

16. Abduo JA, Lyons KL. Effect of vertical misfit on strain within screw-retained implant titanium and zirconia frameworks. J Prostho- dont Res. 2012;56:102-109.

17. Jemt T. Failures and complications in 391 consecutively inserted fixed prostheses supported by Branemark implants in edentulous jaws: a study of treatment from the time of prosthesis placement to the first annual checkup. Int J Oral Maxillofac Implants 1991;6:270–276.

18. Wennerberg, A.; Albrektsson, T. Current Challenges in Successful Rehabilitation with Oral Implants. J. Oral Rehabil. 2011, 38, 286–294.

19. Lee Y, Heo SJ, Koak JY, Kim SK. Accuracy of different impression techniques for internal-connection implants. Int J Oral Maxillofac Implants 2009;24(5):823-830.

20. Vigolo P, Fonzi F, Majzoub Z, Cordioli G. An evaluation of impression techniques for multiple internal connection implant prostheses. J Prosthet Dent 2004;92(5):470-476.

21. Vigolo P, Majzoub Z, Cordioli G. Evaluation of the accuracy of three techniques used for multiple implant abutment impressions. J Prosthet Dent 2003;89(2):186-192.

22. Lee H, So JS, Hochstedler JL, Ercoli C. The accuracy of implant impressions: a systematic review. J Prosthet Dent 2008;100:285-91.

23. Kim JH, Kim KR, Kim S. Critical appraisal of implant impression accuracies: a systematic review. J Prosthet Dent 2015;114:185-92.

24. Hsu CC, Millstein PL, Stein RS. A comparative analysis of the accuracy of implant transfer techniques. J Prosthet Dent 1993; 69(6):588-593.

25. Stimmelmayr M, Guth JF, Erdelt K, Happe A, Schlee M, Beuer F. Clinical study evaluating the discrepancy of two different impression techniques of four implants in an edentulous jaw. Clin Oral Investig 2013;17(8):1929-1935.

26. Michalakis KX, Asar NV, Kapsampeli V, Magkavali-Trikka P, Pissiotis AL, Hirayama H. Delayed linear dimensional changes of five high strength gypsum products used for the fabrication of definitive casts. J Prosthet Dent. 2012;108:189–95.

27. Kim S, Nicholls JI, Han CH, Lee KW. Displacement of implant components from impressions to definitive casts. Int J Oral Maxillofac Implants. 2006;21:747–55.

28. Amin S, Weber HP, Finkelman M, El Rafie K, Kudara Y, Papaspyridakos P. Digital vs. conventional full-arch implant impressions: A comparative study. Clin Oral Implants Res 2017;28:1360-7.

29. “Active Systems: Short Range.” Active Systems: Short Range - Share 3D Guidelines, 2020, https://carare.gitbook.io/share-3d-guidelines/3d-process/data-capture/short-range-techniques.

30. Mizumoto RM, Yilmaz B. Intraoral scan bodies in implant dentistry: A systematic review. J Prosthet Dent. 2018 Sep;120(3):343-352. doi: 10.1016/j.prosdent.2017.10.029. Epub 2018 Apr 5. PMID: 29627211.

31. 3D Systems. Geomagic Design X User Guide. [Online].; 2013 [cited 2022 July. Available from: https://www.engineeringx.pitt.edu/uploadedFiles/_Content/Sub_Sites/Business/MRW/SCPI/_Library/specs/geomagicdesignx2014userguide.pdf.

32. Andriessen FS, Rijkens DR, van der Meer WJ, Wismeijer DW. Applicability and accuracy of an intraoral scanner for scanning multiple implants in edentulous mandibles: a pilot study. J Prosthet Dent 2014;11:186-94.

33. Giménez B, Özcan M, Martínez-Rus F, Pradíes G. Accuracy of a digital impression system based on active triangulation technology with blue light for implants: effect of clinically relevant parameters. Implant Dent 2015;24: 498-504.

34. Beuer F, Schweiger J, Edelhoff D. Digital dentistry: an overview of recent developments for CAD/CAM generated restorations. Br Dent J 2008; 204(9):505-511.

35. Pradíes G, Zarauz C, Valverde A, Ferreiroa A, Martínez-Rus F. Clinical evaluation comparing the fit of all-ceramic crowns obtained from silicone and digital intraoral impressions based on wavefront sampling technology. J Dent. févr 2015;43(2):201-8.

36. Müller P, Ender A, Joda T, Katsoulis J. Impact of digital intraoral scan strategies on the impression accuracy using the TRIOS Pod scanner. Quintessence Int 2016;47:343-9.

37. Kurz M, Attin T, Mehl A. Influence of material surface on the scanning error of a powder-free 3D measuring system. Clin Oral Investig. 7 mars 2015.

38. Revilla-León M, Subramanian SG, Özcan M, Krishnamurthy VR. Clinical study of the influence of ambient light scanning conditions on the accuracy (trueness and precision) of an intraoral scanner. J Prosthodont 2020;29: 107-13.

39. Tan MY, Yee SHX, Wong KM, Tan YH, Tan KBC. Comparison of three-dimensional accuracy of digital and conventional implant impressions: Effect of interimplant distance in an edentulous arch. Int J Oral Maxillofac Implants 2019;34:366-80.

40. Arcuri L, Pozzi A, Lio F, Rompen E, Zechner W, Nardi A. Influence of implant scanbody material, position and operator on the accuracy of digital impression for complete-arch: A randomized in vitro trial. J Prosthodont Res 2020;64:128-36.

41. Lie A, Jemt T. Photogrammetric measurements of implant positions: description of a technique to determine the fit between implants and superstructures. Clin Oral Implants Res 1994; 5(1):30-36.

42. Bratos M, Bergin JM, Rubenstein JE, Sorensen JA. Effect of simulated intraoral variables on the accuracy of a photogrammetric imaging technique for complete-arch implant prostheses. J Prosthet Dent. 2018 Aug;120(2):232-241. doi: 10.1016/j.prosdent.2017.11.002. Epub 2018 Mar 17. PMID: 29559220.

43. Mikhail EM, Bethel JS, McGlone JC. Introduction to Modern Photogrammetry. New YorkL: Wiley; 2001:473.

44. Willomitzer, F. (2019). State of the Art: The Basic Principles of Optical 3D Metrology. In: Single-Shot 3D Sensing Close to Physical Limits and Information Limits. Springer Theses. Springer, Cham. https://doi-org.ezproxy.bu.edu/10.1007/978-3-030-10904-2_3.

45. Geoditic Systems. What is Photogrammetry. [Online].; 2020 [cited 2022 July. Available from: https://www.geodetic.com/v-stars/what-is-photogrammetry/.

46. Revilla-León M, Att W, Özcan M, Rubenstein J. Comparison of conventional, photogrammetry, and intraoral scanning accuracy of complete-arch implant impression procedures evaluated with a coordinate measuring machine. J Prosthet Dent. 2021 Mar;125(3):470-478. doi: 10.1016/j.prosdent.2020.03.005. Epub 2020 May 6. PMID: 32386912.

47. Tohme H, Lawand G, Chmielewska M, Makhzoume J. Comparison between stereophotogrammetric, digital, and conventional impression techniques in implant-supported fixed complete arch prostheses: An in vitro study. J Prosthet Dent. 2021 Jun 7:S0022-3913(21)00269-9. doi: 10.1016/j.prosdent.2021.05.006. Epub ahead of print. PMID: 34112521.

48. Ma B, Yue X, Sun Y, Peng L, Geng W. Accuracy of photogrammetry, intraoral scanning, and conventional impression techniques for complete-arch implant rehabilitation: an in vitro comparative study. BMC Oral Health. 2021 Dec 10;21(1):636. doi: 10.1186/s12903-021-02005-0. PMID: 34893053; PMCID: PMC8665494.

49. Ender A, Mehl A. Accuracy of complete-arch dental impressions: A new method of measuring trueness and precision. J Prosthet Dent 2013;109:121-8.

50. ISO 5725-1. Accuracy (trueness and precision) of measuring methods and results. Part-I: general principles and definitions. Berlin: Beuth Verlag GmbH; 1994.

51. Mutwalli H, Braian M, Mahmood D, Larsson C. Trueness and Precision of Three-Dimensional Digitizing Intraoral Devices. Int J Dent. 2018 Nov 26;2018:5189761. doi: 10.1155/2018/5189761. PMID: 30598665; PMCID: PMC6287154.

52. Papaspyridakos P, Gallucci GO, Chen C-J, Hanssen S, Naert I, Vandenberghe B. Digital versus conventional implant impressions for edentulous patients: accuracy outcomes. Clin Oral Implants Res 2016;27: 465-72.

53. Flügge T, Att W, Metzger M, Nelson K. Precision of dental implant digitization using intraoral scanners. Int J Prosthodont 2016;29:277-83.

54. Sallorenzo A, Gómez-Polo M. Comparative study of the accuracy of an implant intraoral scanner and that of a conventional intraoral scanner for complete-arch fixed dental prostheses. J Prosthet Dent. 2021 Apr 6:S0022-3913(21)00083-4. doi: 10.1016/j.prosdent.2021.01.032. Epub ahead of print. PMID: 33836855.

55. Nobel Biocare. Nobel Biocare. [Online].; 2021 [cited 2021 Aug. Available from: https://store.nobelbiocare.com/hk/en/media/eifu/IFU2003_EN_GB_00.pdf.

56. Mojon P, Oberholzer JP, Meyer JM, Belser UC. Polymerization shrinkage of index and pattern acrylic resins. J Prosthet Dent. 1990 Dec;64(6):684-8. doi: 10.1016/0022-3913(90)90296-o. PMID: 2079675.

57. Nateghi M, Negahdari R, Molaei S, Barzegar A, Bohlouli S. Comparison of the Accuracy of Fixture-Level Implant Impression Making with Different Splinting Techniques. Int J Dent. 2021 Oct 14;2021:2959055. doi: 10.1155/2021/2959055. PMID: 34691181; PMCID: PMC8531793.

58. Heshmati RH, Nagy WW, Wirth CG, Dhuru VB. Delayed linear expansion of improved dental stone. J Prosthet Dent. 2002 Jul;88(1):26-31. PMID: 12239476.

59. 3Shape. 3Shape. [Online].; 2015 [cited 2022 July. Available from: https://www.3shape.com/en/press/2015/3shape-d-series-lab-scanners-add-new.

60. Dentsply Sirona. Dentsply Sirona. [Online].; 2022 [cited 2022 July. Available from: https://www.dentsplysirona.com/en-us/discover/discover-by-brand/ineos-x5.html.

61. O'Toole S, Osnes C, Bartlett D, Keeling A. Investigation into the accuracy and measurement methods of sequential 3D dental scan alignment. Dent Mater. 2019 Mar;35(3):495-500. doi: 10.1016/j.dental.2019.01.012. Epub 2019 Jan 23. PMID: 30683418.

62. Nakhaei M, Ghanbarzadeh J, Dashti H, Karamad R, Alikhasi M. Effect of tightening torque on the marginal adaptation of cement-retained implant-supported fixed dental prostheses Dent. Res J (Isfahan) 2015;12: 359-64.

63. Pereira LMS, Sordi MB, Magini RS, Duarte ARC, Souza JCM. Abutment misfit in implant-supported prostheses manufactured by casting technique: An integrative review. Eur J Dent 2017;11:553-8.

64. Zurutuza J, Caporali A, Bertocco M, Ishchenko M, Khoda O, Steffen H, Figurski M, Parseliunas E, Berk S, Nykiel G. The Central European GNSS Research Network (CEGRN)

dataset. Data Brief. 2019 Nov 12;27:104762. doi: 10.1016/j.dib.2019.104762. PMID: 31788511; PMCID: PMC6880095.

65. Zhang YJ, Shi JY, Qian SJ, Qiao SC, Lai HC. Accuracy of full-arch digital implant impressions taken using intraoral scanners and related variables: A systematic review. Int J Oral Implantol (Berl). 2021 May 12;14(2):157-179. PMID: 34006079.

66. Kavadia V, Kourtis S, Zoidis P, Sarafianou A. The influence of impression coping splinting on the accuracy of the open-tray technique. Gen Dent. 2019 May-Jun;67(3):e5-e9. PMID: 31199752.

67. Abduo J, Palamara JEA. Accuracy of digital impressions versus conventional impressions for 2 implants: an in vitro study evaluating the effect of implant angulation. Int J Implant Dent. 2021 Jul 30;7(1):75. doi: 10.1186/s40729-021-00355-6. PMID: 34327601; PMCID: PMC8322372.

68. Gibbs SB, Versluis A, Tantbirojn D, Ahuja S. Comparison of polymerization shrinkage of pattern resins. J Prosthet Dent. 2014 Aug;112(2):293-8. doi: 10.1016/j.prosdent.2014.02.006. Epub 2014 Apr 14. Erratum in: J Prosthet Dent. 2015 Dec;114(6):872. PMID: 24726587.

69. Katsoulis J, Takeichi T, Sol Gaviria A, Peter L, Katsoulis K. Misfit of implant prostheses and its impact on clinical outcomes. Definition, assessment and a systematic review of the literature. Eur J Oral Implantol 2017;10 Suppl 1: 121-38.

70. Sanda, M., Miyoshi, K. & Baba, K. Trueness and precision of digital implant impressions by intraoral scanners: a literature review. Int J Implant Dent 7, 97 (2021). https://doi.org/10.1186/s40729-021-00352-9.

71. Buzayan MM, Yunus NB. Passive Fit in Screw Retained Multi-unit Implant Prosthesis Understanding and Achieving: A Review of the Literature. J Indian Prosthodont Soc. 2014 Mar;14(1):16-23. doi: 10.1007/s13191-013-0343-x. Epub 2013 Dec 28. PMID: 24604993; PMCID: PMC3935037.

72. Menini M, Setti P, Pera F, Pera P, Pesce P. Accuracy of multi-unit implant impression: traditional techniques versus a digital procedure. Clin Oral Investig. 2018;22:1253–62.

73. Chochlidakis K, Papaspyridakos P, Tsigarida A, Romeo D, Chen YW, Natto Z, et al. Digital versus conventional full-arch implant impressions: A prospective study on 16 edentulous maxillae. J Prosthodont 2020;29:281-6.

74. Kim KM, Lee JS, Kim KN, Shin SW. Dimensional changes of dental impression materials by thermal changes. J Biomed Mater Res 2001;58: 217-20.

75. Endo T, Finger WJ. Dimensional accuracy of a new polyether impression material. Quintessence Int. 2006 Jan;37(1):47-51. PMID: 16429703.

76. Flügge T, van der Meer WJ, Gonzalez BG, Vach K, Wismeijer D, Wang P. The accuracy of different dental impression techniques for implant-supported dental prostheses: a systematic review and meta-analysis. Clin Oral Implants Res 2018;29:374-92.

77. Gómez-Polo M, Álvarez F, Ortega R, Gómez-Polo C, Barmak AB, Kois JC, Revilla-León M. Influence of the implant scan body bevel location, implant angulation and position on intraoral scanning accuracy: An in vitro study. J Dent. 2022 Jun;121:104122. doi: 10.1016/j.jdent.2022.104122. Epub 2022 Apr 6. PMID: 35395345.

78. Gimenez-Gonzalez B, Hassan B, Özcan M, Pradíes G. An in vitro study of factors influencing the performance of digital intraoral impressions operating on active wavefront sampling technology with multiple implants in the edentulous maxilla. J Prosthodont 2017;26:650-5.

79. Giménez B, Özcan M, Martínez-Rus F, Pradíes G. Accuracy of a digital impression system based on active wavefront sampling technology for implants considering operator experience, implant angulation, and depth. Clin Implant Dent Relat Res 2015;17:e54-64.

80. Lin WS, Harris BT, Elathamna EN, Abdel-Azim T, Morton D. Effect of implant divergence on the accuracy of definitive casts created from traditional and digital implant-level impressions: an in vitro comparative study. Int J Oral Maxillofac Implants 2015;30:102-9.

81. Marghalani A, Weber HP, Finkelman M, Kudara Y, El Rafie K, Papaspyridakos P. Digital versus conventional implant impressions for partially edentulous arches: an evaluation of accuracy. J Prosthet Dent. 2018;119:574–9.

82. Iturrate M, Eguiraun H, Etxaniz O, Solaberrieta E. Accuracy analysis of complete-arch digital scans in edentulous arches when using an auxiliary geometric device. J Prosthet Dent. 2019;121:447–54.

83. Pozzi A, Arcuri L, Lio F, Papa A, Nardi A, Londono J. Accuracy of complete-arch digital implant impression with or without scanbody splinting: An in vitro study. Journal of Dentistry. 2022 Apr 1;119:104072.

84. Tan, M.Y.; Hui Xin Yee, S.; Wong, K.M.; Tan, Y.H.; Tan, K.B.C. Comparison of three-dimensional accuracy of digital and conventional implant impressions: Effect of interimplant distance in an edentulous arch. Int. J. Oral Maxillofac. Implant. 2019, 34, 366–380.

85. Albayrak B, Korkmaz İH, Wee AG, Sukotjo C, Bayındır F. Assessing the Effect of Interimplant Distance and Angle on Different Impression Techniques. Machines. 2022 Apr 21;10(5):293.

86. Schmidt, A.; Billig, J.W.; Schlenz, M.A.; Wöstmann, B. The influence of using different types of scan bodies on the transfer accuracy of implant position: An in vitro study. Int. J. Prosthodont. 2021, 34, 254–260.

87. Hariharan R, Shankar C, Rajan M, Baig MR, Azhagarasan NS. Evaluation of accuracy of multiple dental implant impressions using various splinting materials. Int J Oral Maxillofac Implants. 2010 Jan-Feb;25(1):38-44. PMID: 20209185.

88. Mizumoto RM, Yilmaz B, McGlumphy EA Jr, Seidt J, Johnston WM. Accuracy of different digital scanning techniques and scan bodies for complete-arch implant-supported prostheses. J Prosthet Dent 2020;123:96-104.

89. Mizumoto RM, Alp G, Özcan M, Yilmaz B. The effect of scanning the palate and scan body position on the accuracy of complete-arch implant scans. Clin Implant Dent Relat Res 2019;21:987-94.

90. Motel C, Kirchner E, Adler W, Wichmann M, Matta RE. Impact of different scan bodies and scan strategies on the accuracy of digital implant impressions assessed with an intraoral scanner: An in vitro study. J Prosthodont 2019;29: 309-14.

91. Alikhasi M, Siadat H, Nasirpour A, Hasanzade M. Three-dimensional accuracy of digital impression versus conventional method: Effect of implant angulation and connection type. Int J Dent 2018;2018:1-9.

92. Chia VA, Esguerra RJ, Teoh KH, Teo JW, Wong KM, Tan KB. In vitro three-dimensional accuracy of digital implant impressions: the effect of implant angulation. Int J Oral Maxillofac Implants 2017;32:313-21.

93. Fluegge T, Att W, Metzger M, Nelson K. A novel method to evaluate precision of optical implant impressions with commercial scan bodies-an experimental approach. J Prosthodont 2017;26:34-41.

94. Rudolph H, Quaas S, Luthardt RG. Matching point clouds: limits and possibilities. Int J Comput Dent 2002;5:155-64.

95. Mangano F, Lerner H, Margiani B, Solop I, Latuta N, Admakin O. Congruence between Meshes and Library Files of Implant Scanbodies: An In Vitro Study Comparing Five Intraoral Scanners. J Clin Med. 2020 Jul 9;9(7):2174. doi: 10.3390/jcm9072174. PMID: 32660070; PMCID: PMC7408706.

96. Gómez-Polo M, Sallorenzo A, Ortega R, Gómez-Polo C, Barmak AB, Att W, Revilla-León M. Influence of implant angulation and clinical implant scan body height on the accuracy of complete arch intraoral digital scans. J Prosthet Dent. 2022 Mar 22:S0022-3913(21)00651-X. doi: 10.1016/j.prosdent.2021.11.018. Epub ahead of print. PMID: 35337658.

97. Stimmelmayr M, Güth JF, Erdelt K, Edelhoff D, Beuer F. Digital evaluation of the reproducibility of implant scanbody fitdan in vitro study. Clin Oral Investig 2012;16:851-6.

98. Semper W, Kraft S, Kruger T, Nelson K (2009) Theoretical considerations: implant positional index design. J Dent Res 88:725–730.

99. Semper W, Kraft S, Mehrhof J, Nelson K (2010) Impact of abutment rotation and angulation on marginal fit: theoretical considerations. Int J Oral Maxillofac Implants 25:752–758.

100. JemtT,BackT,PeterssonA.Photogrammetry—An alternative to conventional impressions in implant dentistry? A clinical pilot study. Int J Prosthodont 1999;12:363–368.

101. Kan JY, Rungcharassaeng K, Bohsali K, Goodacre CJ, Lang BR (1999) Clinical methods for evaluating implant framework fit. J Prosthet Dent 81:7–13.

102. Zimmermann M, Koller C, Rumetsch M, Ender A, Mehl A. Precision of guided scanning procedures for full-arch digital impressions in vivo. J Orofac Orthop 2017;78:466-71.

103. Ender A, Attin T, Mehl A. In vivo precision of conventional and digital methods of obtaining complete-arch dental impressions. J Prosthet Dent 2016;115:313-20.

CURRICULUM VITAE